RESEARCH ARTICLE

Quantifying microbial fitness in high-throughput experiments

Justus Wilhelm Fink[1,2*†], **Michael Manhart**[1,2,3,4*]

[1]Center for Advanced Biotechnology and Medicine, Rutgers University, Piscataway, United States; [2]Institute of Integrative Biology, Department of Environmental Systems Science, ETH Zurich, Zurich, Switzerland; [3]Department of Environmental Microbiology, Swiss Federal Institute of Aquatic Science and Technology (Eawag), Dübendorf, Switzerland; [4]Department of Biochemistry and Molecular Biology, Robert Wood Johnson Medical School, Rutgers University, Piscataway, United States

***For correspondence:** justus.fink@caltech.edu (JWF); mmanhart@rutgers.edu (MM)

Present address: †Division of Geological and Planetary Sciences, California Institute of Technology, Pasadena, United States

Competing interest: The authors declare that no competing interests exist.

Funding: See page 20

Preprint posted 20 August 2024
Sent for Review 06 September 2024
Reviewed preprint v1 09 December 2024
Reviewed preprint v2 20 May 2026
Reviewed preprint v3 13 August 2026
Version of Record 02 November 2026

Reviewing Editor: Sara Mitri, University of Lausanne, Switzerland

© Copyright Fink and Manhart. This article is distributed under the terms of the Creative Commons Attribution License, which permits unrestricted use and redistribution provided that the original author and source are credited.

eLife Assessment

This manuscript applies a theoretical analysis to two published datasets on yeast and bacterial evolution to compare different ways of quantifying fitness. It makes an **important** advance by clarifying how discrepancies can arise by using different approaches and provides recommendations for best practices. Overall, this is an impressive and highly beneficial study that is based on **convincing** evidence and has the potential of setting standards in this rapidly growing field.

Abstract Few concepts are as central to evolution as is fitness, and yet the quantification of fitness is often ambiguous. In particular, high-throughput experiments to measure mutant fitness in microbes are increasingly common, but vary widely in their definitions of fitness, which makes their results difficult to compare. What are the consequences of these different fitness statistics, and is there a best way to quantify fitness in a given context? Here, we systematize the set of possible fitness statistics according to the following three choices: (1) the encoding of relative abundance (e.g., transforming by a log or logit function), (2) the time scale over which to measure the change in relative abundance, and (3) the choice of a reference subpopulation for calculating relative fitness in bulk competition experiments, such as those using DNA-barcoded mutants. We show that these different choices can lead to significantly different interpretations of mutant fitness in *Saccharomyces cerevisiae* and *Escherichia coli*, affecting the magnitude of fitness effects, the apparent presence of epistasis, and even the fitness ranking across mutants. This can confound predictions for evolutionary dynamics and gene functions. Altogether, our results demonstrate the importance of consistent fitness definitions for reproducible results across experiments.

Introduction

The concept of fitness is supposed to describe the fate of mutations as they arise in a population (***Gillespie, 2004***) and defines other core evolutionary concepts such as trade-offs (***Stearns, 1989***). At the same time, fitness is often a confusing term in evolutionary biology (***de Jong, 1994***; ***Ariew and Lewontin, 2004***; ***Kokko, 2021***). It is possible to classify fitness measures by their role in theory (***Smith et al., 2024***) and their scale of measurement (***Chevin, 2011***; ***Houle et al., 2011***; ***Wagner, 2010***), but these arguments offer little guidance on how to measure fitness in practice. Empirical fitness measurements have become widespread in the microbial sciences—to test evolutionary theory (***Paquin and Adams, 1983***; ***Wiser et al., 2013***; ***Kryazhimskiy et al., 2014***; ***Levy et al., 2015***; ***Nguyen Ba et al., 2019***; ***Couce et al., 2024***), detect microbial interactions (***Schreier et al., 2023***; ***Pierce et al., 2021***),

annotate gene functions (**Wetmore et al., 2015**; **Price et al., 2018**), and understand the spread of antibiotic resistance genes (**Andersson, 2006**; **San Millan and MacLean, 2017**)—but the approaches to quantifying fitness in these studies vary widely.

The classic approach to measuring the fitness effects of mutations uses pairwise competition experiments, where the mutant competes with its ancestral wild-type in coculture (**Elena et al., 1998**; **Zeyl and DeVisser, 2001**; **Gordo et al., 2012**). This approach is ideal because it mimics the dynamics of spontaneous mutations, and thus is typically used in experimental evolution (**Paquin and Adams, 1983**; **Kryazhimskiy et al., 2014**; **Dykhuizen, 1990**; **Lenski et al., 1991**; **Spiers et al., 2002**). For example, the Long-Term Evolution Experiment (LTEE) has evolved *Escherichia coli* over tens of thousands of generations and measured the fitness of each evolved lineage in competition with the ancestor (**Wiser et al., 2013**; **Lenski et al., 1991**; **Barrick et al., 2023**). However, pairwise competition experiments require a way to distinguish mutants from the wild-type in cocultures (e.g., fluorescent labeling or selection markers), which is not always feasible to engineer. A second approach is thus to measure properties of genotypes in monocultures, like the growth rate, and estimate relative fitness between genotypes from these measurements. Monoculture growth curves are straightforward to measure, even for large numbers of mutants (**Warringer et al., 2003**; **Chevereau et al., 2015**; **Campos et al., 2018**), but empirical tests have shown that the monoculture growth rate is insufficient to predict the relative fitness between genotypes (**Concepción-Acevedo et al., 2015**; **Durão et al., 2021**; **Ram et al., 2019**). Summary statistics of whole growth curves, like the area under the curve (AUC), perform better (**Sprouffske and Wagner, 2016**; **Worthan et al., 2023**; **Schmitz et al., 2024**). However, this approach breaks down for strains that engage in cross-feeding or toxin production, and attempts to improve monoculture-based fitness estimates require additional experiments (**Ram et al., 2019**; **Schmitz et al., 2024**) and do not go beyond qualitative fitness rankings (**Schmitz et al., 2024**).

A third and more recent approach is to measure relative fitness in bulk competition experiments using high-throughput sequencing, often of DNA barcodes (**Levy et al., 2015**; **Johnson et al., 2023**). For example, transposon-insertion mutagenesis generates libraries of gene knockouts that can be tracked as they grow in a single batch culture (**van Opijnen and Camilli, 2013**). Estimating the fitness of each mutant allows us to identify genes that are particularly important in the growth environment (**Wetmore et al., 2015**; **Price et al., 2018**; **Nguyen et al., 2020**), in the given genetic background (**Nguyen Ba et al., 2019**; **Couce et al., 2024**; **Johnson et al., 2019**; **Ascensao et al., 2023**), and in the context of an ecological community (**Schreier et al., 2023**; **Pierce et al., 2021**; **Ascensao et al., 2023**; **Martinson et al., 2023**). Bulk fitness estimation also plays a major role in identifying beneficial lineages in experimental evolution (**Levy et al., 2015**; **Blundell and Levy, 2014**) (not unlike the tracking of viral pathogens in public health; **Davies et al., 2021**; **Sohail et al., 2022**; **Meijers et al., 2023**) and especially testing their fitness in new environments (**Venkataram et al., 2016**; **Li et al., 2019**; **Kinsler et al., 2020**; **Bakerlee et al., 2021**; **Schmidlin et al., 2024**). Many of these studies make different choices about the design of experiments and the calculation of fitness, without explaining why a certain fitness measure was used or how to compare between data sets.

The inconsistent choices for quantifying microbial fitness make it difficult to compare fitness across experiments, especially because different groups tend to use different definitions. For example, the LTEE reports relative fitness per-generation (**Wiser et al., 2013**; **Lenski et al., 1991**), whereas other evolution experiments exclusively report relative fitness per-cycle of batch growth (**Kryazhimskiy et al., 2014**; **McDonald et al., 2011**). New techniques, like barcode sequencing, often spark their own fitness metrics (**Wetmore et al., 2015**; **Nguyen et al., 2020**; **Li et al., 2016**; **Frey et al., 2021**; **Gabzi et al., 2022**). A different choice of fitness metric might lead to a different ranking of mutants in a genetic screen (and the importance we assign to those genes) or change statistical properties of the distribution of mutant fitness effects, which is essential to predict the probability of mutant fixation (**Good et al., 2012**), the speed of adaptation (**Desai and Fisher, 2007**), and the effect size in statistical tests of gene function (**Wetmore et al., 2015**; **Price et al., 2018**). This raises three key questions: (1) How do these fitness statistics differ? (2) Can we say which choices are optimal, in the light of first principles or some practical considerations? (3) Does this tell us how we should design these experiments? Previous work has addressed aspects of these questions (**Smith et al., 2024**; **Chevin, 2011**; **Houle et al., 2011**; **Wagner, 2010**; **Matuszewski et al., 2016**) but the arguments are scattered across disciplines and based on generic models of population growth (**Smith et al., 2024**; **Chevin, 2011**; **Wagner, 2010**; **Limdi and Baym, 2023**), rather than incorporating the specific dynamics of microbes

in laboratory experiments. Here, we address these questions from a unified framework, using realistic microbial population dynamics with empirical traits to systematically test different fitness metrics.

Results

Predictive power of fitness depends on the encoding of relative abundance

We distinguish between three related but distinct notions of fitness (***Smith et al., 2024***), all based on predicting dynamics of a population (***Mills and Beatty, 1979***; ***Takacs and Bourrat, 2022***;

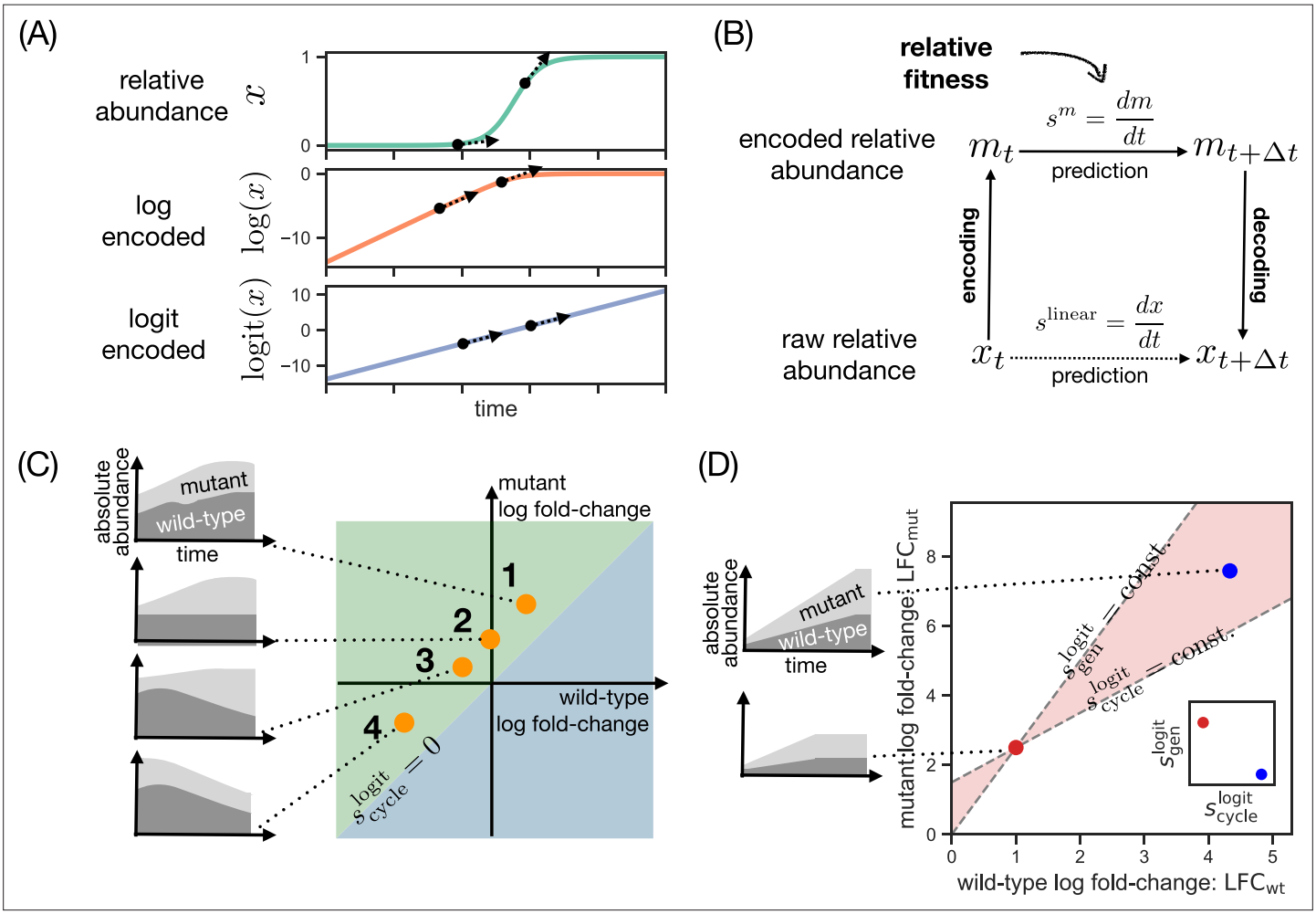


Figure 1. Overview of the choice of encoding and the choice of time scale for quantifying relative fitness. (**A**) Example trajectory of relative abundance x (top panel) for a mutant invading and eventually replacing a wild-type population. The same trajectory is plotted under the encoding $\log x$ (middle panel) and the encoding $\mathrm{logit}\, x = \log(x/(1-x))$ (bottom panel). (**B**) Flowchart to predict the future relative abundance of a mutant given a relative fitness value $s^m = dm/dt$ for some encoding m. The current relative abundance x_t is transformed into the new variable $m_t = m(x_t)$, then projected into the future through a linear extrapolation using s^m (upper horizontal arrow) and finally converted back into a frequency $x_{t+\Delta t}$ using the decoding function m^{-1}. (**C**) Four scenarios for a mutant with the same relative fitness per-cycle but with different underlying population dynamics. For each scenario, we show an example trajectory of absolute abundance (stacked) for the wild-type (dark gray) and mutant population (light gray). Each scenario is mapped as a single-dot onto the fold-change diagram (center plot) and colored areas indicate positive (green area) and negative relative fitness per-cycle (blue area; compare ***Equation 9***). Fitness per-cycle has isoclines that are parallel to the identity in the log fold-change (LFC) diagram. (**D**) Scenario for rank discrepancy between relative fitness per-cycle $s^{\mathrm{logit}}_{\mathrm{cycle}}$ and relative fitness per-generation $s^{\mathrm{logit}}_{\mathrm{gen}}$. For a given competition (red dot), rank discrepancy occurs in a bow tie-shaped area of the fold-change space (shaded red). Any competition in the right half of this area (blue dot) will have higher mutant fitness $s^{\mathrm{logit}}_{\mathrm{cycle}}$ but lower mutant fitness $s^{\mathrm{logit}}_{\mathrm{gen}}$ (right inset). As small plots on the left, we show possible population dynamics that generate this fold-change variation. Here, the growth rates of the mutant and wild-type are identical in the two scenarios, but the growth period is different (e.g., from additional resources).

Charlesworth, 1993; ***Charlesworth, 1994***). The first type of fitness is *absolute fitness*, which is a property of a single genotype by itself and serves to predict the change in the genotype's absolute abundance $N(t)$ over a future time window Δt (***Appendix 1—figure 1A***). This is important for questions about extinction and evolutionary rescue (***Alexander et al., 2014***). The second type of fitness is *relative fitness*, which is a property of two genotypes as it describes how the relative abundance $x(t)$ of one genotype changes compared to the other over a time Δt (***Appendix 1—figure 1B***). This is important to determine the fixation probability of new mutations (***Good et al., 2012***; ***Kimura, 1962***; ***Patwa and Wahl, 2008***). In general, these dynamics are stochastic (***Kimura, 1962***; ***Hansen, 2017***; ***Doebeli et al., 2017***), but throughout this paper we focus on their average behavior across replicate cultures (as sketched in ***Appendix 1—figure 1C***).

A practical challenge of working with relative fitness is that it must be measured between all pairs of genotypes in coculture competitions. Therefore, it is common to infer relative fitness of two genotypes based on some individual properties of the genotypes (***Drlica, 2003***; ***Sprouffske et al., 2018***; ***Pinheiro et al., 2021***; ***Diaz-Colunga et al., 2023***). We denote this third notion of fitness as the *fitness potential*. Like absolute fitness, fitness potential is a property of an individual genotype, but unlike the absolute fitness, it has no meaning by itself. In analogy with the potential energy of physical systems, fitness potential is intended only to be compared between two genotypes (e.g., by taking the difference or ratio) to estimate the relative fitness between those genotypes (***Worthan et al., 2023***; ***Schmitz et al., 2024***). The collection of fitness potential values across a large set of genotypes forms a fitness landscape (***de Visser and Krug, 2014***; ***Bank, 2022***). Note that the term 'fitness potential' has been used with a related but somewhat different meaning in the population genetics literature (***Manrubia et al., 2021***; ***Kondrashov and Kondrashov, 2001***; ***Milkman, 1978***).

We emphasize that fitness as defined here gives information about short-time dynamics but not necessarily the long-term outcome (compare ***Smith et al., 2024***). For example, this excludes the ratio of growth rates (***Chevin, 2011***; ***Diaz-Colunga et al., 2023***) or the resource concentration R^* in chemostat equilibrium (***Grover, 1997***) since these quantities cannot tell you how fast the absolute or relative abundance is changing. We also note that in all these definitions, the fitness of a genotype is specific to one environment, including all abiotic and biotic factors. How fitness in one environment is related to fitness in other environments is important (***Nguyen Ba et al., 2019***; ***Price et al., 2018***; ***Ascensao et al., 2023***; ***Martinson et al., 2023***; ***Li et al., 2019***; ***Kinsler et al., 2020***; ***Diaz-Colunga et al., 2023***; ***Morin et al., 2018***; ***Morin et al., 2022***) but beyond the scope of this article, as we focus on specific laboratory measurements of fitness rather than abstract concepts.

In this article, we will focus on relative fitness as this is the most common object of high-throughput laboratory experiments in microbes (***Wetmore et al., 2015***; ***Lenski et al., 1991***; ***Nguyen et al., 2020***; ***Frey et al., 2021***; ***Gabzi et al., 2022***) and also has the most straightforward connection to key evolutionary outcomes such as fixation (***Good et al., 2012***; ***Kimura, 1962***; ***Patwa and Wahl, 2008***). We define a genotype's relative fitness as any number that is sufficient to predict the genotype's relative abundance $x(t)$ over a short time period (***Appendix 1—figure 1***). The simplest approach is to take a linear expansion of $x(t)$ and use its slope at time t to predict the change over a time Δt (e.g., ***Figure 1A***, top panel):

$$x(t+\Delta t) = x(t) + \left.\frac{dx}{dt}\right|_t \Delta t. \tag{1}$$

The slope

$$s^{\text{linear}} = \left.\frac{dx}{dt}\right|_t \tag{2}$$

qualifies as a fitness statistic but often will incorrectly estimate the actual change in relative abundance because $x(t)$ is nonlinear (***Figure 1A***, top panel).

Alternatively, we can *encode* the relative abundance x in a new variable $m(x)$ (any smooth, strictly increasing function) whose dynamics may be easier to linearly approximate (***Figure 1B***; compare ***Denniston and Crow, 1990***):

$$m(x(t+\Delta t)) = m(x(t)) + s^m \Delta t, \tag{3}$$

where

$$s^m = \left.\frac{dm}{dt}\right|_t \tag{4}$$

is the relative fitness under the encoding m. In Appendix 1—section S1 we show examples of the encoded relative fitness for an explicit model of population dynamics, and in Appendix 1—section S2 we show how this concept generalizes to absolute fitness as well.

The ideal encoding transforms the relative abundance $x(t)$ into a linear trajectory that can be fully predicted from the slope s^m. While the log-encoding $m(x) = \log x$ is common in many TnSeq studies (***Pierce et al., 2021***; ***Wetmore et al., 2015***; ***Price et al., 2018***; ***Martinson et al., 2023***; ***Morin et al., 2018***; ***Morin et al., 2022***) (and is implicit in plots of relative abundance on a logarithmic scale; ***Blundell and Levy, 2014***), the log-encoded fitness $s^{\log}$ tends to overestimate the change at high relative abundance (***Figure 1A***, middle panel). Instead, the best encoding in most cases is the logit function (***Figure 1A***, bottom panel):

$$\operatorname{logit} x = \log\left(\frac{x}{1-x}\right). \tag{5}$$

This is because the relative abundance $x(t)$ typically follows logistic dynamics (Appendix 1—section S1), at least as a first-order approximation (Appendix 1—section S3, ***Appendix 1—figure 2***), and the logit function is linearly related to the inverse function of logistic $x(t)$. The logit-encoded relative fitness of a mutant is equivalent to the standard definition of its selection coefficient in population genetics (***Fisher, 1930***). For this reason we focus on the logit-encoded relative fitness for the remainder of this work. Note that the logit encoding and logistic dynamics apply to relative abundance and are not to be confused with the logistic growth model used with microbial growth curves, where it describes the absolute abundance (***Zwietering et al., 1990***).

Estimating relative fitness requires a choice of time scale

Since the relative abundance of a genotype can only be measured at discrete times, we must estimate the instantaneous relative fitness of ***Equation 4*** using a finite difference between consecutive time points (***Appendix 1—figure 1C***, Appendix 1—section S4):

$$s^m \approx \frac{m(x(t)) - m(x(t-\Delta t))}{\Delta t}. \tag{6}$$

For the logit-encoding this becomes

$$s^{\text{logit}} = \frac{1}{\Delta t}\left[\log\frac{x(t)}{1-x(t)} - \log\frac{x(t-\Delta t)}{1-x(t-\Delta t)}\right]. \tag{7}$$

In the case of a single mutant competing against a wild-type strain, we can rewrite ***Equation 7*** in terms of the log fold-changes (LFCs) of the mutant and wild-type strains:

$$s^{\text{logit}} = \frac{\text{LFC}_{\text{mut}} - \text{LFC}_{\text{wt}}}{\Delta t}, \tag{8}$$

where the LFC of each strain is $\text{LFC} = \log N(t)/N(t-\Delta t)$ and N is the biomass of the strain. The LFC is sometimes also referred to as a Malthusian parameter (***Wagner, 2010***; ***Lenski et al., 1991***; ***Alexander et al., 2014***).

Therefore, a key element of estimating relative fitness from discrete time data is the choice of time interval Δt. There are two common choices in empirical measurements of microbial fitness. The first is to use a time scale extrinsic to the population. In particular, microbial populations in laboratory experiments (***Lenski et al., 1991***; ***Cooper, 2018***) but also in some natural environments (***Thaiss et al., 2014***; ***Martin-Platero et al., 2018***; ***Muratore et al., 2022***) grow in discrete growth cycles dictated by external pulses of nutrients (e.g., batch culture). In this case, it is convenient to quantify relative fitness *per-cycle*, by choosing time units in ***Equation 8*** such that $\Delta t = 1$:

$$s^{\text{logit}}_{\text{cycle}} = \text{LFC}_{\text{mut}} - \text{LFC}_{\text{wt}}. \tag{9}$$

The second common choice for Δt is a time scale intrinsic to the population, typically its generation time. The relative fitness per-cycle may depend on the number of generations in the growth cycle, and it can be valuable to normalize for this dependence, especially when comparing across environments (***Lenski et al., 1991***). However, defining the number of generations for a population with multiple genotypes growing at different rates is ambiguous. In the case of a single mutant competing with a wild-type, it is common to consider only the number of generations experienced by the wild-type strain, which is estimated by its log fold-change $\mathrm{LFC}_{\mathrm{wt}}$. It is convenient to express the generations in base e to match the natural logarithm in the logit-encoding, but this could equivalently be done by converting all logarithms in ***Equation 8*** to base 2. Thus, the relative fitness of a mutant *per-generation* is defined by choosing $\Delta t = \mathrm{LFC}_{\mathrm{wt}}$ in ***Equation 8***:

$$s_{\mathrm{gen}}^{\mathrm{logit}} = \frac{\mathrm{LFC}_{\mathrm{mut}}}{\mathrm{LFC}_{\mathrm{wt}}} - 1. \tag{10}$$

This quantity is equivalent to the fitness statistic $W = 1 + s_{\mathrm{gen}}^{\mathrm{logit}}$ used in the LTEE (***Lenski et al., 1991***) and other studies (***DelaFuente et al., 2020***; ***Peterson et al., 2024***; ***Moger-Reischer et al., 2023***; ***Baake et al., 2019***; ***Pearl Mizrahi et al., 2023***). Some authors assume a fixed number of generations per growth cycle (***Kryazhimskiy et al., 2014***; ***Couce et al., 2024***), but since this may not be true, we use the term 'per-generation' strictly for fitness statistics where the wild-type generations are explicitly measured.

Relative fitness per-cycle and per-generation can rank mutants differently when wild-type growth depends on mutant

Although relative fitness of a mutant per growth-cycle (***Equation 9***) and per-generation (***Equation 10***) differ only by choice of time scale, they are not just equivalent quantities in different units. First, while fitness per-cycle is well-defined regardless of whether the population undergoes net growth or death (***Figure 1C***), fitness per-generation is not defined when the wild-type undergoes no change or net death (denominator of ***Equation 10*** is not positive) (***Kokko, 2021***; ***Lenski, 2021***). This can occur for microbes under high drug concentrations, as well as for microbial populations under harsh environmental conditions as found in sediments or wastewater (***Koch et al., 2018***; ***Wang et al., 2022***).

However, even when the wild-type LFC is positive, the relative fitness per-cycle and per-generation are not necessarily proportional to each other across a set of mutants competed against the same wild-type. The reason is that while the growth cycle time scale is extrinsic to a population and therefore the same across all pairs of genotypes, the generation time scale depends on the growth of the wild-type, which may be affected by the specific mutant it is competing against. This discrepancy can be quantitative as well as qualitative, producing different rankings of mutants. For example, ***Figure 1D*** shows two mutant genotypes (red and blue) that have opposite rankings under these fitness statistics: the blue mutant has higher relative fitness per-cycle $s_{\mathrm{cycle}}^{\mathrm{logit}}$, but the red mutant has higher relative fitness per-generation $s_{\mathrm{gen}}^{\mathrm{logit}}$. The disagreement in ranking requires positive covariation in the LFCs (red bow tie-shaped area in ***Figure 1D***), such that the mutant with higher LFC also induces a higher LFC in the wild-type (see illustration in ***Appendix 1—figure 3*** and exact conditions in Appendix 1—section S5).

Basic features of microbial population dynamics are sufficient to cause rank discrepancy between fitness statistics

Since the discrepancy between fitness per-cycle $s_{\mathrm{cycle}}^{\mathrm{logit}}$ and per-generation $s_{\mathrm{gen}}^{\mathrm{logit}}$ occurs when the wild-type LFC varies across pairwise competitions with different mutants, we need to determine what biological mechanisms cause this. One way to explore this is to use a minimal model of microbial population dynamics parameterized by empirical data on a set of mutants. While a minimal model does not capture all possible mechanisms, it provides a null expectation for how common these discrepancies should be in real populations.

We use a model that approximates microbial population dynamics as three growth phases—a lag phase, an exponential growth phase, and a stationary phase (***Figure 2A***)—where strains compete for a single limiting resource with no other interactions (***Manhart et al., 2018***; ***Manhart and Shakhnovich, 2018***), since resource competition is likely to be the main interaction between a wild-type and a mutant with only small genetic differences (e.g., a point mutation or gene knockout). This

model captures the minimal dynamics of microbial growth under laboratory conditions, and therefore serves as a baseline for possible outcomes. We parameterize the model using growth curves of single-gene knockout mutants in *Saccharomyces cerevisiae* (***Warringer et al., 2003***; ***Giaever et al., 2002***; ***Appendix 1—figures 4 and 5***, Appendix 1—section S6). We simulate a pairwise competition for each knockout against the wild-type (***Figure 2A***) and calculate relative fitness per-cycle $s^{\text{logit}}_{\text{cycle}}$ and per-generation $s^{\text{logit}}_{\text{gen}}$ for each knockout (Methods). While the relative fitness per-cycle and per-generation in the model are highly correlated across mutants overall (***Appendix 1—figure 6***), the model predicts major differences in individual mutants when we rank them by fitness (***Figure 2B***). Indeed, when we plot all simulated mutant competitions on the LFC diagram, we find that there are many pairs of points that have positive covariation in the mutant and wild-type LFC and thus give rise to rank differences (compare ***Figures 1D and 2C***). Since these rankings often serve to select important mutants from a functional genomics screen or an evolution experiment, discrepancies between fitness definitions may lead analyses down different paths.

This model therefore shows that the basic features of microbial population dynamics and resource competition with realistic parameters are sufficient to cause substantial disagreement between fitness per-cycle and per-generation, underscoring the importance of this analysis choice. Furthermore, the model reveals a basic mechanism that causes this discrepancy: mutants must have lower biomass yield plus variation in one additional trait (lag time or growth rate), and a high mutant relative abundance (e.g., 50%) at the start of the competition (***Appendix 1—figure 7***). These conditions are necessary because they allow mutants both to have variation in fitness and to alter the wild-type LFC in pairwise competition. Even though the wild-type growth rate is unaffected by mutants, the wild-type LFC will change in the presence of mutants that have lower yield because the population on average consumes more resources per cell division (Appendix 1—section S7). By this mechanism, it is possible to concoct a set of growth traits where relative fitness per-generation and per-cycle deliver completely opposite rankings (***Appendix 1—figure 8***).

Fitness statistics can disagree on epistasis and long-term fitness trends

Since the relative fitness of single mutants differs depending on whether fitness is quantified per-cycle or per-generation, how does that choice impact the apparent epistatic interactions between multiple mutations and the long-term evolutionary trend in fitness? Using the same minimal model of

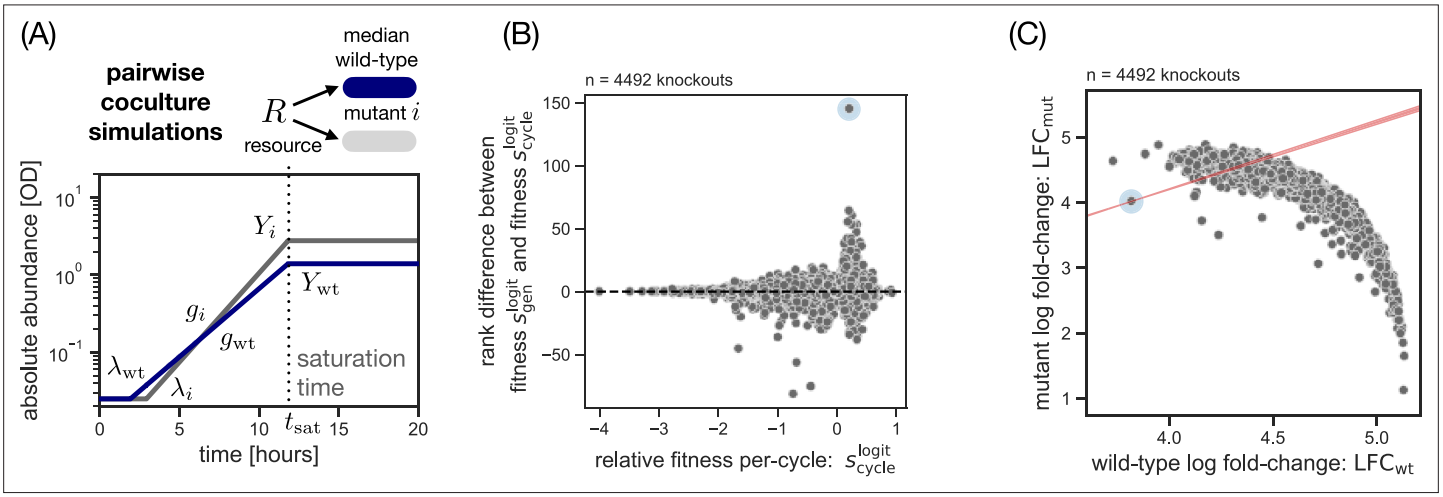


Figure 2. Comparison of mutant fitness rankings with different time scales using empirical trait variation. (**A**) Overview of pairwise coculture simulations. For each mutant strain (gray), we simulate a competition growth cycle against a reference wild-type strain (blue) using the estimated traits and laboratory parameters for the initial condition ($N_0 = 0.05$ OD, $R_0 = 111$ mM glucose, $x = 0.5$; Methods and see ***Appendix 1—figure 4*** for the underlying trait distribution). (**B**) Rank discrepancy between relative fitness per-cycle $s^{\text{logit}}_{\text{cycle}}$ and per-generation $s^{\text{logit}}_{\text{gen}}$. Higher rank is defined as higher fitness, and the rank difference is defined as the rank in $s^{\text{logit}}_{\text{gen}}$ minus the rank in $s^{\text{logit}}_{\text{cycle}}$. The blue halo marks the mutant with the greatest rank difference. (**C**) Covariation between wild-type and mutant fold-change across all simulated competitions for all mutant strains (gray dots). The blue halo marks the same mutant as in panel B, with its red bow tie-shaped area defining the space of log fold-changes (LFCs) that would have a rank discrepancy with it (compare ***Figure 1D***), which includes many other mutant competitions.

population dynamics as in ***Figure 2A***, we simulate a set of six mutants, each one having an increase or decrease in each of the three quantitative traits in the model (lag time, growth rate, and yield), and calculate the relative fitness per-cycle and per-generation for all pairs of those mutations (assuming the mutation effects on the traits themselves are additive; Methods). We quantify epistasis as the fitness difference (in 1:1 competition with the wild-type; Methods) between the double mutant and the sum of the single mutants (***Figure 3A***; ***Krug, 2018***).

Figure 3B shows that almost all the double mutants differ in their apparent epistasis per-cycle versus per-generation. Epistasis per-cycle occurs when one of the mutations affects growth rate (***Figure 3C***), while epistasis per-generation occurs when one of the mutations affects lag time (***Figure 3D***). This is because the effect of a change in growth rate accrues per-generation (and hence is non-epistatic when measured over that time scale; Appendix 1—section S8), while the effect of a change in lag time accrues once per-cycle (and hence is non-epistatic in the per-cycle statistic). See ***Appendix 1—figures 9–14*** for growth curves in all cases. As an example, the double mutant in ***Appendix 1—figure 12***, row D has two lag time-reducing mutations that are perfectly additive in the per-cycle statistic. However, the lag time mutations also reduce the saturation time of the growth cycle such that the fitness of the double mutant is spread over a smaller number of wild-type generations $\mathrm{LFC}_{\mathrm{wt}}$, creating synergistic magnitude epistasis in the per-generation statistic. Note that this depends on measuring fitness for a mutant at relatively high abundance in the pairwise competition with the wild-type; when the mutant is rare, the wild-type fold-change $\mathrm{LFC}_{\mathrm{wt}}$ is effectively constant across mutants and epistasis measured per-cycle is proportional to its value measured per-generation (***Appendix 1—figure 15***). Differences in apparent epistasis can also lead to differences in apparent

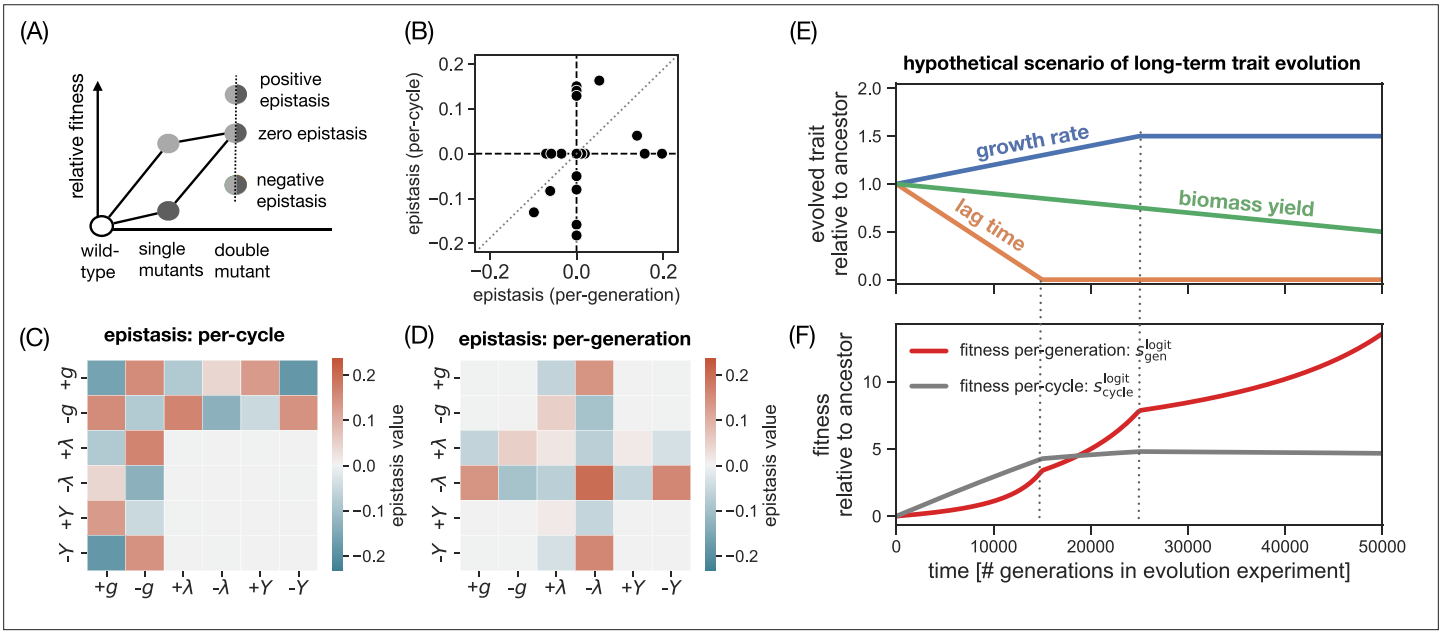


Figure 3. Discrepancy between fitness per-generation and per-cycle in epistasis detection and long-term evolutionary trend. (**A**) Schematic detection of epistasis for two single mutants (light and dark circle). Epistasis occurs if the corresponding double mutant (two-component circles) deviates from the additive fitness (parallelogram shape in solid lines; Methods). (**B**) Correlation between epistasis in relative fitness per-cycle s_{cycle} and per-generation s_{gen}. Each dot corresponds to a hypothetical double mutant that combines pairs of mutations systematically perturbing each of the three growth traits (***Figure 2A***) in our minimal model of population dynamics (Methods). (**C**) Heatmap for epistasis in the per-cycle fitness s_{cycle} for all double mutants in our simulated data set; same data as in panel B. The rows and columns correspond to the six single mutations in our model of population dynamics (Methods): an increase or decrease in lag time ($+\lambda$, $-\lambda$), an increase or decrease in maximum growth rate ($+g$, $-g$), or an increase or decrease in biomass yield ($+Y$, $-Y$). (**D**) Heatmap for epistasis in the per-generation fitness s_{gen}; same data as in panel B. All epistasis plots are based on 1:1 competition growth cycles with the wild-type (***Appendix 1—figures 9–14***). See ***Appendix 1—figure 15*** for epistasis patterns at low mutant relative abundance. (**E**) Hypothetical scenario for trait evolution in an evolution experiment. An evolving population decreases lag time to zero (orange line), increases growth rate until saturation (blue line), and gradually decreases biomass yield (green line). This trend is similar to initial observations from the Long-Term Evolution Experiment (LTEE) (***Vasi et al., 1994***). (**F**) Corresponding long-term trend in relative fitness based on the trait evolution in panel E. We estimate relative fitness per-cycle $s^{\mathrm{logit}}_{\mathrm{cycle}}$ (gray line) and per-generation $s^{\mathrm{logit}}_{\mathrm{gen}}$ (red line) every 250 generations. Dotted vertical lines mark the end of trait evolution in lag time and growth rate in panel E. For the actual fitness trend in the LTEE, see ***Appendix 1—figure 16***.

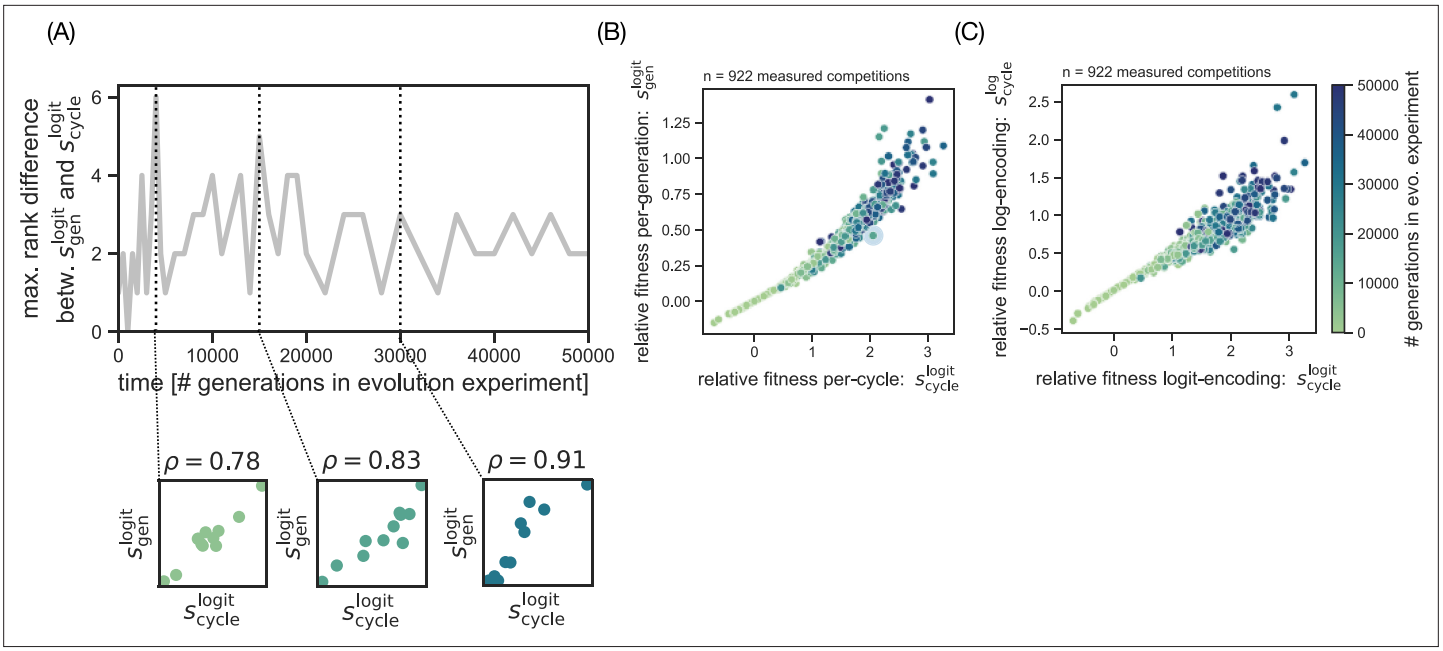


Figure 4. Rank discrepancies between fitness statistics in Long-Term Evolution Experiment (LTEE) competition data. (**A**) Rank difference between relative fitness per-cycle and per-generation as a function of time in the LTEE. For each of the 12 lines in the LTEE, we compute the relative fitness per-cycle $s^{\text{logit}}_{\text{cycle}}$ and per-generation $s^{\text{logit}}_{\text{gen}}$ as a function of time, by averaging the data from the LTEE competition data set (***Wiser et al., 2013***) across replicate measurements (Appendix 1—section S9). For some lines, the time series is truncated due to measurement difficulties (***Wiser et al., 2013***). Based on the quantitative fitness values $s^{\text{logit}}_{\text{cycle}}$ and $s^{\text{logit}}_{\text{gen}}$, we compute fitness rankings between the replicate lines at any given time point (higher rank means higher fitness; compare ***Figure 2B***). The rank difference is defined as the rank in $s^{\text{logit}}_{\text{gen}}$ minus the rank in $s^{\text{logit}}_{\text{cycle}}$, and we combine the rank differences for all evolving lines to compute the maximum rank difference at each time point. Insets: At three chosen time points ($t = 4000$, $t = 15,000$, $t = 30,000$ generations), we show the correlation between relative fitness per-cycle $s^{\text{logit}}_{\text{cycle}}$ and relative fitness per-generation $s^{\text{logit}}_{\text{gen}}$ (each dot corresponds to one of the 12 lines in the LTEE). We quantify the correlation between $s^{\text{logit}}_{\text{cycle}}$ and $s^{\text{logit}}_{\text{gen}}$ with the Spearman rank correlation ρ (panel title). Colors indicate the time point and correspond to the color bar in panel C. (**B**) Covariation between relative fitness per-cycle $s^{\text{logit}}_{\text{cycle}}$ and per-generation $s^{\text{logit}}_{\text{gen}}$ for evolved populations of the LTEE. Each line of the LTEE contributes roughly two competitions per time point due to replicate measurements (Appendix 1—section S9) (***Wiser et al., 2013***). The color of the points indicates evolutionary time point; see panel C for the color bar. We highlight the evolved population with the greatest rank difference (blue halo; same as in ***Appendix 1—figure 17***). (**C**) Same as panel B but comparing relative fitness under the logit-encoding $s^{\text{logit}}_{\text{cycle}}$ and under the log-encoding $s^{\text{log}}_{\text{cycle}}$.

long-term trends of fitness per-cycle and per-generation in an evolution experiment. For example, if growth traits of a population in the minimal model evolve according to ***Figure 3E***, then fitness per-cycle will saturate at an early time while fitness per-generation will continue to increase (***Figure 3F***). This is because the long-term decrease in yield reduces the wild-type LFC in 1:1 competitions between an evolved mutant and the wild-type, which causes fitness per-generation to increase (***Equation 10***).

Different fitness time scales agree on LTEE trend but not on mutant ranking

As an empirical test for discrepancies between relative fitness per-generation and per-cycle, we test how the choice of fitness time scale affects conclusions from the LTEE (Appendix 1—section S9). We reanalyze competition data from the LTEE (***Wiser et al., 2013***) using the relative fitness per-generation $s^{\text{logit}}_{\text{gen}}$ (equivalent to the original definition used in those studies, $W = 1 + s^{\text{logit}}_{\text{gen}}$) and relative fitness per-cycle $s^{\text{logit}}_{\text{cycle}}$. Note these competitions are between the ancestral wild-type and each of the 12 evolved populations, rather than single mutants, across time points. We confirm that the long-term fitness trend in the LTEE is the same for $s^{\text{logit}}_{\text{gen}}$ and $s^{\text{logit}}_{\text{cycle}}$ (***Appendix 1—figure 16***). When we look more closely at the fitness ranking between lineages, we find that the two statistics disagree on the fitness ranking at almost every time point (***Figure 4A***) and on the fittest population overall (***Figure 4B***; see ***Appendix 1—figure 17A*** for rankings). This discrepancy arises from positive covariation across pairs of LFC values in the LTEE competition data set (***Appendix 1—figure 17B***).

While we have focused on the logit encoding so far since logistic dynamics are usually the best null model of mutant frequency dynamics (***Figure 1A***), the log encoding is common in many TnSeq studies (***Pierce et al., 2021***; ***Wetmore et al., 2015***; ***Price et al., 2018***; ***Martinson et al., 2023***; ***Morin et al., 2018***; ***Morin et al., 2022***). The LTEE competition data is a valuable opportunity to empirically test the consequences of this choice as well. ***Figure 4C*** shows that the relative fitness per-cycle under the log-encoding $s^{\log}_{\text{cycle}}$ differs from the logit-based fitness $s^{\text{logit}}_{\text{cycle}}$ for evolved LTEE populations, leading to ranking discrepancies especially for the fittest populations (***Appendix 1—figure 18A***). The discrepancy in fitness between encodings has a different mechanism compared to the discrepancy from fitness time scale: it arises from variation in the initial relative abundance in mutant-to-wild-type competitions in the LTEE data set. Although these pairwise competitions are intended to start with equal abundances of the evolved population and of the wild-type (1:1), ***Appendix 1—figure 18B*** shows that there is a systematic trend toward lower initial frequencies of the evolved populations over time. This trend is a side effect of the inoculation method in LTEE competition experiments, where a fixed volume of the evolved population is transferred to the competition growth cycle but the cell density for the evolved population in pre-culture decreases (***Vasi et al., 1994***; ***Grant et al., 2021***).

Fitness in bulk competitions is distorted by higher-order effects depending on reference subpopulation

So far we have focused on relative fitness in pairwise competition experiments, but this is often not practical for large numbers of mutants due to the required strain labeling (e.g., with fluorescent proteins or selection markers). One alternative is to measure a fitness potential (as defined at the beginning of the Results section), such as growth rate or area under the growth curve (AUC) (***Concepción-Acevedo et al., 2015***; ***Ram et al., 2019***; ***Worthan et al., 2023***; ***Schmitz et al., 2024***), from monoculture experiments, under the assumption that true relative fitness is proportional to the difference in this quantity between genotypes. Using our minimal model of population dynamics parameterized by single-gene knockouts in yeast (***Figure 2A***), we find that common fitness potentials perform poorly overall (***Appendix 1—figure 19***; see ***Concepción-Acevedo et al., 2015***; ***Ram et al., 2019***; ***Worthan et al., 2023***; ***Schmitz et al., 2024*** for empirical tests), with some success for the AUC but strongly depending on the choice of time window (***Appendix 1—figure 20***, Appendix 1—section S10).

Another approach to measuring relative fitness for a large number of mutants is to use bulk competition experiments, where many mutant genotypes compete simultaneously in a single culture and each genotype is tracked through high-throughput sequencing (***van Opijnen and Camilli, 2013***; ***Blundell and Levy, 2014***). This raises the question of how well relative fitness of a mutant in bulk competition corresponds to its relative fitness in a pairwise competition with the wild-type, since the growth in bulk might be influenced by the presence of other mutant genotypes, a phenomenon known as a higher-order interaction (***Morin et al., 2022***; ***Manhart and Shakhnovich, 2018***; ***Friedman et al., 2017***).

An important choice in bulk competition experiments is the relative abundance of the library of all mutant genotypes compared to the wild-type. The invasion of a spontaneous mutation into an existing population is best captured by pairwise competitions with low initial relative abundance of the mutant (case I, ***Figure 5A***), and one way to recreate this scenario in a bulk competition is to use a low relative abundance of the mutant library overall (case II, ***Figure 5A***; ***Venkataram et al., 2016***; ***Li et al., 2019***; ***Kinsler et al., 2020***; ***Bakerlee et al., 2021***; ***Schmidlin et al., 2024***). A practical problem with case II is that individual genotypes in the library will have low absolute abundances, which leads to stochasticity in the population dynamics and the sequencing process (***Levy et al., 2015***; ***McGee et al., 2024***; ***Kinsler et al., 2023***). Therefore, it is common to compete the mutant library by itself (case III, ***Figure 5A***; ***Couce et al., 2024***; ***Pierce et al., 2021***; ***Wetmore et al., 2015***; ***Price et al., 2018***; ***Morin et al., 2018***).

A second important choice is whether to quantify fitness of a mutant relative to the whole population ('total relative fitness'; ***Wetmore et al., 2015***; ***Price et al., 2018***; ***Morin et al., 2018***) or relative to another specific genotype, like the wild-type ('pairwise relative fitness'; see ***Figure 5B***; ***Nguyen et al., 2020***; ***Venkataram et al., 2016***; ***Li et al., 2019***; ***Kinsler et al., 2020***; ***Bakerlee et al., 2021***; ***Schmidlin et al., 2024***). In the case of a mutant library growing by itself (case III), it is still possible to estimate a pairwise fitness by using a few known neutral mutants as the reference population (***Couce***

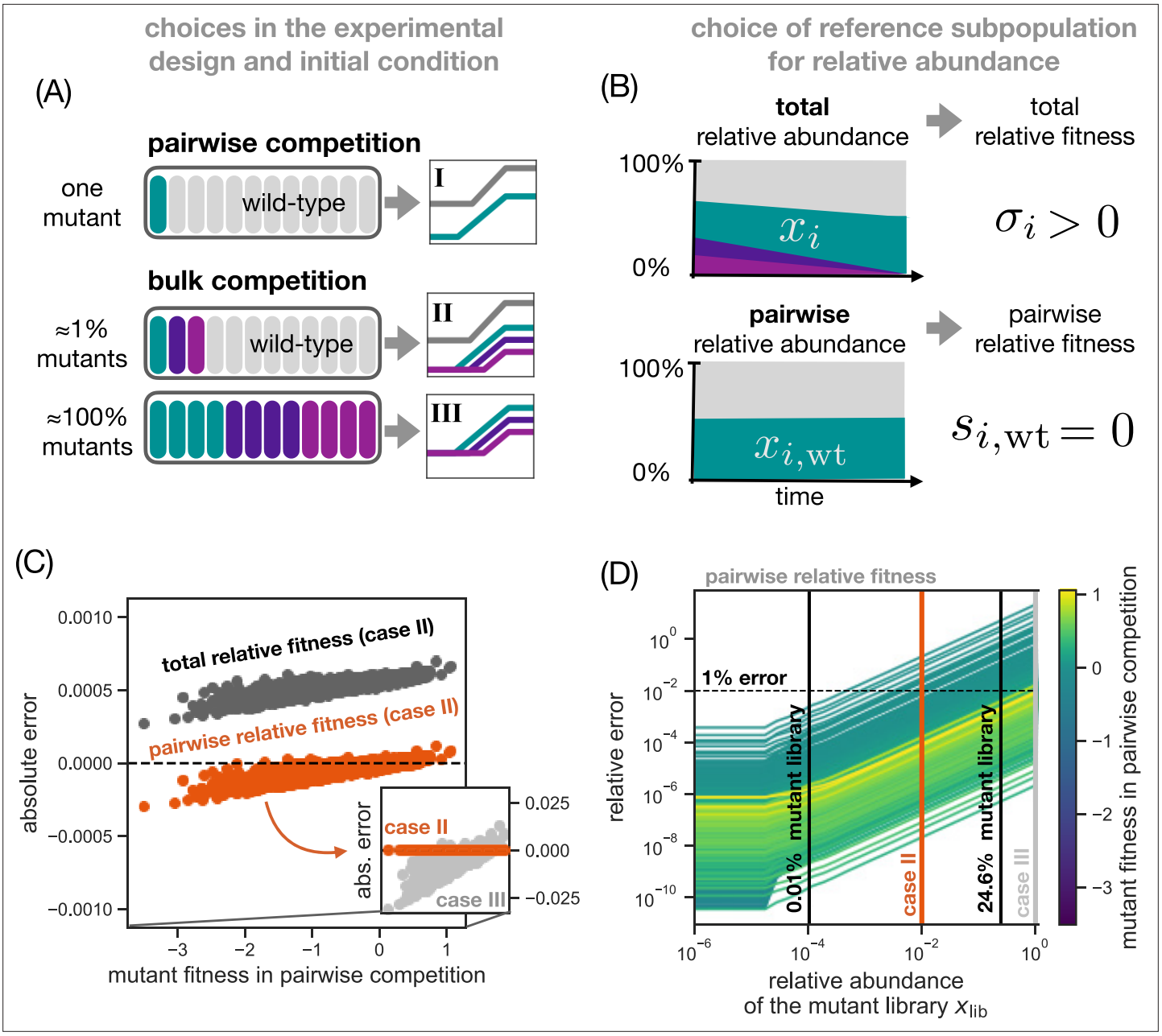


Figure 5. The choice of library abundance and reference group in bulk competition experiments. (**A**) Overview of a pairwise competition experiment with one mutant (top row) and scenarios for bulk competition experiments with many different mutants (middle and bottom rows). The two bulk competition scenarios differ in their initial fraction of the mutant library (colored ovals) in the inoculum (open box). For each scenario, we show a schematic growth cycle (log absolute abundance) in the inset on the right. (**B**) Schematic relative abundance trajectories for a mutant compared to two alternative subpopulations. We distinguish between the total relative abundance x_i with respect to the population as a whole (height of teal band in the top box) and the pairwise relative abundance $x_{i,\mathrm{wt}}$ with respect to the wild-type (height of teal band in the bottom box; ***Equation 20***). We indicate the sign of total relative fitness (***Equation 24***) and pairwise relative fitness (***Equation 25***) on the right. (**C**) The absolute error between bulk and pairwise competition experiments. The total relative fitness (dark gray dots; ***Equation 24***) and the pairwise relative fitness (orange dots; ***Equation 25***) for mutants in the minimal population dynamics model (***Figure 2A***, Methods) parameterized by the yeast knockout data (***Appendix 1—figure 4***) in bulk competition growth cycle with low mutant library abundance (panel A, case II; Methods). The absolute error is defined as the bulk fitness statistic minus the relative fitness in pairwise competition (***Equation S92*** in Appendix 1—section S15). In the inset, the absolute error for pairwise relative fitness (***Equation 25***) for a bulk competition growth cycle with 99.9% library abundance (light gray dots; case III). This still includes a wild-type reference at small percentage to be able to compute a pairwise relative fitness. The *x*-axis and the orange dots in the inset are identical to the main plot. (**D**) The relative error in bulk competition experiments as a function of mutant library abundance in the inoculum. Each line corresponds to a knockout mutant in our data set and represents the relative error between the pairwise relative fitness in bulk competition and the relative fitness in pairwise competition

Figure 5 continued on next page

Figure 5 continued

(***Equation S102*** in Appendix 1—section S16). The black vertical lines show the recommended mutant library abundance for our data set based on ***Equation 11*** ($x_{\text{lib}} \approx 24.6\%$) and based on the more conservative ***Equation S118*** ($x_{\text{lib}} \approx 0.02\%$, Appendix 1—section S16). Note these bounds are calculated a priori and are not the result of a fitting procedure.

et al., 2024; ***Pierce et al., 2021***) and calculating fitness relative to this group (Methods; Appendix 1—section S11 and Appendix 1—section S12).

To test the consequences of these choices, we use the minimal population dynamics model (***Figure 2A***) parameterized by yeast single-gene knockouts and compare the estimates of total and pairwise relative fitness in bulk competitions to fitness measured in pairwise competition, which we use as the ground truth (Methods). ***Figure 5C*** shows that in bulk competitions, the error in total relative fitness (compared to fitness in pairwise competitions) is systematically offset from the error in pairwise relative fitness. For example, a mutant that grows identically to the wild-type (neutral phenotype) does not change in abundance relative to the wild-type, but it may have a net increase in its total relative abundance due to the poor growth of other mutants (compare top and bottom panel in ***Figure 5B***). This offset affects the total relative fitness of all mutants in a uniform way (***Figure 5C***), such that total and pairwise relative fitness completely agree in the ranking of genotypes (***Appendix 1—figure 21***). Note that this offset between total and relative fitness is general and does not depend on our minimal population dynamics model (Appendix 1—section S13).

While the pairwise relative fitness is the preferred method for estimating fitness in bulk competitions, the presence of higher-order interactions means it still deviates from the fitness in pairwise competitions. ***Figure 5C*** shows the absolute error for pairwise fitness has a positive trend with fitness and increases with the relative abundance of the mutant (case III, inset in ***Figure 5C***). For the specific population dynamics in our simulation, we decompose the higher-order interaction into two terms (Appendix 1—section S14 and Appendix 1—section S15): a fitness-independent term and a fitness-dependent term that acts as an amplifier for fitness values (***Appendix 1—figure 22***) and drives the positive error trend in ***Figure 5C***. Intuitively, the population in bulk competition consumes resources more slowly and gives more time for growth rate differences to accrue. The amplification of mutant pairwise fitness in bulk is important because it widens the apparent distribution of fitness effects (leading to, for example, higher estimates for the speed of adaptation) than if fitness was measured in pairwise competition.

In order to control the error from higher-order interactions, we derive an explicit error bound. ***Figure 5D*** shows the relative error from higher-order interactions for each mutant across a range of mutant library abundances. Using the specific population dynamics of our model, we derive the following estimate: Assuming that the mutants in the library only have variation in growth rate, the mutant library abundance should satisfy

$$x_{\text{lib}} < \epsilon \cdot \frac{g_{\text{wt}}}{|g_{\text{lib}} - g_{\text{wt}}|}, \tag{11}$$

where ϵ is the desired threshold on the relative error (***Appendix 1—figure 23***), g_{wt} is the wild-type growth rate, and g_{lib} is the growth rate of the library as a whole (Appendix 1—section S16). In the case of our single-gene knockout library, ***Equation 11*** predicts a maximum library abundance of 24.6% based on the wild-type and library growth rate ($g_{\text{wt}} = 0.406$, $g_{\text{lib}} = 0.389$) for a relative error $\epsilon = 1\%$. ***Figure 5D*** shows that this maximum library abundance keeps the relative error below 1% for high-fitness mutants (bright yellow), because they are dominated by growth rate effects, but fails for mutants close to neutrality because they have a trade-off between growth rate and lag time, which the estimate in ***Equation 11*** neglects. It is possible to derive a more precise bound that keeps the relative error below 1% for all mutant genotypes (in this case $x_{\text{lib}} = 0.01\%$, see vertical line in ***Figure 5D***), but this requires prior knowledge of the trait covariation in the mutant library (Appendix 1—section S16).

Previous benchmark experiments show deviation of bulk fitness from pairwise competition

Our models predict that higher-order effects amplify pairwise fitness measured in bulk compared to the fitness in a pairwise competition experiment. To test this prediction, we reanalyze two published benchmark experiments of bulk fitness measurements. The first data set by ***van Opijnen et al., 2009***

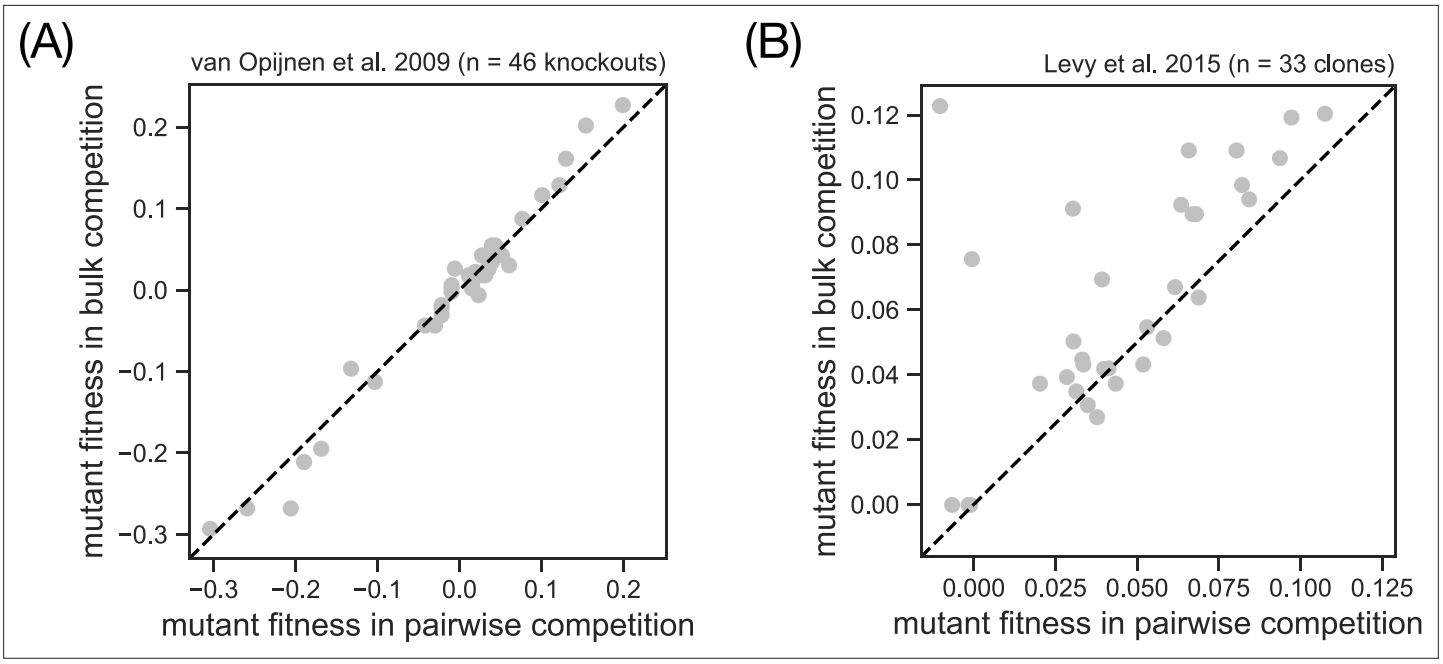


Figure 6. Empirical benchmarks of bulk fitness against pairwise competition experiments. (**A**) Fitness measurements as reported by ***van Opijnen et al., 2009*** for knockouts of *S. pneumoniae*. Pairwise fitness was measured in 1:1 competitions of knockout strains with the wild-type over a single growth cycle using the per-generation statistic $W = 1 + s_{\text{gen}}^{\text{logit}}$ (***Lenski et al., 1991***). Bulk fitness was measured from a single growth cycle using 100% initial abundance of the mutant library and a set of neutral strains as the reference to calculate a per-generation fitness, replacing LFC_{wt} with the library LFC in ***Equation 10***. Since we were unable to obtain the original data, we extracted these fitness data from Figure 3C in the original publication and subtracted 1 to plot as $s_{\text{gen}}^{\text{logit}}$. See ***Appendix 1—figure 24*** for the absolute and relative error of bulk fitness based on these data. (**B**) Fitness measurements as reported by ***Levy et al., 2015*** for evolved genotypes of *S. cerevisiae* after 80 generations of the evolution experiment. Pairwise fitness was measured in 1:1 competitions of knockout strains with a fluorescently labeled wild-type over seven growth cycles using relative fitness per-cycle under the log-encoding $s_{\text{cycle}}^{\log}$, divided by a fixed number of generations inferred from the dilution factor. Bulk fitness was measured from relative abundance data throughout the evolution experiment and using a multi-step algorithm, Bayesian inference, and a set of neutral strains as the reference, leading to a pairwise fitness estimate equivalent to $s_{\text{cycle}}^{\text{logit}}$ (compare SI Equation 50 in ***Levy et al., 2015***). We extracted the fitness data from the table presented in SI Sec. 8.1 of the original publication. See ***Appendix 1—figure 25*** for the absolute and relative error of bulk fitness based on these data.

measured pairwise (1:1) and bulk competitions ($x_{\text{lib}} \approx 99.9\%$) of 46 single-gene knockouts in *Streptococcus pneumoniae* using logit-encoded fitness per-generation and neutral strains as the reference group. ***Figure 6A*** shows that the fitness in bulk deviates from the diagonal, and the absolute error has a positive correlation with the underlying true fitness from pairwise competition (***Appendix 1—figure 24A***; Pearson $r = 0.40, p = 0.006$), similar to the pattern observed in our simulations (compare ***Appendix 1—figure 24A*** with ***Figure 5C***, case III, and ***Appendix 1—figure 24B*** with ***Appendix 1—figure 23C***, case III).

The second data set by ***Levy et al., 2015*** measured pairwise competitions (1:1) and relative abundances for 33 lab-evolved genotypes of *S. cerevisiae* with beneficial fitness. The bulk fitness is inferred under the log encoding and per-cycle, with neutral strains as the reference group. ***Figure 6B*** shows that the fitness of strains in the bulk evolution environment is typically higher than in pairwise competition, but the absolute error has no positive correlation (***Appendix 1—figure 25A***; Pearson $r = -0.26, p = 0.140$) and thus does not support the pattern we see in our simulations (compare ***Appendix 1—figure 25A*** with ***Figure 5C***, case III, and ***Appendix 1—figure 25B*** with ***Appendix 1—figure 23C***, case III).

Discussion

Significance of fitness quantification choices for microbial ecology and evolution

In this work, we have introduced a conceptual framework to derive common statistics of relative fitness from three essential choices:

1. The choice of the state variable for relative abundance (encoding m).
2. The choice of the time scale for the change in relative abundance (Δt)
3. In bulk competition experiments, the choice of subpopulation that acts as the reference for relative abundance of a chosen mutant genotype (***Figure 5B***).

The combination of these choices leads to a range of fitness statistics, including those commonly used in population genetics (***Fisher, 1930***), experimental evolution (***Wiser et al., 2013***; ***Kryazhimskiy et al., 2014***; ***Lenski et al., 1991***), and gene knockout screens (***Pierce et al., 2021***; ***Wetmore et al., 2015***; ***Price et al., 2018***; ***Ascensao et al., 2023***; ***Martinson et al., 2023***; ***Morin et al., 2018***; ***Morin et al., 2022***; ***van Opijnen et al., 2009***).

However, as we compare these statistics in simulated competition experiments, we find that the choice of time scale can lead to different mutant rankings (***Figures 2B and 4A, B***), confound apparent epistasis between mutations (***Figure 3B***), and alter the apparent long-term trend in fitness (***Figure 3F***), while the choice of the reference subpopulation can lead to a systematic shift in inferred fitness values (***Figure 5C***). The quantitative differences between relative fitness statistics affect our ability to make evolutionary predictions. Fixation probabilities and other population genetics quantities depend on ratios of parameters defining the rates of selection, mutation, and genetic drift processes (***Kimura, 1962***; ***Patwa and Wahl, 2008***). These rates must be measured in the same units. For example, in batch cultures with serial transfer, genetic drift is set by the dilution bottleneck and thus operates per-cycle (e.g., $1/N$ per-cycle, where N is the bottleneck population size). Thus, quantifying a mutation's relative fitness s (equivalent to the rate of selection) per-generation and comparing to genetic drift per-cycle (Ns) would incorrectly predict the fixation probability, especially in cases where per-generation and per-cycle fitness rank mutants differently. The choice of statistic may also affect the outcome of a significance test in the context of gene essentiality tests (e.g., using log or logit with the test statistic in ***Wetmore et al., 2015***). Since these measurements often serve as a first screen to narrow down the investigation to the top set of genes (***Pierce et al., 2021***; ***Nguyen et al., 2020***), a difference in mutant ranking means the investigation might miss relevant genes because of the choice of fitness statistic.

Best practices for quantifying mutant fitness in high-throughput experiments

Based on these insights, we recommend the following choices for quantifying relative fitness of a mutant:

1. Use the logit encoding of relative abundance, because under the null model of logistic dynamics this linearizes the trajectory of relative abundance. Only use a different encoding if alternate, non-logistic dynamics are known.
2. For batch growth or any experiment with non-steady state growth, use a fixed extrinsic time scale (e.g., a single growth cycle), rather than an intrinsic time scale (e.g., the number of generations), which introduces additional variation between competitions. Only quantify fitness per-generation for experiments that are known to have steady-state growth (e.g., in a chemostat).
3. In bulk competition experiments, always use the pairwise fitness relative to the wild-type (by including a barcoded wild-type or by grouping neutral mutants into a virtual wild-type) because this more closely matches the relative fitness in pairwise competition.
4. To control the error from higher-order interactions, we recommend minimizing relative abundance of the mutant library as practically feasible. For a given error tolerance, ***Equation 11*** gives an estimate for the maximum library abundance.

Our recommendations agree with previous criticisms of relative fitness per-generation (***Kokko, 2021***; ***Houle et al., 2011***; ***Wagner, 2010***; ***Lenski, 2021***) and total relative fitness (***Matuszewski et al., 2016***; ***Li et al., 2018***) but differ from the standard practice in high-throughput genetic screens (***Wetmore et al., 2015***; ***Price et al., 2018***; ***Morin et al., 2018***) and many evolution experiments (***Durão et al., 2021***; ***Moger-Reischer et al., 2023***), including the LTEE (***Wiser et al., 2013***; ***Lenski***

et al., 1991). The choice of the reference group is a well-recognized issue in high-throughput evolutionary studies, in which one first estimates a total relative fitness and then subtracts a correction based on the fitness of the wild-type (*Kryazhimskiy et al., 2014*; *Kinsler et al., 2020*; *Schmidlin et al., 2024*) or a mean population fitness (*Levy et al., 2015*; *Johnson et al., 2019*; *Ascensao et al., 2023*; *Bakerlee et al., 2021*; *Li et al., 2018*). In contrast, we recommend choosing the reference group at the level of relative abundance (see Methods for a step-by-step demonstration). While researchers must ultimately choose how to quantify fitness based on the specific goals and conditions of their experiment, we believe that a more consistent adherence to the recommendations above would be valuable to the field as a whole so that fitness data from one study can be quantitatively compared to fitness from another.

How general is the disagreement between fitness statistics in pairwise competition?

The discrepancy in mutant ranking for relative fitness per-cycle $s^{\text{logit}}_{\text{cycle}}$ and per-generation $s^{\text{logit}}_{\text{gen}}$ requires positive covariation between the wild-type and mutant LFCs across a set of pairwise competition experiments. This condition is not dependent on any particular mechanism or model, although our minimal model of population dynamics (*Figure 2A*) demonstrates one way this covariation can occur: when mutants have lower yields and are present at sufficiently high abundances to affect wild-type LFCs (*Appendix 1—figure 7*).

Our model focused on the effect of resource competition on fitness discrepancies since that interaction is almost always present between microbial genotypes, providing a baseline expectation. Moreover, resource competition is likely to be the only interaction in high-throughput fitness measurements of mutants with only small genetic differences (e.g., point mutations or gene knockouts) relative to a wild-type. We expect that in cases with additional interactions between mutants and the wild-type, there will be further variation in wild-type LFCs across competitions and thus even more discrepancies between fitness statistics. For example, mutants that stimulate wild-type growth via the secretion of nutrients should create positive LFC covariation across mutants and thus be ranked differently per-cycle and per-generation. Indeed, our reanalysis of LTEE competition data shows that fitness per-cycle $s^{\text{logit}}_{\text{cycle}}$ and per-generation $s^{\text{logit}}_{\text{gen}}$ (equivalent to the statistic $W = 1 + s^{\text{logit}}_{\text{gen}}$ used in the LTEE) disagree on the fitness ranking at almost every time point (*Figure 4A*) and in the first 50,000 generations overall (*Figure 4B*).

How general is the deviation of bulk fitness statistics from pairwise competition experiments?

The offset in total relative fitness (between gray and orange points in *Figure 5C*), equivalent to the mean library fitness (*Equation S88* in Appendix 1—section S13), is independent from the population dynamics (*Figure 5B*, Appendix 1—section S13). In contrast, the error between pairwise fitness in bulk competition and in pairwise competition (orange points in *Figure 5C*) is specific to the population dynamics studied here, although it points to more general mechanisms. Specifically, we expect pairwise fitness in bulk competition to deviate from pairwise competition as soon as the mutant library is able to influence the chemical environment of the competition, for example, when a large fraction of mutants fails to complete respiration of the main carbon source and instead turns to fermentation (*Molenaar et al., 2009*; *Sonenshein, 2007*; *Battjes et al., 2024*), with the release of pathway intermediates like acetate that indirectly lower the pH in the growth medium (*Wolfe, 2005*; *Tran et al., 2024*).

The choice of fitness statistic in the light of other sources of discrepancy

Besides the conceptual choices of fitness quantification discussed in this article, experimental limitations can create discrepancies between replicate fitness measurements of the same mutant (*Worthan et al., 2023*; *Kinsler et al., 2020*; *Borchert et al., 2022*). For example, relative abundance measurements entail sampling uncertainties (when we sample liquid for colony counting or DNA sequencing) (*Blundell and Levy, 2014*; *Matuszewski et al., 2016*; *Limdi and Baym, 2023*), copy number variation (*Wetmore et al., 2015*; *Blundell and Levy, 2014*), as well as PCR jackpots and sequencing read errors (*Levy et al., 2015*; *McGee et al., 2024*; *Kinsler et al., 2023*). Furthermore, there will inevitably

be some variation in initial conditions between replicates and fluctuations during the fitness assay (**Worthan et al., 2023**; **Kinsler et al., 2023**; **Borchert et al., 2022**).

Methods

Inferring growth traits for the single-gene knockout collection in yeast

We used a previously published data set (**Warringer et al., 2003**) for the single-gene knockout collection in *S. cerevisiae* (**Giaever et al., 2002**), where the authors track growth of each genotype for 47 hr in monoculture, using microwell plates with defined growth medium. We downloaded this growth curve data set from the PROPHECY database (**Fernandez-Ricaud et al., 2005**), choosing specifically the data set measured in Synthetic Defined medium. We last accessed the PROPHECY website (http://prophecy.lundberg.gu.se/) on March 30, 2020, but as of November 15, 2025 the website is no longer accessible. We have included a reformatted version of the data with our code repository (https://github.com/justuswfink/24FitnessQuantification, copy archived at **Fink, 2026**). From the raw time series of optical density, the authors subtracted a background correction based on blank wells, applied another correction for nonlinearity at high optical densities, and smoothed the growth curve to remove electrical noise (**Warringer et al., 2003**).

We start with the curves in the published data set (9951 curves) and apply further trimming and smoothing steps (Appendix 1—section S6). From this data, we calculate the time series of instantaneous per-capita growth rate $N^{-1}dN/dt$ (where N is the optical density) and identify time windows where the rate is approximately constant, which we interpret as distinct growth phases (Appendix 1—section S6). We only include curves that have a single phase of constant exponential growth followed by a stationary phase of approximately zero growth (9424 curves).

We quantify the biomass yield, maximum growth rate, and the lag time from each remaining curve as follows. First, we estimate the initial abundance N_{initial} (average optical density over first three time points) and the final abundance N_{final} (average optical density over stationary phase) from the growth curve. Then we calculate the biomass yield as $Y = (N_{\text{final}} - N_{\text{initial}})/R(0)$, where $R(0) = 111$ mM (20 g/l) is the initial concentration of glucose (assuming glucose is the single limiting resource). To estimate the maximum growth rate, we average the instantaneous growth rate over the exponential phase. Finally, we estimate the lag time from the intersection of the log initial abundance ($\log N_0$) with the slope of the maximum growth rate during the exponential growth phase (**Zwietering et al., 1990**). We excluded curves with negative initial OD, curves with negative inferred lag times, and curves with a low quality of fit between the measured time series and a simulated curve based on the inferred trait values ($R^2 < 0.95$; see below for the model). Our final database includes trait estimates for 9195 curves, which represents 92.4% of the original data set (**Warringer et al., 2003**).

Each single-gene deletion strain was measured in two technical replicate growth curves, using a second plate with identical layout in the same plate reader. Some genotypes have only one estimate of the growth traits because the other replicate did not pass our filters (273 genotypes), but for most genotypes, we retain two replicate estimates in our final data set (4163 genotypes); a few genotypes even have three (2 genotypes) or four replicate estimates (54 genotypes) because these genotypes were included multiple times by the original authors (**Warringer et al., 2003**). From these replicates, we finally calculate the average yield, growth rate, and lag time for each genotype. The data set also contained many replicate growth curves of the wild-type strain, 374 of which passed our filters. Since wild-type traits inferred from these replicates had large variation (potentially due to measuring the wild-type across many different plates and days), we define the wild-type trait as the median, not the mean, of these replicates. Although the wild-type measurements included in this data set have large trait variation (orange dots in **Appendix 1—figure 4B,C**), the fact that the variation across knockouts is significantly greater than for the wild-type replicates in terms of growth rate (Levene's test $p = 1.3 \times 10^{-9}$) and lag time (Levene's test $p = 0.025$), and that the replicate measurements of gene knockouts are correlated (**Appendix 1—figure 5**), suggests that these trait measurements do capture true genetic variation. In contrast, the variation in biomass yield across knockouts is not significantly different from the variation across wild-type replicates (Levene's test $p = 0.44$), suggesting that the variation in biomass yield is driven by non-genetic factors like the abundance or batch of resources used for each growth measurement.

Simulating population dynamics in competition experiments

Throughout this work, we model the competition between a set of genotypes during a single batch culture growth cycle using the following model of population dynamics (**Manhart et al., 2018**; **Manhart and Shakhnovich, 2018**):

$$\frac{1}{N_j}\frac{dN_j}{dt} = g_j(t,R), \qquad N_j(0) = x_j(0)N_0, \tag{12a}$$

$$\frac{dR}{dt} = -\sum_j \frac{1}{Y_j}\frac{dN_j}{dt}, \qquad R(0) = R_0, \tag{12b}$$

where for each genotype j, N_j is the absolute abundance, $x_j(0)$ the initial relative abundance, $g_j(t,R)$ the growth rate, and Y_j the biomass yield, where the genotypes include a wild-type as well as one or more mutants. The initial absolute abundance of all genotypes together is N_0, and the concentration of the single limiting resource is R with initial value R_0. Note that **Equation 12b** assumes that cells consume resources only for biomass growth and not for maintenance of existing biomass.

To capture the sigmoidal shape of typical growth curves with a lag phase, exponential growth phase, and saturation phase (e.g., **Appendix 1—figure 4A**), we model the dependence of growth rate on time and resource concentration as

$$g_j(t,R) = g_j\Theta(t-\lambda_j)\Theta(R), \tag{13}$$

where Θ is the step function:

$$\Theta(z) = \begin{cases} 0 & z \leq 0, \\ 1 & z > 0. \end{cases} \tag{14}$$

In this model, a genotype has an initial lag phase of time λ_j where no growth occurs, followed by a phase of constant exponential growth at rate g_j, and ending when the resource concentration R reaches zero. The time to resource depletion, which we also call the saturation time, is defined by the implicit equation $R(t_{\text{sat}}) = 0$. The simple form of the growth response (**Equation 13**) means that the absolute abundance of genotype j at saturation is

$$N_j(t_{\text{sat}}) = N_j(t_0)e^{g_j(t_{\text{sat}}-\lambda_j)\Theta(t_{\text{sat}}-\lambda_j)} \tag{15}$$

and its LFC is

$$\text{LFC}_j = g_j(t_{\text{sat}}-\lambda_j)\Theta(t_{\text{sat}}-\lambda_j). \tag{16}$$

To calculate relative fitness per-cycle (**Equation 9**) and per-generation (**Equation 10**), we numerically determine the saturation time t_{sat} by integrating the biomass and resource dynamics (**Equation 12**) as described in previous work (**Manhart et al., 2018**; **Manhart and Shakhnovich, 2018**). We note that it is also possible to derive an approximate expression for the saturation time t_{sat} which we use for our analytical calculations (Appendix 1—section S7).

Testing epistasis between mutations in the population dynamics model

Consider a wild-type strain with growth rate $g_{\text{wt}} = 1$, lag time $\lambda_{\text{wt}} = 2$, and biomass yield $Y_{\text{wt}} = 1$. We define six basic mutations that represent the six directions of the trait space in our model: a mutation that increases growth rate ($g_{\text{mut}} = 1.2$; symbol $+g$), a mutation that decreases growth rate ($g_{\text{mut}} = 0.8$; symbol $-g$), a mutation that increases lag time ($\lambda_{\text{mut}} = 3$; symbol $+\lambda$), a mutation that decreases lag time ($\lambda_{\text{mut}} = 1$; symbol $-\lambda$), a mutation that increases yield ($Y_{\text{mut}} = 4$; symbol $+Y$), and a mutation that decreases yield ($Y_{\text{mut}} = 0.25$; symbol $-Y$).

We combine these mutations into double mutants as follows: mutations are additive at the level of traits (e.g., the double mutant $(+g,-g)$ is neutral), and mutations in different traits are independent. For a given pair of mutations, epistasis is defined as (**Krug, 2018**)

$$E = s(A,B) - s(A) - s(B), \tag{17}$$

where $s(A)$ is the relative fitness of the single mutant with mutation A, $s(B)$ is the relative fitness of the single mutant with mutation B, and $s(A,B)$ is the relative fitness of the double mutant with both A and B. We estimate the fitness of each mutant by simulating one growth cycle of competition with the wild-type (at initially equal abundance) using an initial biomass of $N_0 = 0.01$ and initial resource concentration $R_0 = 0.5$. These conditions are chosen such that mutations that increase biomass yield reach a maximum density of up to $N(t_{\text{sat}}) = 2$, on the same scale as the optical density measured for the empirical knockouts of *S. cerevisiae* (***Appendix 1—figure 4C***).

Quantifying total and pairwise relative fitness in bulk competition experiments

We define total and pairwise relative fitness, two alternative measures of fitness in bulk competition experiments, as follows. Consider a population with multiple genotypes such that each genotype i has absolute abundance $N_i(t)$ at time t. The *total relative abundance* of the genotype is

$$x_i(t) = \frac{N_i(t)}{\sum_j N_j(t)}. \tag{18}$$

The 'total' here refers to the fact that this is the abundance of genotype i relative to all other genotypes in the population. Similarly, we can think of the definition of relative fitness discussed in the main text (***Equation 4***) as the *total relative fitness* of this genotype under an encoding m:

$$\sigma_i^m = \frac{d}{dt} m(x_i(t)). \tag{19}$$

However, sometimes we want to track the dynamics of a genotype relative to another specific genotype; for example, to follow the fate of a mutant against the wild-type in a bulk competition experiment. For a pair of genotypes $i \neq j$, we thus define the *pairwise relative abundance*

$$x_{ij}(t) = \frac{x_i(t)}{x_i(t) + x_j(t)}, \tag{20}$$

which is the relative abundance of genotype i in a subpopulation of only genotypes i and j. To predict the change in the pairwise relative abundance, we can use the slope

$$s_{ij}^m = \frac{d}{dt} m(x_{ij}(t)), \tag{21}$$

which defines the *pairwise relative fitness* of genotype i with respect to genotype j (see Appendix 1—section S12 for a generalized definition that covers the case $i = j$). In the special case of a population with only two strains, the pairwise relative fitness and total relative fitness are identical ($\sigma_2^m = s_{21}^m$), but they may differ with more than two genotypes (Appendix 1—section S13).

It is also possible to define the total and pairwise relative fitness statistics as finite differences over a time interval, rather than as instantaneous derivatives. For example, we can define them over a growth cycle starting at $t = 0$ and ending at $t = t_{\text{sat}}$:

$$\sigma_{i,\text{cycle}}^m = m(x_i(t_{\text{sat}})) - m(x_i(0)), \tag{22}$$

$$s_{ij,\text{cycle}}^m = m(x_{ij}(t_{\text{sat}})) - m(x_{ij}(0)). \tag{23}$$

For these fitness statistics in the bulk competitions, we use the logit encoding

$$\sigma_{i,\text{cycle}}^{\text{logit}} = \log \frac{x_i(t_{\text{sat}})}{1 - x_i(t_{\text{sat}})} - \log \frac{x_i(0)}{1 - x_i(0)}, \tag{24}$$

$$s_{ij,\text{cycle}}^{\text{logit}} = \log \frac{x_i(t_{\text{sat}})}{x_i(0)} - \log \frac{x_j(t_{\text{sat}})}{x_j(0)}, \tag{25}$$

where we have rewritten $s_{ij,\text{cycle}}^{\text{logit}}$ in the form that it is presented in bulk competition experiments (***Couce et al., 2024***; ***Bakerlee et al., 2021***; ***Schmidlin et al., 2024***). The logit encoding has mathematical advantages for coarse-graining the relative fitness of genotype groups (Appendix 1—section S11), but using the log encoding is another common choice in the literature (***Pierce et al., 2021***; ***Johnson***

et al., 2019; *Kinsler et al., 2020*). However, the relative abundances of the individual mutants in our simulated bulk competition experiments are low enough that these two encodings are approximately equivalent ($\text{logit}\, x \approx \log x$ for $x \ll 1$).

Unlike the comparison between per-cycle and per-generation relative fitness where we focused on rank differences (*Figure 2B*), here we can evaluate absolute differences in fitness estimates because the total and pairwise fitness in bulk fitness are measured in the same units as the relative fitness in pairwise competition. For all mutant genotypes, we calculate the absolute error between these bulk fitness estimates (*Equation 24; Equation 25*) and the relative fitness in pairwise competitions (*Equation 9*), which we take as the ground truth (*Figure 5C*). Note that the pairwise competition could depend on the initial relative abundance of the mutant; we have chosen a very low relative abundance (10^{-6}) that mimics a mutant arising de novo and where this dependence is very weak.

Clearly, minimizing the abundance of the mutant library minimizes the strength of higher-order interactions (also reducing ranking disagreement, *Appendix 1—figure 21B, C*). As low mutant abundances create practical problems for experiments, it is valuable to identify a maximum abundance for the mutant library that keeps the error from bulk fitness estimates below a desired threshold (*Equation 11*). It is convenient to express this threshold in relative rather than absolute terms (compare *Appendix 1—figure 23* to *Figure 5C*).

A guide to calculate pairwise relative fitness under the logit encoding from bulk competition data

Here, $r_i(t)$ represents the best estimate of read numbers for lineage i after correcting for experimental artifacts, like jackpot events in the sequencing (e.g., see discussion in *Levy et al., 2015*).

1. Calculate the total relative abundance x_i of each lineage i by dividing with the total number of reads:

$$x_i(t) = \frac{r_i(t)}{\sum_{i=1}^{n} r_i(t)}, \tag{26}$$

   where the sum is over all n lineages in the experiment.
2. Define a group of lineages $i = 1, \ldots, k$ as the reference (e.g., a group of neutral mutants) and sum their total relative abundance

$$x_{\text{ref}}(t) = \sum_{i=1}^{k} x_i(t). \tag{27}$$

3. Calculate the pairwise relative abundance $x_{i,\text{ref}}$ of each lineage by

$$x_{i,\text{ref}}(t) = \frac{x_i(t)}{x_i(t) + x_{\text{ref}}(t)}. \tag{28}$$

4. Calculate the pairwise fitness per-cycle for each strain i under the logit encoding

$$s_{i,\text{ref}}^{\text{logit}} = \frac{1}{\Delta t}\left[\log \frac{x_{i,\text{ref}}(t_2)}{1 - x_{i,\text{ref}}(t_2)} - \log \frac{x_{i,\text{ref}}(t_1)}{1 - x_{i,\text{ref}}(t_1)}\right], \tag{29}$$

where is the Δt number of growth cycles between time t_1 points and t_2.

Acknowledgements

JWF wishes to thank Luis-Miguel Chevin, Olivier Tenaillon, Henrique Teotónio, and the participants of the 2021 ENS autumn course on Experimental Evolution for valuable discussions early on. The authors are grateful to Jeremy Schreier, Benjamin Raach, and Gatwa Tshinsele-Van Bellingen for a critical reading of the manuscript. JWF and MM were supported by an Ambizione grant from the Swiss National Science Foundation (PZ00P3_180147).

Additional information

Funding

Funder	Grant reference number	Author
Swiss National Science Foundation	PZ00P3_180147	Justus Wilhelm Fink Michael Manhart

The funders had no role in study design, data collection, and interpretation, or the decision to submit the work for publication.

Author contributions

Justus Wilhelm Fink, Michael Manhart, Conceptualization, Investigation, Writing – original draft, Writing – review and editing

Author ORCIDs

Justus Wilhelm Fink https://orcid.org/0000-0002-1138-4009
Michael Manhart https://orcid.org/0000-0003-3791-9056

Peer review material

Version of Record:
Reviewer #1 (Public review): https://doi.org/10.7554/eLife.102635.4.sa1
Reviewer #2 (Public review): https://doi.org/10.7554/eLife.102635.4.sa2
Reviewer #3 (Public review): https://doi.org/10.7554/eLife.102635.4.sa3
Author response https://doi.org/10.7554/eLife.102635.4.sa4

Reviewed preprint v3
Reviewer #1 (Public review): https://doi.org/10.7554/eLife.102635.3.sa3
Reviewer #2 (Public review): https://doi.org/10.7554/eLife.102635.3.sa2
Reviewer #3 (Public review): https://doi.org/10.7554/eLife.102635.3.sa1
Author response: https://doi.org/10.7554/eLife.102635.3.sa0
eLife Assessment https://doi.org/10.7554/eLife.102635.3.sa4

Reviewed preprint v2
Reviewer #1 (Public review): https://doi.org/10.7554/eLife.102635.2.sa3
Reviewer #2 (Public review): https://doi.org/10.7554/eLife.102635.2.sa2
Reviewer #3 (Public review): https://doi.org/10.7554/eLife.102635.2.sa1
Author response: https://doi.org/10.7554/eLife.102635.2.sa0
eLife Assessment https://doi.org/10.7554/eLife.102635.2.sa4

Reviewed preprint v1
Reviewer #1 (Public review): https://doi.org/10.7554/eLife.102635.1.sa3
Reviewer #2 (Public review): https://doi.org/10.7554/eLife.102635.1.sa2
Reviewer #3 (Public review): https://doi.org/10.7554/eLife.102635.1.sa1
Author response: https://doi.org/10.7554/eLife.102635.1.sa0
eLife Assessment https://doi.org/10.7554/eLife.102635.1.sa4

Additional files

Supplementary files

MDAR checklist

Data availability

All data and code are available at https://github.com/justuswfink/24FitnessQuantification (copy archived at ***Fink, 2026***).

References

Alexander HK, Martin G, Martin OY, Bonhoeffer S. 2014. Evolutionary rescue: linking theory for conservation and medicine. *Evolutionary Applications* **7**:1161–1179. DOI: https://doi.org/10.1111/eva.12221, PMID: 25558278

Andersson DI. 2006. The biological cost of mutational antibiotic resistance: any practical conclusions? *Current Opinion in Microbiology* **9**:461–465. DOI: https://doi.org/10.1016/j.mib.2006.07.002, PMID: 16890008

Ariew A, Lewontin RC. 2004. The confusions of fitness. *The British Journal for the Philosophy of Science* **55**:347–363. DOI: https://doi.org/10.1093/bjps/55.2.347

Ascensao JA, Wetmore KM, Good BH, Arkin AP, Hallatschek O. 2023. Quantifying the local adaptive landscape of a nascent bacterial community. *Nature Communications* **14**:248. DOI: https://doi.org/10.1038/s41467-022-35677-5, PMID: 36646697

Baake E, González Casanova A, Probst S, Wakolbinger A. 2019. Modelling and simulating Lenski's long-term evolution experiment. *Theoretical Population Biology* **127**:58–74. DOI: https://doi.org/10.1016/j.tpb.2019.03.006, PMID: 30974115

Bakerlee CW, Phillips AM, Nguyen Ba AN, Desai MM. 2021. Dynamics and variability in the pleiotropic effects of adaptation in laboratory budding yeast populations. *eLife* **10**:e70918. DOI: https://doi.org/10.7554/eLife.70918, PMID: 34596043

Bank C. 2022. Epistasis and adaptation on fitness landscapes. *Annual Review of Ecology, Evolution, and Systematics* **53**:457–479. DOI: https://doi.org/10.1146/annurev-ecolsys-102320-112153

Barrick JE, Blount ZD, Lake DM, Dwenger JH, Chavarria-Palma JE, Izutsu M, Wiser MJ. 2023. Daily transfers, archiving populations, and measuring fitness in the long-term evolution experiment with *Escherichia coli*. *Journal of Visualized Experiments* **198**:e65342. DOI: https://doi.org/10.3791/65342, PMID: 37607082

Battjes J, Grigaitis P, Hoving M, Visser TD, Stampfl K, Miguel GA, van Heerden J, Andersen JK, Bruggeman FJ, Teusink B. 2024. Mitochondrial efficiency determines crabtree effect across yeasts. *bioRxiv*. DOI: https://doi.org/10.1101/2024.11.01.621473

Blundell JR, Levy SF. 2014. Beyond genome sequencing: lineage tracking with barcodes to study the dynamics of evolution, infection, and cancer. *Genomics* **104**:417–430. DOI: https://doi.org/10.1016/j.ygeno.2014.09.005, PMID: 25260907

Boffi NM, Guo Y, Rycroft CH, Amir A. 2024. How microscopic epistasis and clonal interference shape the fitness trajectory in a spin glass model of microbial long-term evolution. *eLife* **12**:RP87895. DOI: https://doi.org/10.7554/eLife.87895, PMID: 38376390

Borchert AJ, Bleem A, Beckham GT. 2022. Experimental and analytical approaches for improving the resolution of randomly barcoded transposon insertion sequencing (RB-TnSeq) Studies. *ACS Synthetic Biology* **11**:2015–2021. DOI: https://doi.org/10.1021/acssynbio.2c00119, PMID: 35657709

Campos M, Govers SK, Irnov I, Dobihal GS, Cornet F, Jacobs-Wagner C. 2018. Genomewide phenotypic analysis of growth, cell morphogenesis, and cell cycle events in *Escherichia coli*. *Molecular Systems Biology* **14**:e7573. DOI: https://doi.org/10.15252/msb.20177573, PMID: 29941428

Charlesworth B. 1993. Book review: Two new books on life-history evolution. *The Quarterly Review of Biology* **68**:262–264. DOI: https://doi.org/10.1086/418074

Charlesworth B. 1994. *Evolution in Age-Structured Populations*. Cambridge University Press. DOI: https://doi.org/10.1017/CBO9780511525711

Chevereau G, Dravecká M, Batur T, Guvenek A, Ayhan DH, Toprak E, Bollenbach T. 2015. Quantifying the determinants of evolutionary dynamics leading to drug resistance. *PLOS Biology* **13**:e1002299. DOI: https://doi.org/10.1371/journal.pbio.1002299, PMID: 26581035

Chevin LM. 2011. On measuring selection in experimental evolution. *Biology Letters* **7**:210–213. DOI: https://doi.org/10.1098/rsbl.2010.0580, PMID: 20810425

Concepción-Acevedo J, Weiss HN, Chaudhry WN, Levin BR. 2015. Malthusian parameters as estimators of the fitness of microbes: a cautionary tale about the low side of high throughput. *PLOS ONE* **10**:e0126915. DOI: https://doi.org/10.1371/journal.pone.0126915, PMID: 26114477

Cooper VS. 2018. Experimental evolution as a high-throughput screen for genetic adaptations. *mSphere* **3**:e00121-18. DOI: https://doi.org/10.1128/mSphere.00121-18, PMID: 29743200

Couce A, Limdi A, Magnan M, Owen SV, Herren CM, Lenski RE, Tenaillon O, Baym M. 2024. Changing fitness effects of mutations through long-term bacterial evolution. *Science* **383**:eadd1417. DOI: https://doi.org/10.1126/science.add1417, PMID: 38271521

Davies NG, Abbott S, Barnard RC, Jarvis CI, Kucharski AJ, Munday JD, Pearson CAB, Russell TW, Tully DC, Washburne AD, Wenseleers T, Gimma A, Waites W, Wong KLM, van Zandvoort K, Silverman JD, Diaz-Ordaz K, Keogh R, Eggo RM, Funk S, et al. 2021. Estimated transmissibility and impact of SARS-CoV-2 lineage B.1.1.7 in England. *Science* **372**:eabg3055. DOI: https://doi.org/10.1126/science.abg3055, PMID: 33658326

de Jong G. 1994. The fitness of fitness concepts and the description of natural selection. *The Quarterly Review of Biology* **69**:3–29. DOI: https://doi.org/10.1086/418431

DelaFuente J, Rodriguez-Beltran J, San Millan A. 2020. Methods to study fitness and compensatory adaptation in plasmid-carrying bacteria. *Horizontal Gene Transfer* **2075**:371–382. DOI: https://doi.org/10.1007/978-1-4939-9877-7_26

Denniston C, Crow JF. 1990. Alternative fitness models with the same allele frequency dynamics. *Genetics* **125**:201–205. DOI: https://doi.org/10.1093/genetics/125.1.201, PMID: 2341032

Desai MM, Fisher DS. 2007. Beneficial mutation selection balance and the effect of linkage on positive selection. *Genetics* **176**:1759–1798. DOI: https://doi.org/10.1534/genetics.106.067678, PMID: 17483432
de Visser J, Krug J. 2014. Empirical fitness landscapes and the predictability of evolution. *Nature Reviews. Genetics* **15**:480–490. DOI: https://doi.org/10.1038/nrg3744, PMID: 24913663
Diaz-Colunga J, Sanchez A, Ogbunugafor CB. 2023. Environmental modulation of global epistasis in a drug resistance fitness landscape. *Nature Communications* **14**:8055. DOI: https://doi.org/10.1038/s41467-023-43806-x, PMID: 38052815
Doebeli M, Ispolatov Y, Simon B. 2017. Towards a mechanistic foundation of evolutionary theory. *eLife* **6**:e23804. DOI: https://doi.org/10.7554/eLife.23804, PMID: 28198700
Dos Santos AR, Di Martino R, Testa SEA, Mitri S. 2022. Classifying interactions in a synthetic bacterial community is hindered by inhibitory growth medium. *mSystems* **7**:e0023922. DOI: https://doi.org/10.1128/msystems.00239-22, PMID: 36197097
Drlica K. 2003. The mutant selection window and antimicrobial resistance. *The Journal of Antimicrobial Chemotherapy* **52**:11–17. DOI: https://doi.org/10.1093/jac/dkg269, PMID: 12805267
Durão P, Amicone M, Perfeito L, Gordo I. 2021. Competition dynamics in long-term propagations of *Schizosaccharomyces pombe* strain communities. *Ecology and Evolution* **11**:15085–15097. DOI: https://doi.org/10.1002/ece3.8191, PMID: 34765162
Dykhuizen DE. 1990. Experimental studies of natural selection in bacteria. *Annual Review of Ecology and Systematics* **21**:373–398. DOI: https://doi.org/10.1146/annurev.es.21.110190.002105
Elena SF, Ekunwe L, Hajela N, Oden SA, Lenski RE. 1998. Distribution of fitness effects caused by random insertion mutations in *Escherichia coli*. *Genetica* **102–103**:349–358 PMID: 9720287.
Fernandez-Ricaud L, Warringer J, Ericson E, Pylvänäinen I, Kemp GJL, Nerman O, Blomberg A. 2005. PROPHECY--a database for high-resolution phenomics. *Nucleic Acids Research* **33**:D369–D373. DOI: https://doi.org/10.1093/nar/gki126, PMID: 15608218
Fink J. 2026. 24FitnessQuantification. swh:1:rev:7d3c4a5798de9e6159de3647253c53891f6d52a0. Software Heritage. https://archive.softwareheritage.org/swh:1:dir:3218272a754bda4ea8720d441ddf02e6a6116af1;origin=https://github.com/justuswfink/24FitnessQuantification;visit=swh:1:snp:b25b446b4098b73464a8ea3046824e7699d5a02c;anchor=swh:1:rev:7d3c4a5798de9e6159de3647253c53891f6d52a0
Fisher RA. 1930. *The Genetical Theory of Natural Selection*. Clarendon Press. DOI: https://doi.org/10.5962/bhl.title.27468
Frey PM, Baer J, Bergada-Pijuan J, Lawless C, Bühler PK, Kouyos RD, Lemon KP, Zinkernagel AS, Brugger SD. 2021. Quantifying variation in bacterial reproductive fitness: a high-throughput method. *mSystems* **6**:e01323-20. DOI: https://doi.org/10.1128/mSystems.01323-20, PMID: 33531411
Friedman J, Higgins LM, Gore J. 2017. Community structure follows simple assembly rules in microbial microcosms. *Nature Ecology & Evolution* **1**:109. DOI: https://doi.org/10.1038/s41559-017-0109, PMID: 28812687
Gabzi T, Pilpel Y, Friedlander T. 2022. Fitness landscape analysis of a tRNA gene reveals that the wild type allele is sub-optimal, yet mutationally robust. *Molecular Biology and Evolution* **39**:msac178. DOI: https://doi.org/10.1093/molbev/msac178, PMID: 35976926
Giaever G, Chu AM, Ni L, Connelly C, Riles L, Véronneau S, Dow S, Lucau-Danila A, Anderson K, André B, Arkin AP, Astromoff A, El Bakkoury M, Bangham R, Benito R, Brachat S, Campanaro S, Curtiss M, Davis K, Deutschbauer A, et al. 2002. Functional profiling of the *Saccharomyces cerevisiae* genome. *Nature* **418**:387–391. DOI: https://doi.org/10.1038/nature00935
Gillespie JH. 2004. *Population Genetics: A Concise*. Guide: JHU Press.
Good BH, Rouzine IM, Balick DJ, Hallatschek O, Desai MM. 2012. Distribution of fixed beneficial mutations and the rate of adaptation in asexual populations. *PNAS* **109**:4950–4955. DOI: https://doi.org/10.1073/pnas.1119910109, PMID: 22371564
Good BH, McDonald MJ, Barrick JE, Lenski RE, Desai MM. 2017. The dynamics of molecular evolution over 60,000 generations. *Nature* **551**:45–50. DOI: https://doi.org/10.1038/nature24287, PMID: 29045390
Gordo I, Perfeito L, Sousa A. 2012. Fitness effects of mutations in bacteria. *Microbial Physiology* **21**:20–35. DOI: https://doi.org/10.1159/000332747
Grant NA, Abdel Magid A, Franklin J, Dufour Y, Lenski RE. 2021. Changes in cell size and shape during 50,000 generations of experimental evolution with *Escherichia coli*. *Journal of Bacteriology* **203**:e00469-20. DOI: https://doi.org/10.1128/JB.00469-20, PMID: 33649147
Grover JP. 1997. *Resource Competition*. Springer. DOI: https://doi.org/10.1007/978-1-4615-6397-6
Guo Y, Vucelja M, Amir A. 2019. Stochastic tunneling across fitness valleys can give rise to a logarithmic long-term fitness trajectory. *Science Advances* **5**:eaav3842. DOI: https://doi.org/10.1126/sciadv.aav3842, PMID: 31392265
Guo Y, Amir A. 2022. The effect of weak clonal interference on average fitness trajectories in the presence of macroscopic epistasis. *Genetics* **220**:iyac028. DOI: https://doi.org/10.1093/genetics/iyac028, PMID: 35171996
Hansen TF. 2017. On the definition and measurement of fitness in finite populations. *Journal of Theoretical Biology* **419**:36–43. DOI: https://doi.org/10.1016/j.jtbi.2016.12.024, PMID: 28041891
Houle D, Pélabon C, Wagner GP, Hansen TF. 2011. Measurement and meaning in biology. *The Quarterly Review of Biology* **86**:3–34. DOI: https://doi.org/10.1086/658408, PMID: 21495498
Johnson MS, Martsul A, Kryazhimskiy S, Desai MM. 2019. Higher-fitness yeast genotypes are less robust to deleterious mutations. *Science* **366**:490–493. DOI: https://doi.org/10.1126/science.aay4199, PMID: 31649199

Johnson MS, Venkataram S, Kryazhimskiy S. 2023. Best practices in designing, sequencing, and identifying random DNA barcodes. *Journal of Molecular Evolution* **91**:263–280. DOI: https://doi.org/10.1007/s00239-022-10083-z, PMID: 36651964

Kimura M. 1962. On the probability of fixation of mutant genes in a population. *Genetics* **47**:713–719. DOI: https://doi.org/10.1093/genetics/47.6.713, PMID: 14456043

Kinsler G, Geiler-Samerotte K, Petrov DA. 2020. Fitness variation across subtle environmental perturbations reveals local modularity and global pleiotropy of adaptation. *eLife* **9**:e61271. DOI: https://doi.org/10.7554/eLife.61271, PMID: 33263280

Kinsler G, Schmidlin K, Newell D, Eder R, Apodaca S, Lam G, Petrov D, Geiler-Samerotte K. 2023. Extreme sensitivity of fitness to environmental conditions: lessons from #1BigBatch. *Journal of Molecular Evolution* **91**:293–310. DOI: https://doi.org/10.1007/s00239-023-10114-3, PMID: 37237236

Koch BJ, McHugh TA, Hayer M, Schwartz E, Blazewicz SJ, Dijkstra P, van Gestel N, Marks JC, Mau RL, Morrissey EM, Pett-Ridge J, Hungate BA. 2018. Estimating taxon-specific population dynamics in diverse microbial communities. *Ecosphere* **9**:e02090. DOI: https://doi.org/10.1002/ecs2.2090

Kokko H. 2021. The stagnation paradox: the ever-improving but (more or less) stationary population fitness. *Proceedings. Biological Sciences* **288**:20212145. DOI: https://doi.org/10.1098/rspb.2021.2145, PMID: 34784767

Kondrashov FA, Kondrashov AS. 2001. Multidimensional epistasis and the disadvantage of sex. *PNAS* **98**:12089–12092. DOI: https://doi.org/10.1073/pnas.211214298

Krug J. 2018. Population genetics and evolution. *arXiv*. https://doi.org/10.48550/arXiv.1803.08474

Kryazhimskiy S, Rice DP, Jerison ER, Desai MM. 2014. Global epistasis makes adaptation predictable despite sequence-level stochasticity. *Science* **344**:1519–1522. DOI: https://doi.org/10.1126/science.1250939, PMID: 24970088

Lenski RE, Rose MR, Simpson SC, Tadler SC. 1991. Long-term experimental evolution in *Escherichia coli*. I. adaptation and divergence during 2,000 generations. *The American Naturalist* **138**:1315–1341. DOI: https://doi.org/10.1086/285289

Lenski RE. 2021. On the Use of Selection Rate versus Relative Fitness. Online Blogpost. https://lenski.mmg.msu.edu/ecoli/srvsrf.html [Accessed June 25, 2021].

Levin BR. 1988. Frequency-dependent selection in bacterial populations. *Philosophical Transactions of the Royal Society of London. Series B, Biological Sciences* **319**:459–472. DOI: https://doi.org/10.1098/rstb.1988.0059, PMID: 2905487

Levy SF, Blundell JR, Venkataram S, Petrov DA, Fisher DS, Sherlock G. 2015. Quantitative evolutionary dynamics using high-resolution lineage tracking. *Nature* **519**:181–186. DOI: https://doi.org/10.1038/nature14279, PMID: 25731169

Li C, Qian W, Maclean CJ, Zhang J. 2016. The fitness landscape of a tRNA gene. *Science* **352**:837–840. DOI: https://doi.org/10.1126/science.aae0568, PMID: 27080104

Li F, Salit ML, Levy SF. 2018. Unbiased fitness estimation of pooled barcode or amplicon sequencing studies. *Cell Systems* **7**:521–525. DOI: https://doi.org/10.1016/j.cels.2018.09.004, PMID: 30391162

Li Y, Petrov DA, Sherlock G. 2019. Single nucleotide mapping of trait space reveals Pareto fronts that constrain adaptation. *Nature Ecology & Evolution* **3**:1539–1551. DOI: https://doi.org/10.1038/s41559-019-0993-0

Limdi A, Baym M. 2023. Resolving deleterious and near-neutral effects requires different pooled fitness assay designs. *Journal of Molecular Evolution* **91**:325–333. DOI: https://doi.org/10.1007/s00239-023-10110-7, PMID: 37160452

Mallet J. 2012. The struggle for existence. How the notion of carrying capacity obscures the links between demography Darwinian Evolution and Speciation. *Evolutionary Ecology Research* **14**:627–665.

Manhart M, Adkar BV, Shakhnovich EI. 2018. Trade-offs between microbial growth phases lead to frequency-dependent and non-transitive selection. *Proceedings. Biological Sciences* **285**:20172459. DOI: https://doi.org/10.1098/rspb.2017.2459, PMID: 29445020

Manhart M, Shakhnovich EI. 2018. Growth tradeoffs produce complex microbial communities on a single limiting resource. *Nature Communications* **9**:3214. DOI: https://doi.org/10.1038/s41467-018-05703-6, PMID: 30097583

Manrubia S, Cuesta JA, Aguirre J, Ahnert SE, Altenberg L, Cano AV, Catalán P, Diaz-Uriarte R, Elena SF, García-Martín JA, Hogeweg P, Khatri BS, Krug J, Louis AA, Martin NS, Payne JL, Tarnowski MJ, Weiß M. 2021. From genotypes to organisms: State-of-the-art and perspectives of a cornerstone in evolutionary dynamics. *Physics of Life Reviews* **38**:55–106. DOI: https://doi.org/10.1016/j.plrev.2021.03.004, PMID: 34088608

Martin-Platero AM, Cleary B, Kauffman K, Preheim SP, McGillicuddy DJ, Alm EJ, Polz MF. 2018. High resolution time series reveals cohesive but short-lived communities in coastal plankton. *Nature Communications* **9**:266. DOI: https://doi.org/10.1038/s41467-017-02571-4, PMID: 29348571

Martinson JNV, Chacón JM, Smith BA, Villarreal AR, Hunter RC, Harcombe WR. 2023. Mutualism reduces the severity of gene disruptions in predictable ways across microbial communities. *The ISME Journal* **17**:2270–2278. DOI: https://doi.org/10.1038/s41396-023-01534-6, PMID: 37865718

Matuszewski S, Hildebrandt ME, Ghenu AH, Jensen JD, Bank C. 2016. A statistical guide to the design of deep mutational scanning experiments. *Genetics* **204**:77–87. DOI: https://doi.org/10.1534/genetics.116.190462, PMID: 27412710

McDonald MJ, Cooper TF, Beaumont HJE, Rainey PB. 2011. The distribution of fitness effects of new beneficial mutations in Pseudomonas fluorescens. *Biology Letters* **7**:98–100. DOI: https://doi.org/10.1098/rsbl.2010.0547, PMID: 20659918

McGee RS, Kinsler G, Petrov D, Tikhonov M. 2024. Improving the accuracy of bulk fitness assays by correcting barcode processing biases. *Molecular Biology and Evolution* **41**:msae152. DOI: https://doi.org/10.1093/molbev/msae152, PMID: 39041198

Meijers M, Ruchnewitz D, Eberhardt J, Łuksza M, Lässig M. 2023. Population immunity predicts evolutionary trajectories of SARS-CoV-2. *Cell* **186**:5151–5164. DOI: https://doi.org/10.1016/j.cell.2023.09.022, PMID: 37875109

Milkman R. 1978. Selection differentials and selection coefficients. *Genetics* **88**:391–403. DOI: https://doi.org/10.1093/genetics/88.2.391, PMID: 17248802

Mills SK, Beatty JH. 1979. The propensity interpretation of fitness. *Philosophy of Science* **46**:263–286. DOI: https://doi.org/10.1086/288865

Moger-Reischer RZ, Glass JI, Wise KS, Sun L, Bittencourt DMC, Lehmkuhl BK, Schoolmaster DR Jr, Lynch M, Lennon JT. 2023. Evolution of a minimal cell. *Nature* **620**:122–127. DOI: https://doi.org/10.1038/s41586-023-06288-x

Molenaar D, van Berlo R, de Ridder D, Teusink B. 2009. Shifts in growth strategies reflect tradeoffs in cellular economics. *Molecular Systems Biology* **5**:MSB200982. DOI: https://doi.org/10.1038/msb.2009.82

Morin M, Pierce EC, Dutton RJ. 2018. Changes in the genetic requirements for microbial interactions with increasing community complexity. *eLife* **7**:e37072. DOI: https://doi.org/10.7554/eLife.37072, PMID: 30211673

Morin MA, Morrison AJ, Harms MJ, Dutton RJ. 2022. Higher-order interactions shape microbial interactions as microbial community complexity increases. *Scientific Reports* **12**:22640. DOI: https://doi.org/10.1038/s41598-022-25303-1, PMID: 36587027

Muratore D, Boysen AK, Harke MJ, Becker KW, Casey JR, Coesel SN, Mende DR, Wilson ST, Aylward FO, Eppley JM, Vislova A, Peng S, Rodriguez-Gonzalez RA, Beckett SJ, Virginia Armbrust E, DeLong EF, Karl DM, White AE, Zehr JP, Van Mooy BAS, et al. 2022. Complex marine microbial communities partition metabolism of scarce resources over the diel cycle. *Nature Ecology & Evolution* **6**:218–229. DOI: https://doi.org/10.1038/s41559-021-01606-w

Nguyen BD, Cuenca V. M, Hartl J, Gül E, Bauer R, Meile S, Rüthi J, Margot C, Heeb L, Besser F, Escriva PP, Fetz C, Furter M, Laganenka L, Keller P, Fuchs L, Christen M, Porwollik S, McClelland M, Vorholt JA, et al. 2020. Import of aspartate and malate by DcuABC Drives H2/Fumarate respiration to promote initial salmonella gut-lumen colonization in mice. *Cell Host & Microbe* **27**:922–936. DOI: https://doi.org/10.1016/j.chom.2020.04.013

Nguyen Ba AN, Cvijović I, Rojas Echenique JI, Lawrence KR, Rego-Costa A, Liu X, Levy SF, Desai MM. 2019. High-resolution lineage tracking reveals travelling wave of adaptation in laboratory yeast. *Nature* **575**:494–499. DOI: https://doi.org/10.1038/s41586-019-1749-3, PMID: 31723263

Paquin CE, Adams J. 1983. Relative fitness can decrease in evolving asexual populations of *S. cerevisiae*. *Nature* **306**:368–370. DOI: https://doi.org/10.1038/306368a0, PMID: 16752492

Park SC, Krug J. 2008. Evolution in random fitness landscapes: the infinite sites model. *Journal of Statistical Mechanics* **2008**:04014. DOI: https://doi.org/10.1088/1742-5468/2008/04/P04014

Patwa Z, Wahl LM. 2008. The fixation probability of beneficial mutations. *Journal of the Royal Society, Interface* **5**:1279–1289. DOI: https://doi.org/10.1098/rsif.2008.0248, PMID: 18664425

Pearl Mizrahi S, Goyal A, Gore J. 2023. Community interactions drive the evolution of antibiotic tolerance in bacteria. *PNAS* **120**:e2209043119. DOI: https://doi.org/10.1073/pnas.2209043119

Peterson A, Baskett C, Ratcliff WC, Burnetti A. 2024. Transforming yeast into a facultative photoheterotroph via expression of vacuolar rhodopsin. *Current Biology* **34**:648–654.. DOI: https://doi.org/10.1016/j.cub.2023.12.044, PMID: 38218181

Piccardi P, Vessman B, Mitri S. 2019. Toxicity drives facilitation between 4 bacterial species. *PNAS* **116**:15979–15984. DOI: https://doi.org/10.1073/pnas.1906172116, PMID: 31270235

Pierce EC, Morin M, Little JC, Liu RB, Tannous J, Keller NP, Pogliano K, Wolfe BE, Sanchez LM, Dutton RJ. 2021. Bacterial-fungal interactions revealed by genome-wide analysis of bacterial mutant fitness. *Nature Microbiology* **6**:87–102. DOI: https://doi.org/10.1038/s41564-020-00800-z, PMID: 33139882

Pinheiro F, Warsi O, Andersson DI, Lässig M. 2021. Metabolic fitness landscapes predict the evolution of antibiotic resistance. *Nature Ecology & Evolution* **5**:677–687. DOI: https://doi.org/10.1038/s41559-021-01397-0, PMID: 33664488

Price MN, Wetmore KM, Waters RJ, Callaghan M, Ray J, Liu H, Kuehl JV, Melnyk RA, Lamson JS, Suh Y, Carlson HK, Esquivel Z, Sadeeshkumar H, Chakraborty R, Zane GM, Rubin BE, Wall JD, Visel A, Bristow J, Blow MJ, et al. 2018. Mutant phenotypes for thousands of bacterial genes of unknown function. *Nature* **557**:503–509. DOI: https://doi.org/10.1038/s41586-018-0124-0, PMID: 29769716

Ram Y, Dellus-Gur E, Bibi M, Karkare K, Obolski U, Feldman MW, Cooper TF, Berman J, Hadany L. 2019. Predicting microbial growth in a mixed culture from growth curve data. *PNAS* **116**:14698–14707. DOI: https://doi.org/10.1073/pnas.1902217116, PMID: 31253703

San Millan A, MacLean RC. 2017. Fitness costs of plasmids: a limit to plasmid transmission. *Microbiology Spectrum* **5**:5. DOI: https://doi.org/10.1128/microbiolspec.mtbp-0016-2017, PMID: 28944751

Schmidlin K, Apodaca S, Newell D, Sastokas A, Kinsler G, Geiler-Samerotte K. 2024. Distinguishing mutants that resist drugs via different mechanisms by examining fitness tradeoffs. *eLife* **13**:RP94144. DOI: https://doi.org/10.7554/eLife.94144, PMID: 39255191

Schmitz DA, Wechsler T, Mignot I, Kümmerli R. 2024. Predicting bacterial interaction outcomes from monoculture growth and supernatant assays. *ISME Communications* **4**:ycae045. DOI: https://doi.org/10.1093/ismeco/ycae045, PMID: 39081364

Schreier JE, Smith CB, Ioerger TR, Moran MA. 2023. A mutant fitness assay identifies bacterial interactions in a model ocean hot spot. *PNAS* **120**:e2217200120. DOI: https://doi.org/10.1073/pnas.2217200120, PMID: 36920927

Sibani P, Brandt M, Alstrøm P. 1998. Evolution and extinction dynamics in rugged fitness landscapes. *International Journal of Modern Physics B* **12**:361–391. DOI: https://doi.org/10.1142/S0217979298000259

Smith DJ, Doulcier G, Bourrat P, Takacs P, Masel J. 2024. Why there are so many definitions of fitness in models. EcoEvoRxiv. DOI: https://doi.org/10.32942/X2V61T

Sohail MS, Louie RHY, Hong Z, Barton JP, McKay MR. 2022. Inferring epistasis from genetic time-series data. *Molecular Biology and Evolution* **39**:msac199. DOI: https://doi.org/10.1093/molbev/msac199, PMID: 36130322

Sonenshein AL. 2007. Control of key metabolic intersections in *Bacillus subtilis*. *Nature Reviews. Microbiology* **5**:917–927. DOI: https://doi.org/10.1038/nrmicro1772, PMID: 17982469

Spiers AJ, Kahn SG, Bohannon J, Travisano M, Rainey PB. 2002. Adaptive divergence in experimental populations of Pseudomonas fluorescens. *I. Genetic and Phenotypic Bases of Wrinkly Spreader Fitness: Genetics* **161**:33–46. DOI: https://doi.org/10.1093/genetics/161.1.33, PMID: 12019221

Sprouffske K, Wagner A. 2016. Growthcurver: an R package for obtaining interpretable metrics from microbial growth curves. *BMC Bioinformatics* **17**:172. DOI: https://doi.org/10.1186/s12859-016-1016-7, PMID: 27094401

Sprouffske K, Aguilar-Rodríguez J, Sniegowski P, Wagner A. 2018. High mutation rates limit evolutionary adaptation in *Escherichia coli*. *PLOS Genetics* **14**:e1007324. DOI: https://doi.org/10.1371/journal.pgen.1007324, PMID: 29702649

Stearns SC. 1989. Trade-offs in life-history evolution. *Functional Ecology* **3**:259. DOI: https://doi.org/10.2307/2389364

Swain PS, Stevenson K, Leary A, Montano-Gutierrez LF, Clark IBN, Vogel J, Pilizota T. 2016. Inferring time derivatives including cell growth rates using Gaussian processes. *Nature Communications* **7**:13766. DOI: https://doi.org/10.1038/ncomms13766, PMID: 27941811

Takacs P, Bourrat P. 2022. The arithmetic mean of what? A cautionary tale about the use of the geometric mean as a measure of fitness. *Biology & Philosophy* **37**:12. DOI: https://doi.org/10.1007/s10539-022-09843-4

Tange O. 2018. GNU parallel. V1. Zenodo. https://doi.org/10.5281/zenodo.1146014

Thaiss CA, Zeevi D, Levy M, Zilberman-Schapira G, Suez J, Tengeler AC, Abramson L, Katz MN, Korem T, Zmora N, Kuperman Y, Biton I, Gilad S, Harmelin A, Shapiro H, Halpern Z, Segal E, Elinav E. 2014. Transkingdom control of microbiota diurnal oscillations promotes metabolic homeostasis. *Cell* **159**:514–529. DOI: https://doi.org/10.1016/j.cell.2014.09.048, PMID: 25417104

Tran P, Lander SM, Prindle A. 2024. Active pH regulation facilitates *Bacillus subtilis* biofilm development in a minimally buffered environment. *mBio* **15**:e0338723. DOI: https://doi.org/10.1128/mbio.03387-23, PMID: 38349175

van Opijnen T, Bodi KL, Camilli A. 2009. Tn-seq: high-throughput parallel sequencing for fitness and genetic interaction studies in microorganisms. *Nature Methods* **6**:767–772. DOI: https://doi.org/10.1038/nmeth.1377, PMID: 19767758

van Opijnen T, Camilli A. 2013. Transposon insertion sequencing: a new tool for systems-level analysis of microorganisms. *Nature Reviews. Microbiology* **11**:435–442. DOI: https://doi.org/10.1038/nrmicro3033, PMID: 23712350

Vasi F, Travisano M, Lenski RE. 1994. Long-term experimental evolution in *Escherichia coli*. II. changes in life-history traits during adaptation to a seasonal environment. *The American Naturalist* **144**:432–456. DOI: https://doi.org/10.1086/285685

Venkataram S, Dunn B, Li Y, Agarwala A, Chang J, Ebel ER, Geiler-Samerotte K, Hérissant L, Blundell JR, Levy SF, Fisher DS, Sherlock G, Petrov DA. 2016. Development of a comprehensive genotype-to-fitness map of adaptation-driving mutations in yeast. *Cell* **166**:1585–1596. DOI: https://doi.org/10.1016/j.cell.2016.08.002, PMID: 27594428

Virtanen P, Gommers R, Oliphant TE, Haberland M, Reddy T, Cournapeau D, Burovski E, Peterson P, Weckesser W, Bright J, van der Walt SJ, Brett M, Wilson J, Millman KJ, Mayorov N, Nelson ARJ, Jones E, Kern R, Larson E, Carey CJ, et al. 2020. SciPy 1.0: fundamental algorithms for scientific computing in Python. *Nature Methods* **17**:261–272. DOI: https://doi.org/10.1038/s41592-019-0686-2, PMID: 32015543

Wagner GP. 2010. The measurement theory of fitness. *Evolution; International Journal of Organic Evolution* **64**:1358–1376. DOI: https://doi.org/10.1111/j.1558-5646.2009.00909.x, PMID: 20002165

Wang C, Yang Y, Wang Y, Wang D, Xu X, Wang Y, Li L, Yang C, Zhang T. 2022. Absolute quantification and genome-centric analyses elucidate the dynamics of microbial populations in anaerobic digesters. *Water Research* **224**:119049. DOI: https://doi.org/10.1016/j.watres.2022.119049

Warringer J, Ericson E, Fernandez L, Nerman O, Blomberg A. 2003. High-resolution yeast phenomics resolves different physiological features in the saline response. *PNAS* **100**:15724–15729. DOI: https://doi.org/10.1073/pnas.2435976100, PMID: 14676322

Wetmore KM, Price MN, Waters RJ, Lamson JS, He J, Hoover CA, Blow MJ, Bristow J, Butland G, Arkin AP, Deutschbauer A. 2015. Rapid quantification of mutant fitness in diverse bacteria by sequencing randomly bar-coded transposons. *mBio* **6**:e00306-15. DOI: https://doi.org/10.1128/mBio.00306-15, PMID: 25968644

Wiser MJ, Ribeck N, Lenski RE. 2013. Long-term dynamics of adaptation in asexual populations. *Science* **342**:1364–1367. DOI: https://doi.org/10.1126/science.1243357, PMID: 24231808

Wolfe AJ. 2005. The acetate switch. *Microbiology and Molecular Biology Reviews* **69**:12–50. DOI: https://doi.org/10.1128/MMBR.69.1.12-50.2005, PMID: 15755952

Worthan SB, McCarthy RDP, Behringer MG. 2023. Case Studies in the assessment of microbial fitness: seemingly subtle changes can have major effects on phenotypic outcomes. *Journal of Molecular Evolution* **91**:311–324. DOI: https://doi.org/10.1007/s00239-022-10087-9, PMID: 36752825

Zeyl C, DeVisser JAGM. 2001. Estimates of the rate and distribution of fitness effects of spontaneous mutation in *Saccharomyces cerevisiae*. *Genetics* **157**:53–61. DOI: https://doi.org/10.1093/genetics/157.1.53, PMID: 11139491

Zwietering MH, Jongenburger I, Rombouts FM, van 't Riet K. 1990. Modeling of the bacterial growth curve. *Applied and Environmental Microbiology* **56**:1875–1881. DOI: https://doi.org/10.1128/aem.56.6.1875-1881.1990, PMID: 16348228

Appendix 1

S1. Different types of fitness under example models of population dynamics

In this section, we explicitly calculate relative fitness of a mutant under a few example models of population dynamics, using the different encodings of relative abundance as described in the main text (main text ***Figure 1A***). Consider a competition coculture between a wild-type genotype with absolute abundance $N_{\mathrm{wt}}(t)$ and a mutant genotype with absolute abundance $N_{\mathrm{mut}}(t)$. We can describe their dynamics according to the ordinary differential equations (ODEs)

$$\begin{aligned}\frac{1}{N_{\mathrm{wt}}}\frac{dN_{\mathrm{wt}}}{dt} &= g_{\mathrm{wt}}(t, N_{\mathrm{wt}}, N_{\mathrm{mut}}),\\ \frac{1}{N_{\mathrm{mut}}}\frac{dN_{\mathrm{mut}}}{dt} &= g_{\mathrm{mut}}(t, N_{\mathrm{wt}}, N_{\mathrm{mut}}).\end{aligned} \tag{S1}$$

Note that the per-capita growth rates g_{wt} and g_{mut} of each genotype can depend on both genotypes to reflect competition or other interactions. The relative abundance of the mutant genotype at time t is

$$x(t) = \frac{N_{\mathrm{mut}}(t)}{N_{\mathrm{mut}}(t) + N_{\mathrm{wt}}(t)}. \tag{S2}$$

The dynamics of the mutant relative abundance are therefore described by

$$\frac{dx}{dt} = \left[g_{\mathrm{mut}}(t, N_{\mathrm{wt}}, N_{\mathrm{mut}}) - g_{\mathrm{wt}}(t, N_{\mathrm{wt}}, N_{\mathrm{mut}})\right] \times x(1-x). \tag{S3}$$

As defined in the main text (***Equation 4***), the relative fitness of a mutant is $s^m = dm/dt$ for an encoding $m(x)$ of the relative abundance x. Under the trivial linear encoding ($m(x) = x$), the relative fitness is therefore just the right-hand side of the relative abundance ODE (***Equation S3***):

$$\begin{aligned}s^{\mathrm{linear}} &= \frac{dx}{dt}\\ &= \left[g_{\mathrm{mut}}(t, N_{\mathrm{wt}}, N_{\mathrm{mut}}) - g_{\mathrm{wt}}(t, N_{\mathrm{wt}}, N_{\mathrm{mut}})\right] \times\\ &\quad x(1-x).\end{aligned} \tag{S4}$$

For the log encoding $m(x) = \log x$, we use the identity $d\log x/dt = x^{-1}dx/dt$ to obtain the log-encoded relative fitness:

$$\begin{aligned}s^{\log} &= \frac{d\log x}{dt}\\ &= \left[g_{\mathrm{mut}}(t, N_{\mathrm{wt}}, N_{\mathrm{mut}}) - g_{\mathrm{wt}}(t, N_{\mathrm{wt}}, N_{\mathrm{mut}})\right] \times\\ &\quad (1-x).\end{aligned} \tag{S5}$$

Finally, for the logit encoding $m(x) = \mathrm{logit}\, x = \log(x/(1-x))$, we use the identity $d\,\mathrm{logit}\, x/dt = x^{-1}(1-x)^{-1}dx/dt$ to obtain the logit-encoded relative fitness:

$$\begin{aligned}s^{\mathrm{logit}} &= \frac{d}{dt}\mathrm{logit}\, x\\ &= g_{\mathrm{mut}}(t, N_{\mathrm{wt}}, N_{\mathrm{mut}}) - g_{\mathrm{wt}}(t, N_{\mathrm{wt}}, N_{\mathrm{mut}}).\end{aligned} \tag{S6}$$

By comparing relative fitness values under the linear encoding (***Equation S4***) and under the logit encoding (***Equation S6***), we see how the logit encoding has removed the explicit dependence on the mutant relative abundance (factors of x and $1-x$), although there can be implicit dependence on the mutant relative abundance within the per-capita growth rates of each strain (g_{wt} and g_{mut}) due to density-dependent growth rates.

If the per-capita growth rates g_{wt} and g_{mut} (***Equation S1***) are constants, then these constant growth rates also act as fitness potentials since they each depend only on a single genotype, but

their difference determines relative fitness (under the logit encoding, ***Equation S6***) between the genotypes. The growth rate is not a fitness potential under more complex dynamics, however. For example, consider a competition model with explicit density dependence:

$$\begin{aligned}\frac{1}{N_{\mathrm{wt}}}\frac{dN_{\mathrm{wt}}}{dt} &= r_{\mathrm{wt}}\left(1-\frac{N_{\mathrm{wt}}}{K_{\mathrm{wt}}}-\frac{N_{\mathrm{mut}}}{K_{\mathrm{mut}}}\right),\\ \frac{1}{N_{\mathrm{mut}}}\frac{dN_{\mathrm{mut}}}{dt} &= r_{\mathrm{mut}}\left(1-\frac{N_{\mathrm{wt}}}{K_{\mathrm{wt}}}-\frac{N_{\mathrm{mut}}}{K_{\mathrm{mut}}}\right),\end{aligned} \tag{S7}$$

where the growth rates decrease as the genotype abundances reach their carrying capacities K_{wt} and K_{mut}, and the maximum growth rates at low abundances are r_{wt} and r_{mut}. In this case, the relative fitness under the logit encoding is (from ***Equation S6***)

$$s^{\mathrm{logit}} = (r_{\mathrm{mut}} - r_{\mathrm{wt}})\left(1-\frac{N_{\mathrm{wt}}}{K_{\mathrm{wt}}}-\frac{N_{\mathrm{mut}}}{K_{\mathrm{mut}}}\right). \tag{S8}$$

In this case, there is no fitness potential because it is not possible to separate ***Equation S8*** into a difference between terms that only depend on each genotype separately.

S2. Definition of absolute fitness for a genotype

Here we give an explicit definition of a genotype's absolute fitness, analogous to the definition of relative fitness in the main text (***Equations 1–4***). Conceptually, absolute fitness is any number that is sufficient to predict a genotype's absolute abundance N over a short time window. Let an encoding $m(N)$ be any smooth, strictly increasing function of the absolute abundance N. We can then predict the absolute abundance over a time window Δt using a linear expansion of the encoded abundance (analogous to main text ***Equation 3*** for relative fitness):

$$m(N(t+\Delta t)) \approx m(N(t)) + a^m \Delta t, \tag{S9}$$

where

$$a^m = \frac{dm}{dt} \tag{S10}$$

is defined as the absolute fitness of the genotype under the encoding m (analogous to main text ***Equation 4*** for relative fitness; see also main text ***Figure 1B***). For example, the absolute fitness of a genotype under the log encoding $m(N) = \log N$ is the per-capita growth rate:

$$a^{\log} = \frac{1}{N}\frac{dN}{dt}. \tag{S11}$$

In general, the ideal encoding of absolute abundance is the inverse function of the absolute abundance trajectory $N(t)$ (up to a shift and rescaling), so that the first-order expansion in ***Equation S9*** is exact and the absolute fitness a^m is sufficient to determine changes in absolute abundance up to any future time. The log encoding $m(N) = \log N$ is therefore ideal when absolute abundance grows or decays exponentially at a constant rate, while the logit encoding $m(N) = \mathrm{logit}\, N$ is ideal for a population that grows with logistic density dependence (***Equation S7*** in case of a single genotype).

Absolute fitness and relative fitness are related since the relative abundance of a genotype is determined by normalizing its absolute abundance by the absolute abundance of all genotypes in the population. Specifically, the relative fitness of a genotype is determined by the absolute fitnesses for all genotypes in the population. For example, in the case of two genotypes, the relative fitness under the logit encoding (***Equation S6***) is the difference between the genotypes' absolute fitness under the log encoding (***Equation S11***). In the case of constant per-capita growth rates, these log-encoded absolute fitnesses also act as fitness potentials.

S3. The role of logistic population dynamics in logit-encoded relative fitness

Here we show how the logit encoding of relative abundance is related to the logistic model of population dynamics. For a relative abundance x, logistic dynamics are

$$\frac{dx}{dt} = rx(1-x), \tag{S12}$$

where r is the exponential rate at which relative abundance increases from low values. This form emerges from the general dynamics of relative abundance (***Equation S3***) when the difference in per-capita growth rates g_{mut} and g_{wt} is constant. One can also interpret the logistic model as a lowest-order approximation for more complex dynamics. That is, consider a general equation for relative abundance:

$$\frac{dx}{dt} = f(x), \tag{S13}$$

for an arbitrary function $f(x)$. Since this function must obey the boundary conditions $f(0) = 0$ and $f(1) = 0$ (the relative abundance must stop changing when it either goes extinct or fixes), a polynomial expansion of $f(x)$ must have roots at these values:

$$f(x) = rx(1-x)(1+\mathcal{O}(x)). \tag{S14}$$

Thus, the logistic model in ***Equation S12*** is a lowest-order approximation even when the true dynamics are more complex.

The logistic differential equation in ***Equation S12*** has the solution

$$x(t) = \frac{x(0)e^{rt}}{x(0)e^{rt} + 1 - x(0)}. \tag{S15}$$

The logit encoding of the logistic relative abundance has linear dependence on time:

$$\begin{aligned} m(x) &= \operatorname{logit} x \\ &= rt + \log\left(\frac{1-x(0)}{x(0)}\right). \end{aligned} \tag{S16}$$

This is another way to see why the relative fitness under the logit encoding (the time derivative of ***Equation S16***) is constant under logistic dynamics. Mathematically, this occurs because the logit function is the inverse of the logistic dynamics (***Equation S15***), up to a shift and rescaling. Thus, if the relative abundance dynamics are different from logistic (***Equation S12***), the logit encoding no longer exactly linearizes the trajectory of relative abundance and thus is no longer the optimal encoding for relative fitness (see ***Appendix 1—figure 2*** and the mathematical notes by ***Mallet, 2012*** for more examples).

More generally, the ideal encoding for a given relative abundance dynamics $x(t)$ is any linear function of the inverse $m(x(t)) = at(x) + b$ of those dynamics. Note that the ambiguous scale includes log and logit encodings with a different base of the logarithm (discussed by ***Chevin, 2011***). The inversion of $x(t)$ is equivalent to removing frequency (relative abundance) dependence from the relative fitness statistic s^m(***Levin, 1988***).

S4. Relative fitness predictions in discrete time: additive versus multiplicative form

In our framework, relative fitness is a statistic that predicts relative abundance in an additive equation (main text ***Equation 3***) but sometimes the dynamics of individual genotypes are modeled using a multiplicative form of fitness. In this section, we show how these multiplicative fitness statistics are related to the additive fitness statistics, in particular for the logit encoding.

We consider a population of a wild-type and a mutant genotype, where we track the mutant's relative abundance over multiple rounds of competition (e.g., growth cycles)

$$x(0) \to x(1) \to \cdots \to x(r-1) \to x(r), \tag{S17}$$

and the variable x changes each round according to some underlying population dynamics.

In a modeling approach typical to many studies in population genetics (***Krug, 2018***), these population dynamics are captured in the genotype-specific growth factors

$$f_{\text{mut}} = \frac{N_{\text{mut}}(r+1)}{N_{\text{mut}}(r)}, \qquad f_{\text{wt}} = \frac{N_{\text{wt}}(r+1)}{N_{\text{wt}}(r)}, \tag{S18}$$

which determine the update equation for the mutant relative abundance

$$x(r+1) = \frac{x(r)f_{\text{mut}}}{(1-x(r))f_{\text{wt}} + x(r)f_{\text{mut}}}, \tag{S19}$$

which is the discrete-time analogue to a differential equation (***Equation S1***). We divide ***Equation S19*** by $1 - x(r+1)$ to obtain the form

$$\frac{x(r+1)}{1-x(r+1)} = \frac{x(r)}{1-x(r)}\frac{f_{\text{mut}}}{f_{\text{wt}}}, \tag{S20}$$

which allows us to recognize the ratio of growth factors $f_{\text{mut}}/f_{\text{wt}}$ as a relative fitness statistic, since it is sufficient to predict the relative abundance of the mutant genotype (under the encoding $m(x) = x/(1-x)$). But the statistic $f_{\text{mut}}/f_{\text{wt}}$ acts as a multiplying factor in ***Equation S20***, whereas the general form of relative fitness s^m (main text ***Equation 3***) acts as an additive factor. What is the relationship between the multiplicative and the additive form of discrete-time relative fitness statistics?

To describe discrete rounds of population dynamics in our framework, we treat the relative abundance $x(r)$ as samples from a continuous time series, separated by a time-gap $\Delta t = t(r+1) - t(r)$. For a chosen encoding m, the relative abundance of the mutant genotype in the future round is predicted by

$$m(x(r+1)) = m(x(r)) + s^m \Delta t, \tag{S21}$$

since this is how we defined relative fitness s^m in main text ***Equation 3***. This relative fitness acts as an additive factor, but we apply the exponential function on both sides of ***Equation S21*** to obtain the updated equation

$$\exp\left[m(x(r+1))\right] = \exp\left[m(x(r))\right] \cdot \exp(s^m \Delta t), \tag{S22}$$

where the additive fitness s^{logit} together with the time scale Δt acts as a multiplicative factor. Specifically for the logit encoding $m(x) = \text{logit}\, x$ we have

$$\frac{x(r+1)}{1-x(r+1)} = \frac{x(r)}{1-x(r)} \exp(s^{\text{logit}} \Delta t). \tag{S23}$$

We compare ***Equation S23*** to ***Equation S20*** and solve for the relative fitness of the mutant genotype

$$s^{\text{logit}} = \frac{\log f_{\text{mut}} - \log f_{\text{wt}}}{\Delta t}, \tag{S24}$$

as a function of the growth factors $f_{\text{mut}}, f_{\text{wt}}$. Using the definition of the growth factors (***Equation S18***), we see that ***Equation S24*** is simply the discrete-time relative fitness for the logit encoding in terms of the mutant and wild-type log fold-change (LFC; main text ***Equation 8***). As a general point, we note that the growth-factor f_{mut} qualifies as an absolute fitness (since it is sufficient to predict the absolute abundance $N(r+1)$), but does not constitute a relative fitness statistic (since we also need to know f_{wt}, see ***Equation S20*** or ***Equation S24***).

More generally, for a given encoding function $m(x)$ we define the mutant's multiplicative relative fitness over a discrete growth cycle as

$$w^m = \exp(s^m \Delta t), \tag{S25}$$

where s^m is the additive relative fitness for this growth-cycle under the chosen encoding (main text ***Equation 4***) and Δt is the duration of the growth-cycle in time units that match s^m. ***Equation S25*** shows that the additive fitness s^m has time units, but the multiplicative fitness does not and is formally a dimensionless quantity. These dimensionless units are preserved in the approximate formula

$$w^m \approx 1 + s^m \Delta t, \tag{S26}$$

which is the first-order expansion of ***Equation S25*** in the limit of weak selection ($|s^m \Delta t| \ll 1$). For example, if we choose to measure relative fitness with the logit encoding on the time scale per-cycle ($\Delta t = 1$ cycle), we get

$$w^{\text{logit}} \approx 1 + s^{\text{logit}}_{\text{cycle}} \cdot 1 \text{ cycle}, \tag{S27}$$

which is the same multiplicative fitness as if we choose to measure the relative fitness on the time scale per-generation ($\Delta t = \text{LFC}^{\text{wt}}$):

$$w^{\text{logit}} \approx 1 + s^{\text{logit}}_{\text{gen}} \text{LFC}^{\text{wt}}. \tag{S28}$$

In both cases, the time units for the discrete-time additive fitness cancel in the product term.

So how would a mutant ranking in the multiplicative fitness w^{logit} rank a set of mutant genotypes compared to the fitness statistics $s^{\text{logit}}_{\text{cycle}}$ or $s^{\text{logit}}_{\text{gen}}$? ***Equation S27*** shows that the multiplicative fitness statistic w^{logit} agrees with the relative fitness per-cycle s^{logit}, but can differ from the ranking in the relative fitness per-generation $s^{\text{cycle}}_{\text{gen}}$ as both terms of the product in ***Equation S28*** depend on the mutant.

Finally, we address the question of how the relative fitness $s^{\text{logit}}_{\text{cycle}}$ agrees in the ranking with the multiplicative fitness w^{logit}, but disagrees with the fitness statistic defined in the Long-Term Evolution Experiment (***Lenski et al., 1991***) as

$$W = 1 + s^{\text{logit}}_{\text{gen}}. \tag{S29}$$

By comparing ***Equation S29*** to the multiplicative fitness in ***Equation S26***, we see that the LTEE fitness statistic W does not derive from the general form of the multiplicative fitness (***Equation S25***) as all statistics derived from this approximation have a multiplying factor Δt that cancels the units of time in s^m. The fact that the LTEE fitness statistic W (***Equation S29***) misses the term LFC_{wt} compared to the logit-based multiplicative fitness w^{logit} (***Equation S28***) means that the objects have different units of time and different rankings.

S5. Derivation of mismatch conditions for relative fitness per-cycle and per-generation

In this section, we derive the conditions for a ranking mismatch between the relative fitness per-cycle and per-generation (for the logit-encoded relative abundance) across a set of competition experiments. Consider a batch culture where a competing wild-type and mutant genotype have log fold-changes LFC_{wt} and LFC_{mut} over a single growth cycle. The LFCs are convenient variables to describe these dynamics since we can express the mutant's relative fitness per-cycle as (main text ***Equation 9***)

$$s^{\text{logit}}_{\text{cycle}} = \text{LFC}_{\text{mut}} - \text{LFC}_{\text{wt}}, \tag{S30}$$

and the mutant's relative fitness per-generation as (main text ***Equation 10***)

$$s^{\text{logit}}_{\text{gen}} = \frac{\text{LFC}_{\text{mut}}}{\text{LFC}_{\text{wt}}} - 1. \tag{S31}$$

Here, we assume both LFCs are nonzero (so that measuring fitness per-generation is meaningful; see discussion in main text).

To determine how these two fitness statistics lead to different rankings, we consider two competition experiments *A* and *B*, which may represent two different mutants competing against the same wild-type or the same mutant tested in two different environments. A mismatch in ranking occurs when the fitness per-cycle in competition is higher in *B*, while the fitness per-generation is higher in *A*:

$$\begin{aligned} s^{\text{logit}}_{\text{cycle}}(\text{LFC}^B_{\text{wt}}, \text{LFC}^B_{\text{mut}}) &> s^{\text{logit}}_{\text{cycle}}(\text{LFC}^A_{\text{wt}}, \text{LFC}^A_{\text{mut}}), \\ s^{\text{logit}}_{\text{gen}}(\text{LFC}^B_{\text{wt}}, \text{LFC}^B_{\text{mut}}) &< s^{\text{logit}}_{\text{gen}}(\text{LFC}^A_{\text{wt}}, \text{LFC}^A_{\text{mut}}). \end{aligned} \tag{S32}$$

We insert the expressions for relative fitness per-cycle (***Equation S30***) and per-generation (***Equation S31***) into ***Equation S32*** to rewrite the condition for ranking mismatch in terms of the LFCs:

$$\text{LFC}^B_{\text{mut}} > \text{LFC}^B_{\text{wt}} + \left(\text{LFC}^A_{\text{mut}} - \text{LFC}^A_{\text{wt}}\right), \tag{S33a}$$

$$\text{LFC}^B_{\text{mut}} < \text{LFC}^B_{\text{wt}} \cdot \frac{\text{LFC}^A_{\text{mut}}}{\text{LFC}^A_{\text{wt}}}. \tag{S33b}$$

For a given competition A, ***Equation S33a*** and ***Equation S33b*** define an area in the space of LFCs where competition B can lie such that competitions' fitness is ranked differently per-cycle versus per-generation (main text ***Figure 1D*** shows an example as the red-shaded area). Biologically, these constraints describe a situation where the mutant and wild-type LFCs are both higher or both lower in competition *B* than in competition *A* (i.e., so that the gray point is up and to the right of the red point in ***Figure 1D***, or down and to the left), but the LFC differences must be sufficiently balanced between the mutant and wild-type (i.e., so that the point lies within the red area in ***Figure 1D***).

Typically, however, the LFCs of the wild-type and the mutant are not independent, since these LFCs are jointly constrained by the fact both strains compete for the same finite resources. For example, assume that a single limiting resource with concentration *R* is consumed in proportion to the growth of each genotype's biomass according to

$$\frac{dR}{dt} = -\frac{1}{Y_{\text{wt}}}\frac{dN_{\text{wt}}}{dt} - \frac{1}{Y_{\text{mut}}}\frac{dN_{\text{mut}}}{dt}, \tag{S34}$$

where Y_{wt} and Y_{mut} are the wild-type and mutant biomass yields (stoichiometry of biomass to resource). We can integrate ***Equation S34*** to obtain

$$R(t) = R(0) - \frac{N_{\text{wt}}(t) - N_{\text{wt}}(0)}{Y_{\text{wt}}} - \frac{N_{\text{mut}}(t) - N_{\text{mut}}(0)}{Y_{\text{mut}}}. \tag{S35}$$

The growth cycle stops when no resource remains ($R(t) = 0$), such that

$$R(0) + \frac{N_{\text{wt}}(0)}{Y_{\text{wt}}} + \frac{N_{\text{mut}}(0)}{Y_{\text{mut}}} = \frac{N_{\text{wt}}(0)e^{\text{LFC}_{\text{wt}}}}{Y_{\text{wt}}} + \frac{N_{\text{mut}}(0)e^{\text{LFC}_{\text{mut}}}}{Y_{\text{mut}}}, \tag{S36}$$

where we have expressed the genotype abundances at the end of the growth cycle in terms of their LFCs. ***Equation S36*** thus entails a constraint between the wild-type and mutant LFCs. For a set of mutant competitions with the same initial resource concentration $R(0)$, initial abundances $N_{\text{wt}}(0)$ and $N_{\text{mut}}(0)$, and yields Y_{wt} and Y_{mut}, the mutant and wild-type LFCs are constrained by ***Equation S36*** to fall along a one-dimensional curve (black line in ***Appendix 1—figure 3A***). Geometrically, we see that this constraint on LFCs is incompatible with the requirements for a ranking mismatch between fitness per-cycle and per-generation for a pair of mutant competitions (compare black line and red shaded areas in ***Appendix 1—figure 3A***). However, if some mutant competitions deviate from this constraint, for example by having different yields Y_{mut} or initial conditions $N_{\text{wt}}(0)$ and $N_{\text{mut}}(0)$, then ranking mismatches may be possible (***Appendix 1—figure 3B***).

S6. Analysis of growth curves to identify growth phases

In this section, we describe in more detail how we identify growth phases from the original data set of growth curves and use this to choose a subset of curves that matches the simplified growth dynamics of our population dynamics model (***Appendix 1—figure 4A***). As mentioned in the main text (Methods), we downloaded this original data from the PROPHECY database (http://prophecy.lundberg.gu.se/), downloading specifically the data set for growth in Synthetic Defined medium as first analyzed and reported by ***Warringer et al., 2003***. We last accessed the PROPHECY website (http://prophecy.lundberg.gu.se/) on March 30, 2020, but as of November 15, 2025 the website is no longer accessible. We have included a reformatted version of the data with our code repository

(https://github.com/justuswfink/24FitnessQuantification, copy archived at ***Fink, 2026***). The original growth curve data is already corrected for background and instrument non-linearities (***Warringer et al., 2003***) (summarized in Methods), but we decided to apply additional corrections as follows: To begin with, we concatenate the original 51 data files (for different plate reader runs) into a single, consecutive dataframe and manually handle a duplication in one of the files (Experiment No. 18). This file has no measurements for the first time point ($t = 0$) due to a technical error in the original data export (***Warringer et al., 2003***), and for curves from this experimental run, we set the initial time point to NAN value in Python, meaning that these points will be ignored for any subsequent calculations of averages. More generally, we decided to trim the first four time points of all growth curves (equivalent to 1 hr 20 min from 47 hr total) and remove OD measurement below a noise threshold ($\mathrm{OD} = 0.001$) as this improves the quality of the fit later on.

After pre-processing, we estimate a smooth time series for the instantaneous growth rate in each growth curve, using a previously published script gaussianprocess.py by ***Swain et al., 2016*** that implements the Gaussian Process approach to smoothing (downloaded from https://swainlab.bio.ed.ac.uk/software.html). We apply this script to the logarithmic absolute abundance $\log \mathrm{OD}$, and reconstruct a smoothed trajectory $f(t) \approx \log \mathrm{OD}(t)$ as well as the first derivative df/dt and the second derivative d^2f/dt^2 (***Swain et al., 2016***). Effectively, the script estimates three hyperparameters that capture the shape of each curve, and we find that the estimation works best if we constrain the parameter ranges as outlined in ***Appendix 1—table 1***.

Appendix 1—table 1. Parameter settings for Gaussian Process optimization.

Symbol	Range	Interpretation
th[0]	[−5, 5]	Amplitude of variation on log scale
th[1]	[−5, 5]	Flexibility on log scale
th[2]	[−3.83, 0.478]	Measurement error on log scale

With a smoothed time series at hand, we now identify 'plateaus' of constant growth rate using the functions available in Scipy (***Virtanen et al., 2020***). For each growth curve, we start by identifying so-called 'plateau seeds', which are small intervals where the second derivative is below a chosen threshold $d^2f/dt^2 < 5 \cdot 10^{-6}$. For each plateau seed k in the growth curve, we calculate the average growth rate $\hat{g}_k$ in the time window of the plateau. Due to some noise in the second derivative, we find many plateau seeds that are adjacent and need to be merged. To do so, we iterate over the plateau seeds in the growth curve and merge the current candidate k with the previous plateau $k-1$, except one of the following conditions is true:

- Both plateau seeds have a duration that is too long (equal to or greater than 100 min).
- The transition time between the plateau seeds is too large (equal to or greater than 200 min).
- The first plateau has a significantly different growth rate than the second one, such that the following equation is satisfied

$$|g_{k-1} - g_k| > 0.001 + |g_k| \cdot 0.4, \tag{S37}$$

where g_k, g_{k-1} are the average growth rates in each plateau (per minute).

Empirically, we find that the duration of these merged plateaus is shorter than what one would expect from visually inspecting the growth curve. Therefore, we extend the remaining plateaus in each growth curve as follows: For each plateau, we estimate the lower and upper growth rates df/dt in the time window and take this as a growth rate corridor. We extend the plateau to the left until df/dt leaves that growth rate corridor, and similarly extend to the right. By definition, the resulting plateau is equal to or larger than the original time window, and we recalculate the average growth rate over the time window.

From this analysis, we obtain a list of growth phases for each curve that allows us to choose a subset of curves that match our model of population dynamics (Methods). We only choose curves

that have two plateaus, where the first plateau has significant growth (exponential phase), and the second plateau has no growth (stationary phase). Here, we define significant growth as the average growth rate in the plateau time window being larger than or equal to 0.0011 per minute. This forms the set of growth curves that we use to estimate growth traits (9424 curves).

S7. The saturation time in our model of population dynamics

In this section, we restate an explicit expression for the saturation time t_{sat} in pairwise competition that was derived in earlier work and allows us to see how mutants can influence resource depletion and the wild-type LFC (main text ***Equation 16***). Using the same model of population dynamics (Methods, main text ***Equation 12a***), previous work (***Manhart et al., 2018***; ***Manhart and Shakhnovich, 2018***) derived an approximate formula for t_{sat} that shows how it depends on the underlying parameters:

$$t_{\text{sat}} \approx \bar{\lambda} + \bar{\tau}\text{LFC}, \tag{S38}$$

where

$$\bar{\lambda} = \bar{\tau}\bar{Y}\sum_j \frac{x_j g_j \lambda_j}{Y_j} \tag{S39}$$

is the effective lag time of the population,

$$\bar{\tau} = \left[\sum_j x_j g_j \frac{\bar{Y}}{Y_j}\right]^{-1} \tag{S40}$$

is the effective e-fold growth time (reciprocal exponential growth rate) of the population,

$$\bar{Y} = \left[\sum_j \frac{x_j}{Y_j}\right]^{-1} \tag{S41}$$

is the effective yield of the population, and

$$\text{LFC} = \log\left(1 + \frac{R_0\bar{Y}}{N_0}\right) \tag{S42}$$

is the log fold-change of the total biomass, which depends on the initial absolute abundance N_0 of all genotypes and the initial concentration of resources R_0.

Equation S38 shows how each competing genotype influences the saturation time t_{sat} and thus the LFCs of all other genotypes via main text ***Equation 16***. For example, adding a mutant with a slow growth rate increases the effective doubling time (***Equation S40***), while a mutant with a long lag time will increase the effective lag time (***Equation S39***). Genotypes also influence the saturation time (***Equation S38***) through the effective yield $\bar{Y}$, which is the harmonic average of yields for all genotypes (***Equation S41***). The harmonic average means that adding mutants with low biomass yield Y_j can significantly shorten the saturation time, but mutants that are more efficient (high Y_j) have little influence on the duration of the growth cycle. Note that genotypes must be at sufficiently high relative abundance to significantly influence the effective population traits, since the contribution of each genotype j is weighted by its relative abundance x_j.

For bulk competition experiments, the saturation time of the culture can be expressed as an interpolation between the traits of the wild-type and the mutant library. We rewrite ***Equations S39 and S40*** as a function of mutant library traits

$$\bar{\lambda} = \bar{\tau}\bar{Y}\left((1-x_{\text{lib}})\frac{g_{\text{wt}}\lambda_{\text{wt}}}{Y_{\text{wt}}} + x_{\text{lib}}\frac{g_{\text{lib}}\lambda_{\text{lib}}}{Y_{\text{lib}}}\right), \tag{S43}$$

$$\bar{\tau} = \left((1-x_{\text{lib}})g_{\text{wt}}\frac{\bar{Y}}{Y_{\text{wt}}} + x_{\text{lib}}g_{\text{lib}}\frac{\bar{Y}}{Y_{\text{lib}}}\right)^{-1}, \tag{S44}$$

$$\bar{Y} = \left(\frac{1 - x_{\text{lib}}}{Y_{\text{wt}}} + \frac{x_{\text{lib}}}{Y_{\text{lib}}} \right)^{-1}, \tag{S45}$$

where g_{wt} is the wild-type growth rate, λ_{wt} is the wild-type lag time,

$$x_{\text{lib}} = \sum_{\text{muts } j} x_j, \tag{S46}$$

is the mutant library abundance at the beginning of the bulk competition,

$$\lambda_{\text{lib}} = \sum_{\text{muts } j} \lambda_j \frac{x_j}{x_{\text{lib}}} \frac{g_j}{g_{\text{lib}}} \frac{Y_{\text{lib}}}{Y_j} \tag{S47}$$

is the mutant library lag time,

$$g_{\text{lib}} = \sum_{\text{muts } j} g_j \frac{x_j}{x_{\text{lib}}} \frac{Y_{\text{lib}}}{Y_j} \tag{S48}$$

is the mutant library growth rate, and

$$Y_{\text{lib}} = \left[\sum_{\text{muts } j} \frac{x_j}{x_{\text{lib}}} \frac{1}{Y_j} \right]^{-1} \tag{S49}$$

is the mutant library yield. Note that the effective traits in ***Equations S47–S49*** are independent under a rescaling of the mutant library abundance x_{lib} as long as the relative proportion of the individual lineages x_j/x_{lib} stays constant.

To simplify calculations, we sometimes assume that the mutants have variation in lag time and growth rate, but no variation in biomass yield ($Y_i = Y_j$ for all i and j). Under this assumption, we can rewrite ***Equations S43 and S44*** as

$$\bar{\lambda} = \frac{(1 - x_{\text{lib}}) g_{\text{wt}} \lambda_{\text{wt}} + x_{\text{lib}} g_{\text{lib}} \lambda_{\text{lib}}}{(1 - x_{\text{lib}}) g_{\text{wt}} + x_{\text{lib}} g_{\text{lib}}}, \tag{S50}$$

$$\bar{\tau} = \frac{1}{(1 - x_{\text{lib}}) g_{\text{wt}} + x_{\text{lib}} g_{\text{lib}}}. \tag{S51}$$

S8. Epistasis detection for double mutants using relative fitness per-cycle and per-generation

In this section, we discuss the patterns of epistasis observed in relative fitness per-cycle and relative fitness per-generation for the systematic scan of double mutants in our model of population dynamics (Methods). For relative fitness per-cycle, main text ***Figure 3C*** shows that epistasis occurs if and only if one of the mutations involves a change in growth rate. This is because the selection on growth rate in the per-cycle statistic depends on the duration of the growth cycle (***Manhart et al., 2018***)

$$s_{\text{cycle}}^{\text{logit}} = g_{\text{mut}}(t_{\text{sat}} - \lambda_{\text{mut}}) - g_{\text{wt}}(t_{\text{sat}} - \lambda_{\text{wt}}), \tag{S52}$$

where t_{sat} is the saturation time, $t_{\text{sat}} - \lambda_{\text{mut}}$ is the time of growth for the mutant strain and $t_{\text{sat}} - \lambda_{\text{wt}}$ is the time of growth for the wild-type strain. At high relative abundance of the mutant, the saturation time t_{sat} depends on all three mutant traits (***Equation S38***), leading to quadratic mutant trait terms in ***Equation S52*** and non-zero epistasis in main text ***Equation 17***. For example, a double mutant in growth rate $(+g, +g)$ has lower than expected relative fitness per-cycle (negative epistasis in ***Equation 17***) because the second growth rate mutation shortens the growth window $t_{\text{sat}} - \lambda_{\text{mut}}$ in ***Equation S52*** (see growth curves in ***Appendix 1—figure 9***; row A). Intuitively, there is no epistasis between lag time and yield because changes to lag time play out early in the growth cycle and changes in yield only change the final time point of growth (see ***Appendix 1—figure 11***). Note that here we have chosen examples where both mutants exit the lag phase before saturation—for deleterious mutations with extremely long lag time, a double mutant $(+\lambda, +\lambda)$ eventually shows epistasis in

relative fitness per-cycle since the wild-type growth advantage is bounded from above due to finite resources.

Using relative fitness per-generation s_{gen}, main text ***Figure 3D*** shows that epistasis occurs if and only if one of the mutations involves lag time, a pattern that is distinct from the per-cycle statistic (compare ***Figure 3C, D***). This is because the relative fitness per-generation uses the wild-type LFC as a normalizing time scale (main text ***Equation 10***) and nonlinearities in this time scale with respect to the mutant traits can modify or create new epistasis. For example, epistasis is modified in the per-generation statistic for a double mutant in growth rate and lag time (e.g., $(+g, -\lambda)$; ***Appendix 1—figure 9***, row D). There is positive epistasis in relative fitness per-cycle, since the shorter lag time leads to a longer mutant growth time which amplifies selection on growth rate (compare ***Equation S52***), but there is even higher positive epistasis in the per-generation statistic, because the double mutant growth is spread over less wild-type generations compared to the single mutant growth. Sometimes, the nonlinearity in the time-scale LFC_{wt} works to remove epistasis. For example, a double-mutant of growth rate $(+g, +g)$ (***Appendix 1—figure 9***, row A) is epistatic in the per-cycle statistic but non-epistatic in the per-generation statistic

$$s_{\text{gen}}^{\text{logit}} = \frac{g_{\text{mut}}(t_{\text{sat}} - \lambda_{\text{mut}})}{g_{\text{wt}}(t_{\text{sat}} - \lambda_{\text{wt}})} - 1, \tag{S53}$$

where the mutant growth time $t_{\text{sat}} - \lambda_{\text{mut}}$ and the wild-type $t_{\text{sat}} - \lambda_{\text{wt}}$ are both reduced but happen to cancel. Finally, the mutant-dependent time-scale LFC_{wt} of the per-generation statistic also introduces new epistasis between lag time and yield (***Appendix 1—figure 11***), as well as for mutants with two lag time mutations (***Appendix 1—figure 11***, row C and ***Appendix 1—figure 12***, row D). These mutations have no epistasis in relative fitness per-cycle but the normalization by the wild-type LFC in main text ***Equation 10*** introduces an additional dependence on t_{sat} that renders fitness a quadratic function of lag time.

We repeat the fitness estimates using a 1% mutant relative abundance in the simulated competition experiments (***Appendix 1—figure 15A***). At this low mutant abundance, ***Appendix 1—figure 15B*** shows the epistasis in relative fitness per-cycle s_{cycle} is limited to combinations of mutants that perturb growth rate and lag time. Note that in this low abundance limit, the relative fitness per-generation s_{gen} agrees on the presence and absence of epistasis (***Appendix 1—figure 15C***), simply because the wild-type LFC is approximately constant across mutants.

S9. Analysis of fitness trajectories from the Long-Term Evolution Experiment

A previous analysis of the Long-Term Evolution Experiment (LTEE) performed by ***Wiser et al., 2013*** found that evolved populations of *Escherichia coli* increased in relative fitness over 50,000 generations without converging to a maximum fitness. Here, we re-analyze the same data by directly comparing the relative fitness (under the logit encoding) per-cycle $s_{\text{cycle}}^{\text{logit}}$ and per-generation $s_{\text{gen}}^{\text{logit}}$ to see if the choice of fitness statistic changes the conclusion. The experimental protocol of the LTEE has been described elsewhere (***Lenski et al., 1991***; ***Barrick et al., 2023***), but we briefly summarize the main aspects: Starting with a single ancestral strain of *E. coli*, 12 replicate populations were inoculated in 1988 and are perpetually grown in batch cultures with serial transfers, such that 1% of the population biomass is transferred to fresh growth medium each day. Samples from each replicate population are stored every 500 generations, leading to a record of evolved populations over time (***Barrick et al., 2023***).

Previous work performed competition experiments between the ancestral population and each evolved population (every 500–2000 generations) by combining them in equal proportions and growing them over a single batch culture growth cycle, with measurements of their initial and final absolute abundances taken by colony counting (***Wiser et al., 2013***). This data has been prepared in a convenient format by ***Good et al., 2017*** and is available for download here. The total data set lists n = 928 competition experiments. We remove n=6 entries because either the initial or final abundances are missing.

For a few of the 12 populations, the time series is truncated: population Ara+6 has competition measurements up to generation 4000, population Ara-2 has competition measurements up to generation 30,000, and population Ara+2 has competition measurements up to generation 32,000

(**Wiser et al., 2013**). Note that the evolved population tested in these competitions is not a single genotype, but a sample of many genotypes that were present in that evolving population at that time. From these values of absolute abundance, we compute the log fold-change (LFC) of the evolved and ancestral populations in each competition and then calculate the evolved population's relative fitness per-cycle (main text **Equation 9**) and per-generation (main text **Equation 10**). The original data set has two to four replicate measurements for each evolved sample, corresponding to a repeat of the competition experiment at a different day (**Wiser et al., 2013**). Initially, we collect all competition experiments into a single data set (n = 928 competitions) and find that relative fitness per-generation and per-cycle differ in the ranking of these competitions (main text **Figure 4B**, **Appendix 1—figure 17A**). For example, one competition is ranked 261 positions lower in relative fitness per-generation than per-cycle (where higher rank indicates higher fitness). The scatter occurs because the biomass yield evolves downward over time (**Vasi et al., 1994**; **Grant et al., 2021**). We can understand the ranking mismatch from the underlying LFCs in the competition experiment (**Appendix 1—figure 17B**), that show considerable scatter, with some mutant-wild-type pairs in a positive covariation (compare **Appendix 1—figure 17B** and main text **Figure 1D**). The scatter occurs because the biomass yield evolves downward over time (**Vasi et al., 1994**; **Grant et al., 2021**), shifting the wild-type LFCs downward in 1:1 competitions with the evolved populations (horizontal trend across time points in **Appendix 1—figure 17B**).

We can also construct a time series of relative fitness for each population and compare fitness rankings at individual time points. For each of the 12 populations in the LTEE, we define the relative fitness per-generation $s_{\text{gen}}^{\text{logit}}$ at time t by averaging the value $s_{\text{gen}}^{\text{logit}}$ across all competition experiments with the frozen sample from time t. Similarly, we define a time series of relative fitness per-cycle $s_{\text{cycle}}^{\text{logit}}$ for each population. In summary, we can pool all time series into a single data set (with the truncation described above) and test how the two statistics rank the 12 populations at any point in the experiment. We find that the mismatch between relative fitness per-cycle and per-generation is consistently low at all time points (main text **Figure 4A**), with a few exceptions (for example, at generation 4000 the two statistics disagree on the top six populations).

A key result from previous analysis by **Wiser et al., 2013** on this data set is that the evolving populations increase indefinitely in relative fitness, rather than leveling off at some maximum fitness value. The empirical analysis by **Wiser et al., 2013** tested the long-term trend by fitting the statistic $W = 1 + s_{\text{gen}}^{\text{logit}}$ to a hyperbolic model of the time series:

$$f(t) = 1 + \frac{at}{t+b}, \tag{S54}$$

where t is the evolutionary time point at which the evolved population is measured against its ancestor, and $f(t)$ is the fitness statistic measured from that competition (here fitted to the measured values of W). The important feature of the hyperbolic model is that it assumes that relative fitness saturates at a maximum fitness over long times ($\lim_{t\to\infty} f(t) = 1 + a$). To contrast this model, they also tested a power law

$$f(t) = (\alpha t + 1)^{\beta} \tag{S55}$$

under which fitness increases without bound over long times ($\lim_{t\to\infty} f(t) = \infty$). To repeat this analysis with the fitness statistics $s_{\text{cycle}}^{\text{logit}}$ and $s_{\text{gen}}^{\text{logit}}$ used in this article, we must adjust the models to account for the fact that W takes 1 as its neutral value (occurring at $t = 0$ by definition) while $s_{\text{cycle}}^{\text{logit}}$ and $s_{\text{gen}}^{\text{logit}}$ are zero under neutrality. Thus, we use

$$f(t) = \frac{at}{t+b} \tag{S56}$$

as the hyperbolic model and

$$f(t) = (\alpha t)^{\beta} \tag{S57}$$

as the power law model.

As a control against the original analysis of **Wiser et al., 2013**, we first perform our own fit of the time series of the relative fitness per-generation $s_{\text{gen}}^{\text{logit}}$ to the hyperbolic (**Equation S56**)

and the power law (***Equation S57***) models. Wiser et al. compared their two models using the Bayesian Information Criterion but since the models have the same number of parameters this is mathematically equivalent to comparing the values of R^2. ***Appendix 1—figure 16A*** shows that in our analysis, the power law model has a higher quality of fit ($R^2 = 0.701$) than the hyperbolic model does ($R^2 = 0.682$) for the fitness statistic $s_{\text{gen}}^{\text{logit}}$, consistent with the original result by Wiser et al. for the statistic $W = 1 + s_{\text{gen}}^{\text{logit}}$. Since the equations for the hyperbolic model only differ in the constant offset (compare ***Equations S54 and S56***), our fit of $s_{\text{gen}}^{\text{logit}}$ to ***Equation S56*** is mathematically equivalent to the fit of W to ***Equation S54***. Therefore, our fit should give the exact same results as the original publication (***Wiser et al., 2013***) in the case of the hyperbolic model (although we could not find the fitted values a, b documented in the original publication so we were unable to check them). This is not true for the power law, because the modified power law used by Wiser et al. (***Equation S55***) includes the offset within the parentheses, rather than as an added constant outside (compare ***Equation S55*** to ***Equation S57***). This means that the fit of W to the power law with an initial value of 1 (***Equation S55***, fitted values $\alpha = 0.00515, \beta = 0.0950$; matching ***Wiser et al., 2013***) is different from the fit of $s_{\text{gen}}^{\text{logit}}$ to the power law with an initial value of zero (***Equation S57***, fitted values $\alpha = 0.000007, \beta = 0.299891$).

We next perform a new analysis by calculating the relative fitness per-cycle $s_{\text{cycle}}^{\text{logit}}$ from the same time series data (12 time series pooled together, one for each line) and fitting this fitness statistic to the same hyperbolic (***Equation S56***) and power law (***Equation S57***) models. As shown in ***Appendix 1—figure 16B***, we find that the power law model outperforms the hyperbolic model for the per-cycle fitness, consistent with the model performance for the per-generation fitness. This suggests that Wiser et al.'s original conclusion about fitness increasing without bound (***Wiser et al., 2013***) is robust to the choice of fitness statistic.

As we previously mentioned, the fitness measurements of all replicate populations are not uniform across time (***Appendix 1—figure 16A***): there are fewer fitness measurements at late time points (generation 34,000 and higher) because three populations were eventually excluded from the fitness measurements (***Wiser et al., 2013***). To further corroborate our results, we thus repeat the model fits using a single time series of the evolved fitness, rather than fitting the models to all 12 fitness time series simultaneously. We calculate the average fitness per-generation $s_{\text{gen}}^{\text{logit}}$ and per-cycle $s_{\text{cycle}}^{\text{logit}}$ in the evolution experiment as the average across all 12 populations at each time point and fit this population-averaged time series to the hyperbolic (***Equation S56***) and power law (***Equation S57***) models (Wiser et al. refer to this as a fit to the 'grand mean'). ***Appendix 1—figure 16C, D*** shows that the power law still has a better quality of fit than the hyperbolic model does, and we thus conclude that the increasing fitness trend reported by ***Wiser et al., 2013*** is also robust to the uneven distribution of measurements over time.

We note that the quality of fit R reported in the main text of ***Wiser et al., 2013*** differs from the quality of fit we show on our plots. While both studies performed the fits of the models on all 12 populations simultaneously, ***Wiser et al., 2013***, evaluated the quality of fit by calculating R for the fitted model (blue and pink lines in ***Appendix 1—figure 16A***) against the fitness time series averaged over replicates (gray points in ***Appendix 1—figure 16C***). That is, they fit the model to the data without averaging over population but calculate quality of fit using the population-averaged data. Since we believe this was inconsistent, we have followed a more standard approach of calculating the quality of fit on the same input data used for the fit (i.e., correlating the blue and pink lines in ***Appendix 1—figure 16A*** with gray points in the same plot). As a consequence, the correlations between the fitted models and data reported in the original publication (hyperbolic $R = 0.969$, power law $R = 0.986$; see ***Wiser et al., 2013***) are systematically higher than the values we find in our re-analysis (hyperbolic $R = 0.826$, power law: $R = 0.837$; take square root of the values in ***Appendix 1—figure 16A***). Although the long-term fitness dynamics in the case of the LTEE are robust to the choice of fitness statistic, we note that it is possible to construct scenarios of microbial growth trait evolution where relative fitness saturates in one statistic but not in the other (main text ***Figure 3E–F***). For theory work on the long-term trend of fitness in evolving populations and additional models beyond the power law, see ***Sibani et al., 1998***; ***Park and Krug, 2008***; ***Guo et al., 2019***; ***Guo and Amir, 2022***; ***Boffi et al., 2024***.

S10. Testing AUC and other fitness potentials using simulated competition experiments

In this section, we explain our tests of estimated fitness potentials against true relative fitness in simulated competition experiments. We first focus on the area under the growth curve (AUC), which is defined as

$$\mathrm{AUC} = \int_0^{t_{\mathrm{eval}}} N(t)dt, \tag{S58}$$

where $N(t)$ is a growth curve of absolute abundance (or a proxy such as optical density) and t_{eval} is a cutoff time for evaluating the area. Many previous studies (***Worthan et al., 2023***; ***Schmitz et al., 2024***; ***Sprouffske et al., 2018***; ***Piccardi et al., 2019***; ***Dos Santos et al., 2022***) and growth curve analysis packages (***Sprouffske and Wagner, 2016***) have used this definition. The idea of AUC is that, unlike estimated fitness potentials that only account for individual traits of a genotype's growth (e.g., growth rate or lag time; see below), the AUC literally integrates the whole growth dynamics into a single number. For example, both fast growth rate and short lag time are manifested in greater AUC. Note that while one can attempt to use the AUC as an approximate fitness potential (as we investigate here), it is not a measure of absolute fitness (Appendix 1—section S2) since it is insufficient to predict changes in absolute abundance (i.e., the area under the growth curve does not determine the change in absolute abundance from beginning to end).

To compute the AUC for the set of single-gene deletion genotypes in our data set, we first simulate a growth curve for each genotype under the population dynamics model in main text ***Equation 12a*** with the traits estimated from the yeast single-gene knockout data (Methods). We use simulated growth curves, with trait values inferred from the measured growth curves, rather than the actual measured growth curves since we are comparing the AUCs to relative fitness also from simulations of competitions; we do not have actual competition data for these genotypes, so it would be an apples-to-oranges comparison if we used AUCs from the actual growth curve data. Furthermore, in empirical growth curves, the AUC is also influenced by technical variation in the initial biomass N_0 and the initial concentration of resources R_0, so using simulations removes these effects.

Appendix 1—figure 20A shows the distribution of saturation times t_{sat} (as defined for the population dynamics model in Methods) numerically calculated for all simulated growth curves of the deletion mutants. We calculate the AUC for each growth curve using ***Equation S58*** with an evaluation time of $t_{\mathrm{eval}} = 16$ hr since that includes the stationary phase in the vast majority of our simulated growth curves (***Appendix 1—figure 20A***). From the mutant's AUC, we calculate the AUC-based estimator of the mutant's relative fitness

$$\hat{s}_{\mathrm{AUC}} = \mathrm{AUC}_{\mathrm{mut}} - \mathrm{AUC}_{\mathrm{wt}}, \tag{S59}$$

where $\mathrm{AUC}_{\mathrm{wt}}$ is the AUC for a simulated growth curve of the wild-type (using the median wild-type traits in our database; see Methods). We then simulate a single growth cycle of the mutant competing against the wild-type (***Equation 12a*** with equal initial abundance of the mutant and wild-type) to calculate the mutant's 'true' (under the model assumptions) relative fitness per-cycle with the logit encoding $s^{\mathrm{logit}}_{\mathrm{cycle}}$. We simulate both the coculture and the monoculture growth dynamics with the same initial biomass $N_0 = 0.05$ OD and resource concentration $R_0 = 111$ mM (***Warringer et al., 2003***). Repeating this analysis for all mutant genotypes in the data set, we calculate the Spearman rank correlation between the AUC-predicted relative fitness from monoculture $\hat{s}_{\mathrm{AUC}}$ and the true relative fitness in competition $s^{\mathrm{logit}}_{\mathrm{cycle}}$ (***Appendix 1—figure 19***, column C).

The success of the AUC depends on the evaluation time t_{eval}, which sets the time window from which information is captured from the growth curve by the integral (***Equation S58***). ***Appendix 1—figure 20B–D*** shows the correlation between the relative fitness in coculture $s^{\mathrm{logit}}_{\mathrm{cycle}}$ and the AUC estimator $\hat{s}_{\mathrm{AUC}}$ (***Equation S59***) for three values of t_{eval}: the mean saturation time of all genotypes in monoculture ($t_{\mathrm{eval}} \approx 13$ hr), a significantly longer value ($t_{\mathrm{eval}} \approx 24$ hr), and an intermediate value ($t_{\mathrm{eval}} = 16$ hr; used for ***Appendix 1—figure 19***). For short evaluation times ($t_{\mathrm{eval}} \approx 13$ hr), the AUC underestimates the fitness of mutants with long lag but fast growth, which leads to a nonlinear relationship between the AUC estimator and the true relative fitness (compare ***Appendix 1—figure***

20B, C). For long evaluation times ($t_{\mathrm{eval}} = 24$ hr), there is greater scatter between the AUC predictor and true relative fitness for the highest fitness mutants (compare spread in ***Appendix 1—figure 20C, D***). Intuitively, these mutants have short lag times or fast growth rates and saturate early in monoculture, so their AUC values are effectively set by the biomass yield, which has no predictive value on the competition outcome. In summary, ***Appendix 1—figure 20B–D*** shows a trade-off between accurately ranking highly deleterious mutants (which need long t_{eval}) and ranking highly beneficial mutants (which need short t_{eval}).

Besides AUC, it is possible to use other features of the monoculture growth curve as approximate fitness potentials. For example, one can use the monoculture growth rates alone as fitness potentials:

$$\hat{s}_g = g_{\mathrm{mut}}^{\mathrm{mono}} - g_{\mathrm{wt}}^{\mathrm{mono}}, \tag{S60}$$

or the monoculture lag times:

$$\hat{s}_{\mathrm{lag}} = \lambda_{\mathrm{mut}}^{\mathrm{mono}} - \lambda_{\mathrm{wt}}^{\mathrm{mono}}. \tag{S61}$$

Another possible fitness potential is the absolute abundance at saturation, which in our model of population dynamics (***Equation 12a***) is proportional to the biomass yield:

$$\hat{s}_Y = Y_{\mathrm{mut}}^{\mathrm{mono}} - Y_{\mathrm{wt}}^{\mathrm{mono}}. \tag{S62}$$

Finally, one can also use the difference in the monoculture log fold-changes (LFCs):

$$\hat{s}_{\mathrm{LFC}} = \log\left(\frac{N_{\mathrm{mut}}(t_{\mathrm{sat}}^{\mathrm{mono}})}{N_{\mathrm{mut}}(0)}\right) - \log\left(\frac{N_{\mathrm{wt}}(t_{\mathrm{sat}}^{\mathrm{mono}})}{N_{\mathrm{wt}}(0)}\right). \tag{S63}$$

This looks similar to the definition of relative fitness per-cycle (main text ***Equation 9***) but is distinct because it uses the LFCs in monoculture rather than the true LFCs in coculture (which may be different).

We test each of these fitness potentials against the relative fitness in pairwise competition, using different input data sets of trait variation and the 'GNU Parallel' command to speed up the simulation process (***Tange, 2018***). ***Appendix 1—figure 19*** rows B and C show that growth rate and lag time can act as perfect fitness potentials if that trait is the only trait with variation across mutants. This is because the relative fitness is proportional to differences in each of these traits when they are the only source of variation (see Appendix 1—section S14). Appendix 1—section S14 also shows that differences in biomass yield ($Y_{\mathrm{mut}} - Y_{\mathrm{wt}}$) have no effect on fitness by themselves, which is why the biomass yield of the strains in monoculture is a poor fitness potential to estimate relative fitness. This large but neutral variation in the biomass yield across mutants in our data sets means that the LFC is also a poor fitness potential.

All of these trait-based fitness potentials are outperformed by the AUC, which provides the best approximation of the mutant fitness ranking in coculture under realistic trait variation (***Appendix 1—figure 19***, row A). More broadly, it is important to treat absolute and relative fitness, as well as fitness potentials, as distinct concepts, serving different purposes (***Smith et al., 2024***; ***Gordo et al., 2012***). As we show here in simulation (***Appendix 1—figure 19***), and others have shown in experiments (***Concepción-Acevedo et al., 2015***; ***Durão et al., 2021***; ***Worthan et al., 2023***; ***Schmitz et al., 2024***), measuring fitness potentials is not enough to demonstrate that a mutant genotype will outcompete the wild-type.

S11. Coarse-graining pairwise relative fitness in multi-genotype populations

In this section, we point out the specific advantages of the logit-encoding for coarse-graining pairwise relative fitness in bulk competition experiments. While the pairwise relative fitness is defined for any encoding m, the logit encoding endows it with some convenient mathematical properties not shared by other encodings (e.g., the log encoding). The logit encoding of the pairwise relative abundance has the property

$$\operatorname{logit} x_{ij} = \log x_i - \log x_j, \tag{S64}$$

meaning that it is antisymmetric under exchange of the indices i and j ($\text{logit}\, x_{ij} = -\text{logit}\, x_{ji}$) and additive across pairs of indices ($\text{logit}\, x_{ij} = \text{logit}\, x_{ik} + \text{logit}\, x_{kj}$). Since the logit-encoded pairwise relative fitness is just the time derivative of the logit function (***Equation 21***), it carries equivalent properties of antisymmetry and additivity:

$$s_{ji}^{\text{logit}} = -s_{ij}^{\text{logit}}, \tag{S65}$$

$$s_{ij}^{\text{logit}} = s_{ik}^{\text{logit}} + s_{kj}^{\text{logit}}. \tag{S66}$$

We also note that the logit encoding of the pairwise relative abundance has the property:

$$\text{logit}\left(\frac{ax_i}{ax_i + bx_j}\right) = \text{logit}\left(\frac{x_i}{x_i + x_j}\right) + \log\left(\frac{a}{b}\right). \tag{S67}$$

Rescaling the relative abundances of either genotype thus does not change the pairwise relative fitness (since it only shifts the logit by a constant, which does not affect its derivative). This means that pairwise relative fitness is an 'intensive' property of a genotype, analogous to intensive properties in statistical mechanics (such as temperature) that do not scale with system size. For example, if we split a mutant genotype into two subgroups (e.g., differentiated by a neutral marker), the pairwise relative fitness of each mutant subgroup with respect to the wild-type will be the same as the pairwise relative fitness of the mutant genotype as a whole compared to the wild-type. In contrast, the logit-encoded total relative fitness does not satisfy this property since $\text{logit}\,(ax_i) \neq \text{logit}\, x_i + a$.

When the encoding m is the logit function, the pairwise relative fitness per-cycle still satisfies the above properties (antisymmetry and additivity with respect to indices i, j, and invariance under relative abundance rescaling) since those are properties of the underlying logit encoding. This is also apparent from interpreting the per-cycle fitness statistic as an integral of the instantaneous statistic:

$$s_{ij,\text{cycle}}^{m} = \int_{t_0}^{t_{\text{sat}}} s_{ij}^{m}(t)\, dt. \tag{S68}$$

S12. The relative fitness between coarse-grained groups of genotypes

In this section, we generalize the concept of pairwise relative fitness to pairs of genotype groups rather than pairs of individual genotypes. In a multi-genotype population with subsets of genotypes $\mathcal{A}$ and $\mathcal{B}$, define

$$x_{\mathcal{AB}}(t) = \frac{\sum_{i\in\mathcal{A}} x_i(t)}{\sum_{i\in\mathcal{A}\cup\mathcal{B}} x_i(t)} \tag{S69}$$

as the relative abundance of $\mathcal{A}$ genotypes compared to $\mathcal{B}$ genotypes at time t, where $A \cup B$ is the union of the two index sets. Analogous with main text ***Equation 21***, we define the fitness of group $\mathcal{A}$ relative to group $\mathcal{B}$ as

$$s_{\mathcal{AB}}^{m} = \frac{d}{dt} m(x_{\mathcal{AB}}(t)) \tag{S70}$$

for an encoding m. Under the logit encoding, it turns out that the fitness between these two groups can be conveniently expressed as a weighted average of the pairwise fitness between the member genotypes in each group:

$$s_{\mathcal{AB}}^{\text{logit}} = \frac{1}{\sum_{i\in\mathcal{A}} x_i} \frac{1}{\sum_{j\in\mathcal{B}} x_j} \cdot \sum_{i\in\mathcal{A}} \sum_{j\in\mathcal{B}} x_i x_j s_{ij}^{\text{logit}}. \tag{S71}$$

To prove ***Equation S71***, we first note that

$$\frac{x_{\mathcal{AB}}}{1 - x_{\mathcal{AB}}} = \frac{\sum_{i\in\mathcal{A}} x_i}{\sum_{j\in\mathcal{B}} x_j}. \tag{S72}$$

Thus, we can rewrite the logit-encoded relative pairwise fitness between $\mathcal{A}$ and $\mathcal{B}$ as

$$\begin{aligned} s^{\text{logit}}_{\mathcal{AB}} &= \frac{d}{dt}\text{logit}\, x_{\mathcal{AB}} \\ &= \frac{d}{dt}\log\left(\frac{\sum_{i\in\mathcal{A}} x_i}{\sum_{j\in\mathcal{B}} x_j}\right) \\ &= \frac{d}{dt}\log\left(\sum_{i\in\mathcal{A}} x_i\right) - \frac{d}{dt}\log\left(\sum_{j\in\mathcal{B}} x_j\right), \end{aligned} \tag{S73}$$

where we have invoked ***Equation S72*** on the second line. We can expand each term on the right-hand side of ***Equation S73*** as

$$\frac{d}{dt}\log\sum_{i\in\mathcal{A}} x_i = \frac{1}{\sum_{i\in\mathcal{A}} x_i}\sum_{i\in\mathcal{A}}\frac{dx_i}{dt}, \tag{S74}$$

and then insert ***Equation S74*** into ***Equation S73*** to obtain

$$s^{\text{logit}}_{\mathcal{AB}} = \frac{1}{\sum_{i\in\mathcal{A}} x_i}\frac{1}{\sum_{j\in\mathcal{B}} x_j}\cdot\left[\sum_{j\in\mathcal{B}} x_j\sum_{i\in\mathcal{A}}\frac{dx_i}{dt} - \sum_{i\in\mathcal{A}} x_i\sum_{j\in\mathcal{B}}\frac{dx_j}{dt}\right], \tag{S75}$$

where we have collected the normalization factors (sums over relative abundances in $\mathcal{A}$ and $\mathcal{B}$) as a single pre-factor. We then rewrite each product of sums in ***Equation S75*** as

$$\sum_{j\in\mathcal{B}} x_j\sum_{i\in\mathcal{A}}\frac{dx_i}{dt} = \sum_{j\in\mathcal{B}}\sum_{i\in\mathcal{A}} x_j x_i\frac{d}{dt}\log x_i \tag{S76}$$

to finally obtain

$$\begin{aligned} s^{\text{logit}}_{\mathcal{AB}} &= \frac{1}{\sum_{i\in\mathcal{A}} x_i}\frac{1}{\sum_{j\in\mathcal{B}} x_j} \\ &\cdot\left[\sum_{j\in\mathcal{B}}\sum_{i\in\mathcal{A}} x_j x_i\left(\frac{d}{dt}\log x_i - \frac{d}{dt}\log x_j\right)\right]. \end{aligned} \tag{S77}$$

Identifying the term in the inner parentheses as the pairwise selection coefficient s^{logit}_{ij} (main text ***Equation 21***) then results in ***Equation S71***.

Equation S71 establishes that the relative fitness between a pair of genotype groups is a weighted sum of relative fitnesses between individual pairs of genotypes in those groups, but this holds for relative fitness defined at an instant in time (since it is based on derivatives). For relative fitness defined over a finite time interval (e.g., a growth cycle in batch culture), an analogous but approximate result holds. We first write the relative fitness over a growth cycle time interval as an integral over the instantaneous relative fitness (inserting ***Equation S71*** into ***Equation S68***):

$$\begin{aligned} s^{\text{logit}}_{\mathcal{AB},\text{cycle}} &= \int_0^{t_{\text{sat}}}\frac{1}{\sum_{i\in\mathcal{A}} x_i(t)}\frac{1}{\sum_{j\in\mathcal{B}} x_j(t)} \\ &\cdot\sum_{i\in\mathcal{A}}\sum_{j\in\mathcal{B}} x_i(t)x_j(t)s^{\text{logit}}_{ij}(t)dt, \end{aligned} \tag{S78}$$

where t_{sat} is the end time of the growth cycle (Methods, Appendix 1—section S7). The integral in ***Equation S78*** is difficult to calculate as the relative abundance trajectories $x_i(t), x_j(t)$ depend on the relative fitness of the genotypes $s^{\text{logit}}_{ij}(t)$ in a non-trivial way. Instead, we make the approximation that the relative abundances do not change significantly over time of the growth cycle ($x_i(t) \approx x_i(0)$) and can thus pass the integral through the sums in ***Equation S78*** to show that the per-cycle relative fitness between a pair of genotype groups is approximately also a weighted sum of per-cycle relative fitnesses:

$$\begin{aligned} s^{\text{logit}}_{\mathcal{AB},\text{cycle}} &\approx \frac{1}{\sum_{i\in\mathcal{A}} x_i(0)}\frac{1}{\sum_{j\in\mathcal{B}} x_j(0)} \\ &\cdot\sum_{i\in\mathcal{A}}\sum_{j\in\mathcal{B}} x_i(0)x_j(0)s^{\text{logit}}_{ij,\text{cycle}}. \end{aligned} \tag{S79}$$

Conceptually, assuming the relative abundances are approximately constant over the growth cycle is equivalent to assuming selection is weak; one can also show this mathematically by expressing the relative abundances $x_i(t)$ in terms of the pairwise relative fitnesses s_{ij}^{logit} in ***Equation S78*** and keeping only terms to leading order in s_{ij}^{logit}.

We finally note that the total relative fitness (instantaneous ***Equation 19*** and per-cycle ***Equation 22*** in the main text) is a special case of the relative fitness between groups (***Equations S71 and S79***) where $\mathcal{A}$ is the single genotype i and $\mathcal{B}$ is all other genotypes besides i:

$$\sigma_i^{\text{logit}} = \frac{1}{1-x_i} \cdot \sum_{j \neq i} x_j s_{ij}^{\text{logit}}, \tag{S80}$$

$$\sigma_{i,\text{cycle}}^{\text{logit}} \approx \frac{1}{1-x_i(0)} \cdot \sum_{j \neq i} x_j(0) s_{ij,\text{cycle}}^{\text{logit}}. \tag{S81}$$

S13. Fitness error from the frame of reference in bulk competition experiments

Here, we calculate the error that arises from measuring the total relative fitness of each mutant in a bulk competition experiment of a mutant library, rather than the pairwise relative fitness between each mutant and the wild-type. We call this difference the *error from the frame of reference*, the frame of reference being either the whole population in total fitness or the wild-type in pairwise fitness. Note that this is an error between two different fitness quantifications of the same bulk competition experiment; Appendix 1—section S15 addresses the error (arising from higher-order interactions) between fitness quantifications in bulk versus pairwise competition experiments. Here, we only consider relative fitness under the logit encoding and measured per growth cycle, so we drop these labels to simplify notation.

Consider a bulk competition experiment of a wild-type and a library of large number of mutants over a single batch growth cycle of time t_{sat} (Methods). The total relative fitness of mutant i is (main text ***Equation 22***)

$$\sigma_i = \text{logit}\, x_i(t_{\text{sat}}) - \text{logit}\, x_i(0), \tag{S82}$$

while its pairwise relative fitness compared to the wild-type is (main text ***Equation 23***)

$$s_{i,\text{wt}} = \text{logit}\, x_{i,\text{wt}}(t_{\text{sat}}) - \text{logit}\, x_{i,\text{wt}}(0). \tag{S83}$$

Using the coarse-graining rules from Appendix 1—section S12 (namely ***Equations S79 and S81***), we can express the total relative fitness of mutant i as a weighted sum of the pairwise relative fitnesses between the mutant and the wild-type and between the mutant and the rest of the mutant library:

$$\sigma_i \approx \frac{1}{x_{\text{wt}} + x_{\text{lib}\backslash i}} \left(x_{\text{wt}} s_{i,\text{wt}} + x_{\text{lib}\backslash i} s_{i,\ \text{lib}\backslash i} \right), \tag{S84}$$

where the notation $\text{lib}\backslash i$ refers to the mutant library excluding the mutant i. The approximation here is due to our assumption in ***Equation S79*** that selection is weak enough that the relative abundances of genotypes do not change too much over the growth cycle. Since we can rewrite the pairwise relative fitness between mutant i and the rest of the library as a difference between i and the wild-type and the rest of the library and the wild-type (using ***Equation S66***)

$$s_{i,\text{lib}\backslash i} = s_{i,\text{wt}} - s_{\text{lib}\backslash i,\text{wt}}, \tag{S85}$$

we insert this into ***Equation S84*** to obtain

$$\sigma_i \approx s_{i,\text{wt}} - \frac{x_{\text{lib}\backslash i}}{x_{\text{wt}} + x_{\text{lib}\backslash i}} s_{\text{lib}\backslash i,\text{wt}}. \tag{S86}$$

The difference between the total and pairwise relative fitness is therefore

$$\sigma_i - s_{i,\mathrm{wt}} \approx -\frac{x_{\mathrm{lib}\backslash i}}{x_{\mathrm{wt}} + x_{\mathrm{lib}\backslash i}} s_{\mathrm{lib}\backslash i,\mathrm{wt}}. \tag{S87}$$

Since mutant libraries in these experiments typically contain hundreds or thousands of mutants, the contribution of a single mutant i is small and thus we can assume that the properties of the mutant library excluding mutant i ($\mathrm{lib}\backslash i$) are approximately the same as the library as a whole (so that $x_{\mathrm{lib}\backslash i} \approx x_{\mathrm{lib}}$, $s_{\mathrm{lib}\backslash i,\mathrm{wt}} \approx s_{\mathrm{lib,wt}}$). This allows us to further simplify the error as

$$\sigma_i - s_{i,\mathrm{wt}} \approx -x_{\mathrm{lib}} s_{\mathrm{lib,wt}}. \tag{S88}$$

Equation S88 shows why this offset between the total and pairwise relative fitnesses is approximately independent of the focal mutant i (hence the constant shift for all mutant points in main text ***Figure 5C***). The sign of the error from the frame of reference depends on the mean fitness of the mutant library: a mutant library that is overall deleterious relative to the wild-type ($s_{\mathrm{lib,wt}} < 0$) causes the total relative fitness for a mutant σ_i to overestimate the mutant's pairwise relative fitness $s_{i,\mathrm{wt}}$. Intuitively, this is because the total relative fitness is comparing the mutant to a mixed population of wild-type and other mutants, which are on average worse competitors than the wild-type, which thus makes the mutant appear to be better than if it is just compared to the wild-type alone (compare top and bottom panel in main text ***Figure 5B***). ***Equation S88*** also shows that the error from the frame of reference can be reduced if the mutant library is neutral relative to the wild-type ($s_{\mathrm{lib,wt}} = 0$) or the mutant library has small relative abundance in the culture biomass ($x_{\mathrm{lib}} \ll 1$). In bulk competition experiments with barcoded mutant libraries, these assumptions are often not met since the mutant libraries tend to be overall deleterious (as in our simulated bulk competition for the yeast single-gene knockouts, see ***Appendix 1—figure 6***) and are inoculated at a high relative abundance (***Levy et al., 2015***; ***Pierce et al., 2021***; ***Wetmore et al., 2015***; ***Price et al., 2018***; ***Morin et al., 2018***). Since this makes the error in ***Equation S88*** significant, we instead recommend including barcoded wild-type strains as references in the bulk competition, so that pairwise fitness can be quantified relative to that (***Equation S83***) rather than using the total relative fitness. By using a mix of barcoded wild-type cells and non-barcoded wild-type cells, it is further possible to optimize this protocol and save on sequencing investment (***Schmidlin et al., 2024***).

Finally, we want to point out a difference between the best practice we recommend here (Discussion) and a widespread practice in estimating fitness estimates in bulk competition experiments. In practice, transposon-seq experiments that grow the mutant library by itself start with an estimate of total relative fitness and then subtract the median total relative fitness of the knockouts (***Wetmore et al., 2015***; ***Price et al., 2018***; ***Martinson et al., 2023***; ***Morin et al., 2018***) or a mean total relative fitness (***Levy et al., 2015***; ***Nguyen Ba et al., 2019***; ***Johnson et al., 2019***). However, these corrections are not explicitly founded in the choice of a reference group (like a set of neutral genotypes or a wild-type), making the correction appear ad hoc (***Wetmore et al., 2015***; ***Martinson et al., 2023***; ***Morin et al., 2018***), or the reference is a strain that is not part of the culture, like in the fitness estimates for barcoded lineages that are evaluated against the initial ancestor without that ancestor actually being present (***Levy et al., 2015***; ***Nguyen Ba et al., 2019***; ***Johnson et al., 2019***). To make things more confusing, even those studies that do include a wild-type then describe their method as an estimate of total relative fitness of the mutant under the log encoding, subtracted by the total relative fitness of the wild-type under the log encoding (***Couce et al., 2024***; ***Bakerlee et al., 2021***; ***Schmidlin et al., 2024***). The result is a pairwise relative fitness under the logit encoding (***Equation 25***), but presenting it this way obscures that choice of encoding and the relationship to the classic, logit-based selection coefficient used in pairwise competition experiments (***Equation 7***). We hope that our framework can provide more clarity: The choice of the reference group happens at the level of relative abundance, by calculating a pairwise relative abundance (***Equation 20*** or ***Equation S69***), and this removes the need for any correction on the fitness values themselves.

S14. Pairwise relative fitness using an explicit model of population dynamics

In the model of population dynamics (main text Methods, ***Equation 12a***), we can calculate the pairwise relative fitness of genotypes based on the approximation of the saturation time (Appendix

1—section S7; ***Manhart et al., 2018***; ***Manhart and Shakhnovich, 2018***). The pairwise relative fitness of genotype i relative to genotype j (per-cycle and under the logit encoding) is

$$s^{\text{logit}}_{ij,\text{cycle}} \approx s_{ij,\text{lag}} + s_{ij,\text{growth}} + s_{ij,\text{coupling}}, \tag{S89a}$$

where

$$s_{ij,\text{lag}} = -\frac{\bar{\tau}}{\tau_i \tau_j}\Delta\lambda_{ij}, \tag{S89b}$$

$$s_{ij,\text{growth}} = -\frac{\bar{\tau}}{\tau_i \tau_j}\Delta\tau_{ij}\text{LFC}, \tag{S89c}$$

$$s_{ij,\text{coupling}} = -\frac{\bar{\tau}\bar{Y}}{\tau_i \tau_j} \times \sum_k \frac{x_k}{\tau_k Y_k}\left(\Delta\tau_{ik}\Delta\lambda_{kj} - \Delta\lambda_{ik}\Delta\tau_{kj}\right). \tag{S89d}$$

The e-fold growth time for genotype j is $\tau_j = 1/g_j$, and the terms $\Delta\lambda_{ij} = \lambda_i - \lambda_j$ and $\Delta\tau_{ij} = \tau_i - \tau_j$ are the differences between the two genotypes' lag times and growth times. Since the terms in ***Equation S89d*** depend on the covariation between growth and lag, we interpret these terms as couplings between the growth and lag phases; they are zero if only two genotypes are present.

S15. Fitness error from higher-order interactions between pairwise and bulk competition experiments

In this section, we calculate the error in relative fitness of a mutant arising from higher-order interactions in bulk competition experiments with large mutant libraries, compared to the 'true' relative fitness in pairwise competitions between just the focal mutant and wild-type alone. Here, we only consider relative fitness under the logit encoding and measured per growth cycle, so we drop these labels to simplify notation. Let the pairwise relative fitness of mutant i compared to the wild-type (main text ***Equation 23***) be

$$s^{\text{pair}}_{i,\text{wt}} = \text{logit}\, x^{\text{pair}}_{i,\text{wt}}(t^{\text{pair}}_{\text{sat}}) - \text{logit}\, x_{i,\text{wt}}(0) \tag{S90}$$

in the pairwise competition with the wild-type alone, and

$$s^{\text{bulk}}_{i,\text{wt}} = \text{logit}\, x^{\text{bulk}}_{i,\text{wt}}(t^{\text{bulk}}_{\text{sat}}) - \text{logit}\, x_{i,\text{wt}}(0) \tag{S91}$$

in the bulk competition with all other mutants in the library. The superscripts pair and bulk indicate that the dynamics of $x_{i,\text{wt}}(t)$ and the saturation time t_{sat} may be different in the two competitions. The difference between these two measurements of relative fitness is

$$\begin{aligned}\Delta s_{i,\text{wt}} &= s^{\text{bulk}}_{i,\text{wt}} - s^{\text{pair}}_{i,\text{wt}} \\ &= s^{\text{pair}}_{i,\text{wt}}\left(\frac{s^{\text{bulk}}_{i,\text{wt}}}{s^{\text{pair}}_{i,\text{wt}}} - 1\right).\end{aligned} \tag{S92}$$

Since the difference between the bulk and pairwise competitions is the presence of the other mutants in the library, we interpret this difference as the *fitness error from higher-order interactions* among the mutants.

We now calculate how this error depends on the underlying growth traits of the genotypes using the population dynamics model (main text Methods, ***Equation 12a***) and the explicit expression for relative fitness from Appendix 1—section S14. Based on the approximate pairwise relative fitness in this model (***Equations S89a–S89d***), the relative fitness in the pairwise competition is the sum of two terms

$$s^{\text{pair}}_{i,\text{wt}} = s^{\text{pair}}_{i,\text{wt,lag}} + s^{\text{pair}}_{i,\text{wt,growth}}, \tag{S93}$$

while the relative fitness in the bulk competition is the sum of three terms

$$s_i^{\text{bulk}} = s_{i,\text{lag}}^{\text{bulk}} + s_{i,\text{growth}}^{\text{bulk}} + s_{i,\text{coupling}}^{\text{bulk}}, \tag{S94}$$

where the third term represents the coupling between growth and lag phases present only in populations with more than two genotypes (***Equation S89d***).We define the higher-order effects on the selection for lag time as

$$\Delta s_{i,\text{wt,lag}} = s_{i,\text{wt,lag}}^{\text{bulk}} - s_{i,\text{wt,lag}}^{\text{pair}}. \tag{S95}$$

Using ***Equation S89b***, we can express this in terms of the underlying traits as

$$\Delta s_{i,\text{wt,lag}} = s_{i,\text{wt,lag}}^{\text{pair}} \cdot \frac{\Delta \bar{\tau}_i}{\bar{\tau}^{\text{pair},i}}, \tag{S96}$$

where $\Delta \bar{\tau}_i = \bar{\tau}^{\text{bulk}} - \bar{\tau}^{\text{pair},i}$ is the difference in effective e-fold growth times (***Equation S40***) in the bulk competition and in the pairwise competition of mutant i and the wild-type.

We similarly define the higher-order effects in the selection on growth rate as

$$\Delta s_{i,\text{wt,growth}} = s_{i,\text{wt,growth}}^{\text{bulk}} - s_{i,\text{wt,growth}}^{\text{pair}}, \tag{S97}$$

and calculate $s_{i,\text{wt,growth}}^{\text{bulk}}$ and $s_{i,\text{wt,growth}}^{\text{pair}}$ from ***Equation S89c*** to get the expression

$$\Delta s_{i,\text{wt,growth}} = -\frac{\Delta \tau_{i,\text{wt}}}{\tau_{\text{wt}} \tau_i} \left(\bar{\tau}^{\text{bulk}} \text{LFC}^{\text{bulk}} - \bar{\tau}^{\text{pair},i} \text{LFC}^{\text{pair},i} \right), \tag{S98}$$

where LFC^{bulk} is the log fold-change (***Equation S42***) of the total biomass in the bulk competition and $\text{LFC}^{\text{pair},i}$ is the log fold-change of the total biomass in the pairwise competition between mutant i and the wild-type. We note that total biomass growth in the bulk competition LFC^{bulk} depends on the mutant library through the effective biomass yield (***Equation S41***), but this dependence is weak because the yield enters only logarithmically into ***Equation S42***. We thus assume that the bulk and pairwise competition have equal biomass growth ($\text{LFC}^{\text{bulk}} \approx \text{LFC}^{\text{pair},i}$) for all mutants i such that the higher-order effect on the growth rate selection (***Equation S98***) is proportional to the increase in the mean doubling time

$$\Delta s_{i,\text{wt,growth}} \approx s_{i,\text{wt,growth}}^{\text{pair}} \frac{\Delta \bar{\tau}_i}{\bar{\tau}_{\text{pair},i}}. \tag{S99}$$

Since this has the same form as the higher-order effect on lag time selection in ***Equation S96***, we can combine ***Equations S99 and S96*** into

$$\Delta s_{i,\text{wt,lag}} + \Delta s_{i,\text{wt,growth}} \approx s_{i,\text{wt}}^{\text{pair}} \frac{\Delta \bar{\tau}_i}{\bar{\tau}^{\text{pair},i}}. \tag{S100}$$

Because the effective growth time in the pairwise competition $\bar{\tau}^{\text{pair},i}$ is approximately just the effective growth time of the wild-type alone τ_{wt} (assuming the mutant is competed against it at low initial relative abundance), this means that

$$\frac{\Delta s_{i,\text{wt,lag}} + \Delta s_{i,\text{wt,growth}}}{s_{i,\text{wt}}^{\text{pair}}} \approx \left(\frac{\bar{\tau}^{\text{bulk}}}{\tau_{\text{wt}}} - 1 \right). \tag{S101}$$

That is, the relative error of lag and growth selection from higher-order interactions is approximately independent of the individual mutant, but rather depends on properties of the wild-type (τ_{wt}) and the whole mutant library (through $\bar{\tau}^{\text{bulk}}$). This is why we observe an approximately constant slope across all mutants in ***Appendix 1—figure 22*** (dark orange points) when comparing the error against the pairwise relative fitness. The slight deviation from the constant slope is due to our approximation that the LFCs are the same between the bulk and pairwise competitions; this is a good approximation for the yeast deletion library but not exactly true, and hence causes a slightly different scaling between the growth Δs_{growth} and lag Δs_{lag} error terms compared to ***Equation S101***.

Finally, we note that the growth-lag coupling terms $s^{\text{bulk}}_{i,\text{wt,coupling}}$ do not have a simple scaling with pairwise relative fitness since they depend quadratically on trait differences; this is shown as the bright orange points in ***Appendix 1—figure 22***. In the main text, we therefore refer to $\Delta s_{i,\text{wt,lag}} + \Delta s_{i,\text{wt,growth}}$ as the fitness-dependent error and the $s^{\text{bulk}}_{i,\text{wt,coupling}}$ as the fitness-independent error from higher-order interactions.

S16. Choosing the mutant library abundance in bulk competition experiments

Appendix 1—section S15 showed that measuring relative fitness of a mutant in a bulk competition (with a library of other mutants also present) entails an error due to higher-order interactions among the mutants, compared to measuring relative fitness in a pairwise competition consisting of just the mutant and wild-type. Here, we show how this error depends on the relative abundance of the mutant library in the bulk competition, so that we can estimate the range of library abundances that keep the error below a desired threshold.

Calculating the relative error on fitness

Let the absolute error in relative fitness from higher-order interactions for a mutant i be $\Delta s_{i,\text{wt}}$ (***Equation S92***). Let the relative fitness of this mutant in a pairwise competition be $s^{\text{pair}}_{i,\text{wt}}$ (***Equation S90***). Since the error $\Delta s_{i,\text{wt}}$ depends on the relative abundance x_{lib} of the whole mutant library, our goal is to determine what range of x_{lib} keeps the error in relative fitness (compared to the 'true' relative fitness in the pairwise competition) below a chosen threshold ϵ:

$$\left| \frac{\Delta s_{i,\text{wt}}}{s^{\text{pair}}_{i,\text{wt}}} \right| < \epsilon. \tag{S102}$$

In Appendix 1—section S15 we calculated the dependence of $\Delta s_{i,\text{wt}}$ on the underlying growth traits. However, since here we are mainly concerned with the dependence on the library abundance x_{lib}, we present an alternative calculation that better captures that dependence.

We start by pointing out that we can express the relative fitness in pairwise (***Equation S90***) and bulk competitions (***Equation S91***) in terms of the saturation times for these competitions, using the explicit solution to the population dynamics model in main text ***Equation 15***:

$$s^{\text{pair}}_{i,\text{wt}} = g_i(t^{\text{pair},i}_{\text{sat}} - \lambda_i) - g_{\text{wt}}(t^{\text{pair},i}_{\text{sat}} - \lambda_{\text{wt}}), \tag{S103}$$

$$s^{\text{bulk}}_{i,\text{wt}} = g_i(t^{\text{bulk}}_{\text{sat}} - \lambda_i) - g_{\text{wt}}(t^{\text{bulk}}_{\text{sat}} - \lambda_{\text{wt}}). \tag{S104}$$

We can thus express the error from higher-order interactions (***Equation S92***) as

$$\Delta s_{i,\text{wt}} = \Delta g_{i,\text{wt}}(t^{\text{bulk}}_{\text{sat}} - t_{\text{sat}}{}^{\text{pair},i}), \tag{S105}$$

where $\Delta g_{i,\text{wt}} = g_i - g_{\text{wt}}$. ***Equation S105*** shows that the mutant library affects the fitness of individual mutants $s^{\text{bulk}}_{i\text{wt}}$ by changing the saturation time. Mathematically, this is equivalent to the results of Appendix 1—section S15, which showed how the difference in effective e-fold growth times $\bar{\tau}$ between bulk and pairwise competitions primarily mediated the higher-order effects, but expressed in terms of the saturation time t_{sat} (which is not identical to $\bar{\tau}$ but related through ***Equation S38***). The error in ***Equation S105*** is also proportional to the growth rate advantage of the mutant compared to the wild-type. In particular, mutant genotypes that only differ in lag time are not affected by the mutant library since their advantage is accrued once at the beginning of the growth cycle and therefore does not scale with the total time of competition.

According to ***Equation S38***, the saturation time t_{sat} depends on the effective lag time $\bar{\lambda}$ (***Equation S39***), effective e-fold growth time $\bar{\tau}$ (***Equation S40***), and the log fold-change LFC (***Equation S42***) for the competition. To simplify the calculation, we introduce a few assumptions. We assume all mutants have the same yields as the wild-type ($Y_i = Y_{\text{wt}}$) such that the LFCs in the bulk and pairwise competitions are identical ($\text{LFC}^{\text{bulk}} = \text{LFC}^{\text{pair}}$). We also assume that the relative abundance of the

mutant in the pairwise competition is small enough that the saturation time in that case is set entirely by the wild-type traits:

$$t_{\text{sat}}^{\text{pair},i} \approx \lambda_{\text{wt}} + \tau_{\text{wt}}\text{LFC}. \tag{S106}$$

Note that this means that the difference in saturation times is independent of the specific mutant i; the only dependence of the mutant i on the overall error from higher-order interactions is through the difference in growth rates in ***Equation S105***.

We can thus write the fitness error as

$$\Delta s_{i,\text{wt}} \approx \Delta g_{i,\text{wt}} \left[(\bar{\lambda}^{\text{bulk}} - \lambda_{\text{wt}}) + (\bar{\tau}^{\text{bulk}} - \tau_{\text{wt}})\text{LFC} \right]. \tag{S107}$$

Equation S107 depends on the mutant library abundance x_{lib} through the effective traits $\bar{\lambda}^{\text{bulk}}$ and $\bar{\tau}^{\text{bulk}}$ of the bulk competition (Appendix 1—section S7). Inserting ***Equation S50; Equation S51*** into ***Equation S107***, we obtain

$$\Delta s_{i,\text{wt}} = \Delta g_{i,\text{wt}} \quad \frac{x_{\text{lib}} g_{\text{lib}}}{x_{\text{lib}} g_{\text{lib}} + (1 - x_{\text{lib}}) g_{\text{wt}}} \cdot \left[\Delta\lambda_{\text{lib,wt}} + \text{LFC}\Delta\tau_{\text{lib,wt}} \right], \tag{S108}$$

where $\Delta\lambda_{\text{lib,wt}} = \lambda_{\text{lib}} - \lambda_{\text{wt}}$ is the difference in lag times, and $\Delta\tau_{\text{lib,wt}} = \tau_{\text{lib}} - \tau_{\text{wt}}$ the difference in e-fold growth times (reciprocal growth rates), between the library (defined according to ***Equations S47 and S48***) and the wild-type. All the dependence on the library relative abundance x_{lib} is now contained in the fraction outside the square brackets in ***Equation S108***.

Since the relative fitness of the mutant library as a whole compared to the wild-type in bulk competition is (using ***Equations S89a–S89d***)

$$s_{\text{lib,wt}}^{\text{bulk}} = -\frac{\bar{\tau}^{\text{bulk}}}{\tau_{\text{lib}}\tau_{\text{wt}}}\Delta\lambda_{\text{lib,wt}} - \frac{\bar{\tau}^{\text{bulk}}}{\tau_{\text{lib}}\tau_{\text{wt}}}\Delta\tau_{\text{lib,wt}}\text{LFC}^{\text{bulk}}, \tag{S109}$$

we can rewrite ***Equation S108*** as

$$\Delta s_{i,\text{wt}} = -x_{\text{lib}} s_{\text{lib,wt}}^{\text{bulk}} \frac{\Delta g_{i,\text{wt}}}{g_{\text{wt}}}. \tag{S110}$$

This shows that a mutant library that is neutral relative to the wild-type in the bulk competition ($s_{\text{lib,wt}}^{\text{bulk}} = 0$) removes the error from higher-order interactions, even when that neutrality is based on a trade-off between growth rates and lag times ($\Delta\lambda_{\text{lib,wt}} = -\Delta\tau_{\text{lib,wt}}\text{LFC}^{\text{bulk}}$). We note that the error of higher-order interactions (***Equation S110***) appears similar to the error from the frame of reference (***Equation S88***), but the former includes the relative mutant growth rate $\Delta g_{i,\text{wt}}/g_{\text{wt}}$ as an additional pre-factor.

Calculating the upper bound on relative abundance of the mutant library

To calculate the maximum relative library abundance that keeps the relative error below the threshold ϵ, we input the absolute error in ***Equation S108*** into the relative error bound of ***Equation S102*** and rearrange to isolate the dependence on the library abundance x_{lib}:

$$\frac{x_{\text{lib}} g_{\text{lib}}}{x_{\text{lib}} g_{\text{lib}} + (1 - x_{\text{lib}}) g_{\text{wt}}} < \epsilon A_i, \tag{S111}$$

where

$$A_i = \left| \frac{S_{i,\text{wt}}^{\text{pair}}}{\Delta g_{i,\text{wt}} \left(\Delta\lambda_{\text{lib,wt}} + \text{LFC}\Delta\tau_{\text{lib,wt}} \right)} \right| \tag{S112}$$

depends on the focal mutant i but does not depend on the library abundance x_{lib}. The left-hand side of ***Equation S111*** varies between zero and one as a function of x_{lib}. This means that if $\epsilon A_i > 1$, any value of x_{lib} will satisfy ***Equation S111***, meaning that the relative error on mutant i from higher-order interactions will always be less than ϵ. For example, this holds when the mutant i has the same

growth rate as the wild-type ($\Delta g_{i,\mathrm{wt}} = 0$, which causes $A_i \to \infty$), even if it varies in lag time and/or other mutants have variation in growth rates.

We thus next consider the case where $\epsilon A_i < 1$. We multiply both sides of ***Equation S111*** by the denominator on the left-hand side (always positive) to obtain

$$x_{\mathrm{lib}} g_{\mathrm{lib}} < \epsilon A_i \left(x_{\mathrm{lib}} g_{\mathrm{lib}} + (1 - x_{\mathrm{lib}}) g_{\mathrm{wt}} \right), \tag{S113}$$

and then collect all the terms involving x_{lib} on the left-hand side:

$$x_{\mathrm{lib}}((1 - \epsilon A_i) g_{\mathrm{lib}} + \epsilon A_i g_{\mathrm{wt}}) < \epsilon A_i g_{\mathrm{wt}}. \tag{S114}$$

Since $\epsilon A_i < 1$, the factor multiplying x_{lib} on the left-hand side of ***Equation S114*** must be positive and thus we can divide both sides to obtain an upper bound on the library abundance x_{lib} such that the relative error on fitness is less than ϵ:

$$x_{\mathrm{lib}} < \frac{\epsilon A_i g_{\mathrm{wt}}}{(1 - \epsilon A_i) g_{\mathrm{lib}} + \epsilon A_i g_{\mathrm{wt}}}. \tag{S115}$$

Since ϵ will typically be small, we can simplify the right-hand side of ***Equation S115*** by approximating it to first-order in ϵ:

$$x_{\mathrm{lib}} \lessapprox \epsilon A_i \frac{g_{\mathrm{wt}}}{g_{\mathrm{lib}}}. \tag{S116}$$

This approximation holds as long as $\epsilon A_i (g_{\mathrm{lib}} - g_{\mathrm{wt}})/g_{\mathrm{lib}} \ll 1$.

The maximum mutant library abundance determined by ***Equation S115 or Equation S116*** is specific to a single mutant genotype *i*, meaning that the relative fitness errors for other mutants may exceed ϵ even if the inequality for mutant *i* is satisfied. To keep the relative fitness errors for all mutants less than ϵ, we need to choose a library abundance x^*_{lib} such that

$$\max_{\mathrm{mut}\ j} \left| \frac{\Delta s_{j,\mathrm{wt}}}{s^{\mathrm{pair}}_{j,\mathrm{wt}}} \right| < \epsilon. \tag{S117}$$

This means that ***Equation S116*** must be satisfied for all mutants *j*:

$$x^*_{\mathrm{lib}} = \min_{\mathrm{muts}\ j} \epsilon A_j \frac{g_{\mathrm{wt}}}{g_{\mathrm{lib}}}. \tag{S118}$$

Thus, we must determine the minimum value of A_j over all mutants *j*. Using the definition in ***Equation S112***, A_j is minimized for the mutant with minimum value of

$$\left| \frac{s^{\mathrm{pair}}_{j,\mathrm{wt}}}{\Delta g_{j,\mathrm{wt}}} \right| = \left| \frac{1}{g_{\mathrm{wt}}} \mathrm{LFC} - g_j \frac{\Delta \lambda_{j,\mathrm{wt}}}{\Delta g_{j,\mathrm{wt}}} \right|, \tag{S119}$$

where we have calculated the pairwise relative fitness in ***Equation S103*** using $t^{\mathrm{pair},i}_{\mathrm{sat}}$ from ***Equation S106***. Mutants that minimize ***Equation S119*** are those with trade-offs between lag times and growth rates such that their overall pairwise relative fitness with respect to the wild-type is zero. This makes sense, since these mutants will have a relative fitness close to zero in the pairwise competition ($|s^{\mathrm{pair}}_{j,\mathrm{wt}}| \ll 1$), but nonzero fitness relative to the wild-type in the bulk competition as the relative selection on the lag time and growth rate shifts (e.g., because $\bar{\tau}^{\mathrm{bulk}} > \bar{\tau}^{\mathrm{pair}}$ in ***Equations S89a–S89d***).

Special case of variation in growth rates only

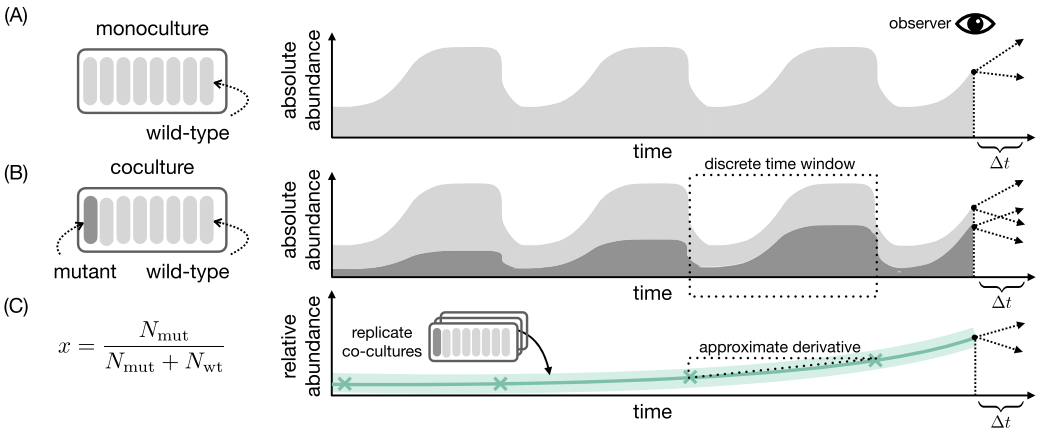
To determine an even simpler estimate on the maximum mutant library abundance, we consider the special case where genotypes vary only in growth rates and not lag times. Using the definition in ***Equation S112***, $A_i = g_{\mathrm{lib}}/(g_{\mathrm{wt}} - g_{\mathrm{lib}})$ for all mutants *i*, and thus there is a single bound on library abundance for all mutants (using ***Equation S116***):

$$x_{\mathrm{lib}} < \epsilon \left| \frac{g_{\mathrm{wt}}}{g_{\mathrm{wt}} - g_{\mathrm{lib}}} \right|. \tag{S120}$$

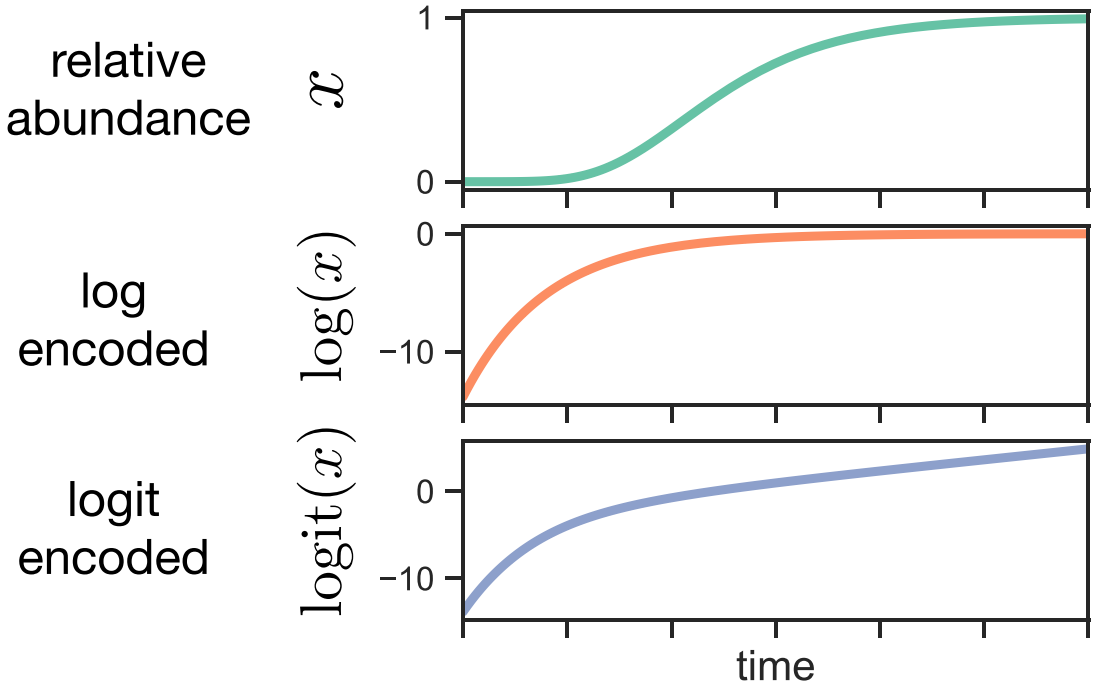
This is the same as ***Equation 11*** in the main text.

We test ***Equation 11*** using our simulated competition data for the yeast single-gene deletion library (Methods) with variation in all three traits: lag time, growth rate, and biomass yield (***Appendix 1—figure 4B, C***). We compute the growth rates of the mutant library ($g_{\mathrm{lib}} = 0.389\,\mathrm{hr}^{-1}$ using ***Equation S40***) and the wild-type ($g_{\mathrm{wt}} = 0.406\,\mathrm{hr}^{-1}$). Using a relative error threshold of $\epsilon = 0.01$, the maximum mutant library relative abundance according to main text ***Equation 11*** is $x_{\mathrm{lib}} = 24.6\%$. ***Figure 5D*** in the main text shows that this mutant library abundance indeed is able to keep the relative error below the threshold for mutants with high relative fitness, but, as expected, this mutant library abundance fails for mutants close to neutrality.

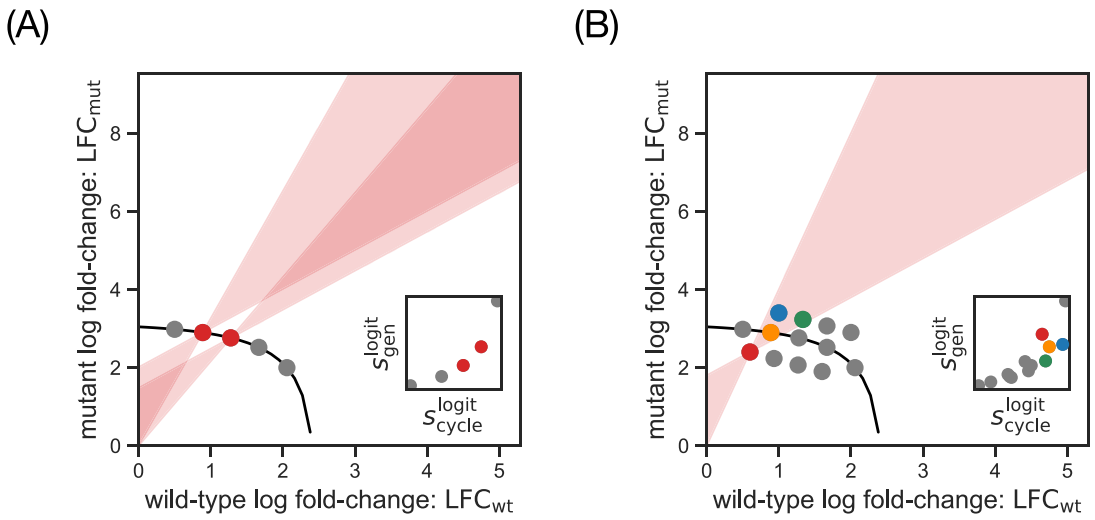
We furthermore compute the maximum library abundance with ***Equation S118***, based on the precise trait variation in our data set. The mutant library has an effective lag time $\lambda_{\mathrm{lib}} = 1.95\,\mathrm{hr}$ (compared to wild-type lag time $\lambda_{\mathrm{wt}} = 1.92\,\mathrm{hr}$) and an effective e-fold growth time $\tau_{\mathrm{lib}} = 2.57\,\mathrm{hr}$ (compared to the wild-type $\tau_{\mathrm{wt}} = 2.46\,\mathrm{hr}$), leading to an overall negative relative fitness $s^{\mathrm{bulk}}_{\mathrm{lib,wt}} = -0.198$ based on an LFC value of $\mathrm{LFC}^{\mathrm{bulk}} = \log 100$ (a typical fold-change in our data set) and the limit of low relative abundance of the library. We insert these trait values into ***Equation S118*** and obtain a maximum mutant library abundance $x^{*}_{\mathrm{lib}} = 0.01\%$. ***Figure 5D*** in the main text shows that this much smaller mutant library abundance is able to keep the relative error below the desired threshold for all mutant genotypes. Note, however, this is still not fully exact since we have ignored the underlying variation in biomass yield in our trait data set.



Appendix 1—figure 1. Predicting the absolute and relative abundance of microbial populations. (**A**) Example time series of absolute abundance for a single microbial population (light gray). The observer (eye symbol) of the time series at time *t* can ask about the future trend in absolute abundance (arrows). (**B**) Same as panel A but for two microbial strains, such as a wild-type and a mutant. The absolute abundance of the wild-type strain (light gray) is stacked on top of the absolute abundance of the mutant strain (dark gray). (**C**) The relative abundance for the mutant strain corresponding to panel B. We sketch the mean relative abundance *x* over time (green line) inferred from multiple replicate cocultures. An error band (light green) around the time series demonstrates the variation between replicates.



Appendix 1—figure 2. The effect of encodings on a non-logistic relative abundance trajectory. Example trajectory of relative abundance x (top panel) for a mutant invading and eventually replacing a wild-type population, simulated with the Gompertz equation $dx/dt = rx\log(1/x)$. Below, we show the Gompertz trajectory under the encodings $\log x$ and $\mathrm{logit}\, x = \log(x/(1-x))$. Compare to main text ***Figure 1A*** for a trajectory simulated with the logistic equation.

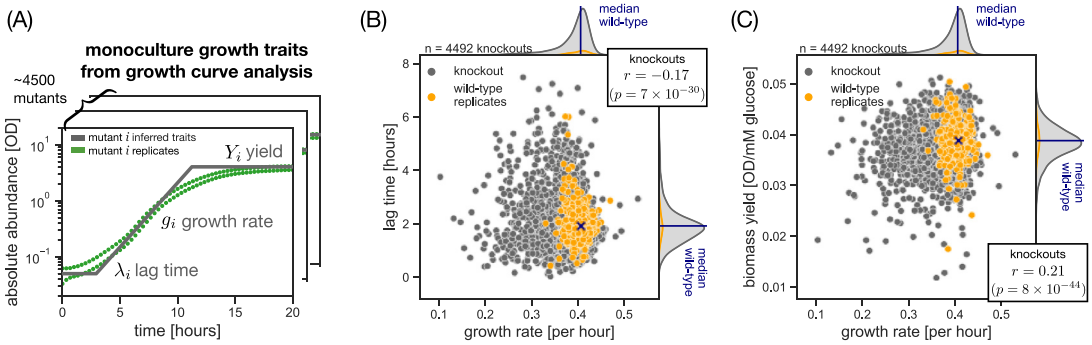


Appendix 1—figure 3. The variation of wild-type and mutant log fold-change under resource consumption constraints. (**A**) Schematic fold-change variation under a perfect resource consumption constraint between wild-type and mutant. Each dot corresponds to a mutant strain in a 1:1 competition growth cycle with the wild-type strain (Appendix 1—section S5). There is negative covariation between mutant and wild-type LFCs because the resource constraint forces one to decrease if the other increases. For our model of population dynamics, we can calculate this constraint exactly (black line: ***Equation S36*** in Appendix 1—section S5). For two mutants (red points) we highlight the bow tie-shaped areas (red shading; compare to main text ***Figure 1D***) where other competitions must lie to have a rank discrepancy between relative fitness per-cycle $s^{\mathrm{logit}}_{\mathrm{cycle}}$ and per-generation $s^{\mathrm{logit}}_{\mathrm{gen}}$ with those mutants, but they are inevitably empty due to the negative covariance across competitions from the resource constraint. Inset: Correlation of fitness per-cycle and per-generation for these same competitions, showing no rank discrepancy. (**B**) Same as panel A but schematically showing how a deviation from the resource consumption

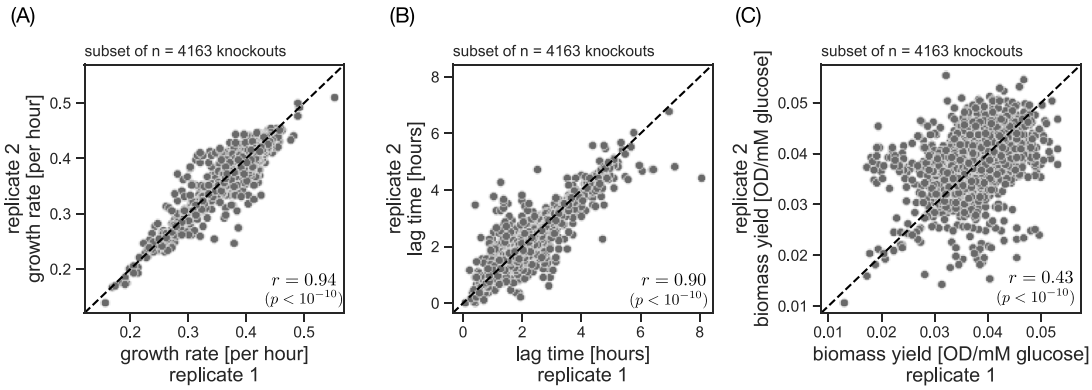
Appendix 1—figure 3 continued on next page

Appendix 1—figure 3 continued

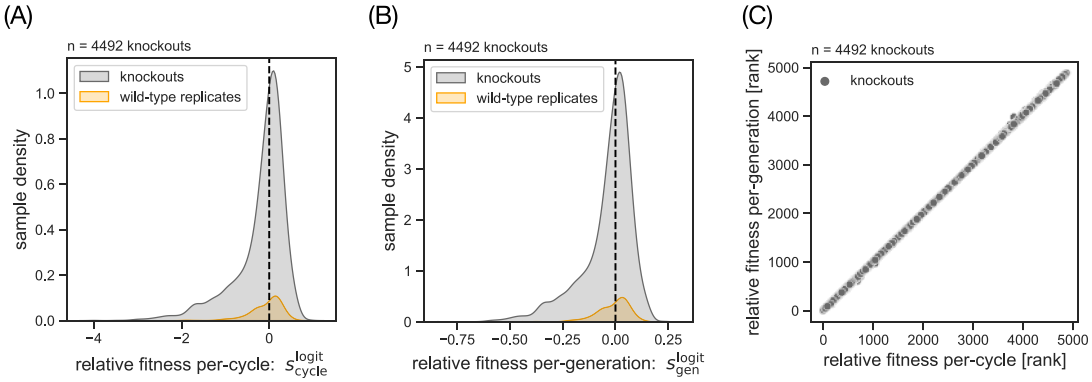
constraint can allow competitions to fall in each other's red bow tie-shaped regions (e.g., blue, orange, and green competitions compared to the red one), and thus have a rank discrepancy between relative fitness per-cycle $s^{\text{logit}}_{\text{cycle}}$ and per-generation $s^{\text{logit}}_{\text{gen}}$ (inset).



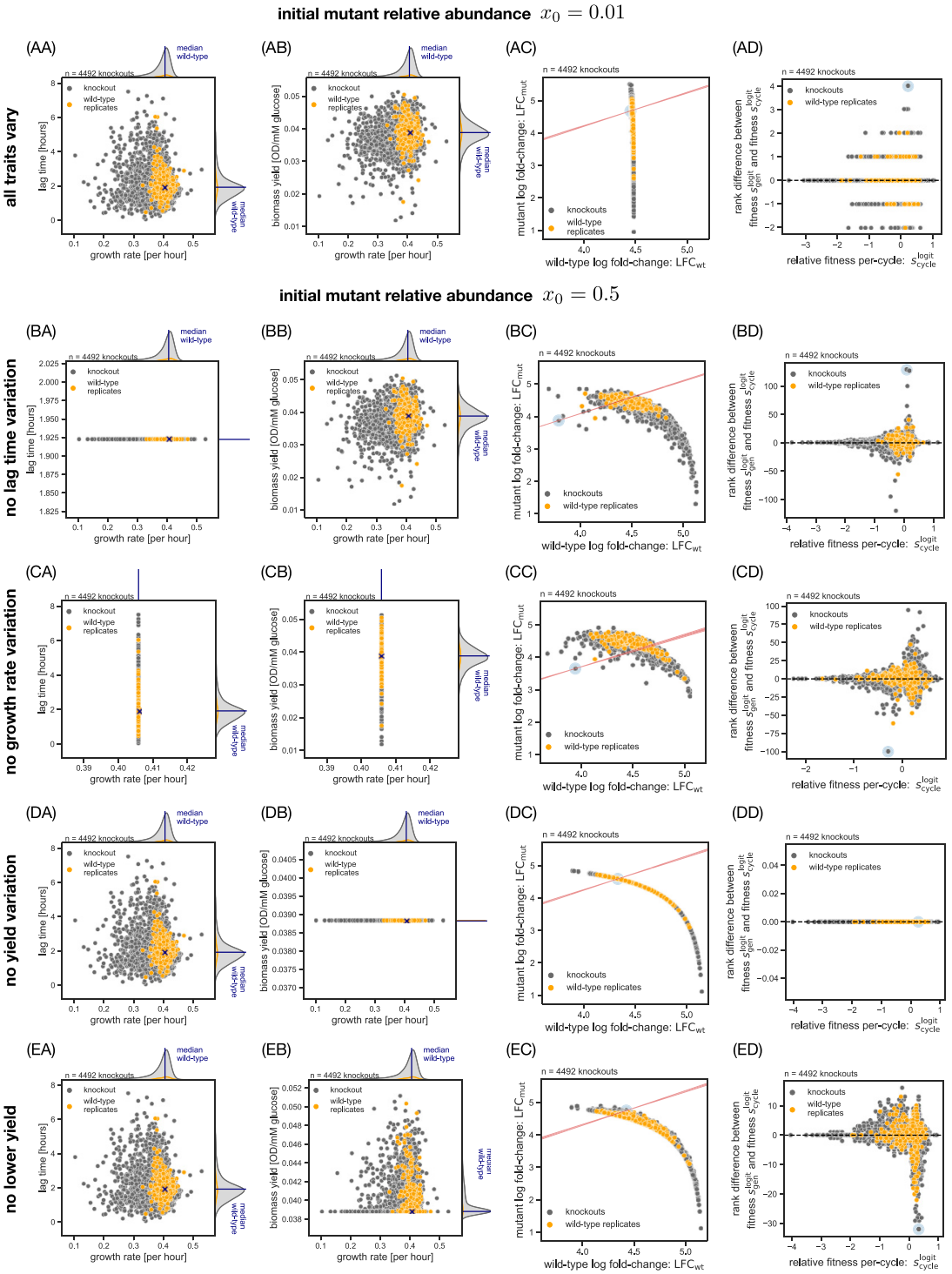
Appendix 1—figure 4. Empirical trait distribution for single gene-knockouts of yeast. (**A**) Overview of the growth curve data set and the estimated growth traits for the knockout library of *Saccharomyces cerevisiae* (Methods) (***Warringer et al., 2003***). (**B**) Covariation between estimated maximum growth rate g and lag time λ across all mutant strains (gray dots; Pearson correlation coefficient $r = -0.17$, $p = 7 \times 10^{-30}$) as well as wild-type replicates (orange dots; $r = -0.16$, $p = 0.002$). The reference wild-type strain for our pairwise coculture simulations is defined by the median trait values (black cross) of all wild-type replicates. (**C**) Covariation between measured maximum growth rate g and biomass yield Y across all mutant strains (gray dots; $r = 0.21$, $p = 8 \times 10^{-44}$) as well as wild-type replicates (orange dots; $r = -0.06$, $p = 0.25$). Histograms on the top and right sides of panels B and C are marginal distributions along each axis, with colors matching the scatter points and the vertical black line marking the median wild-type trait value.



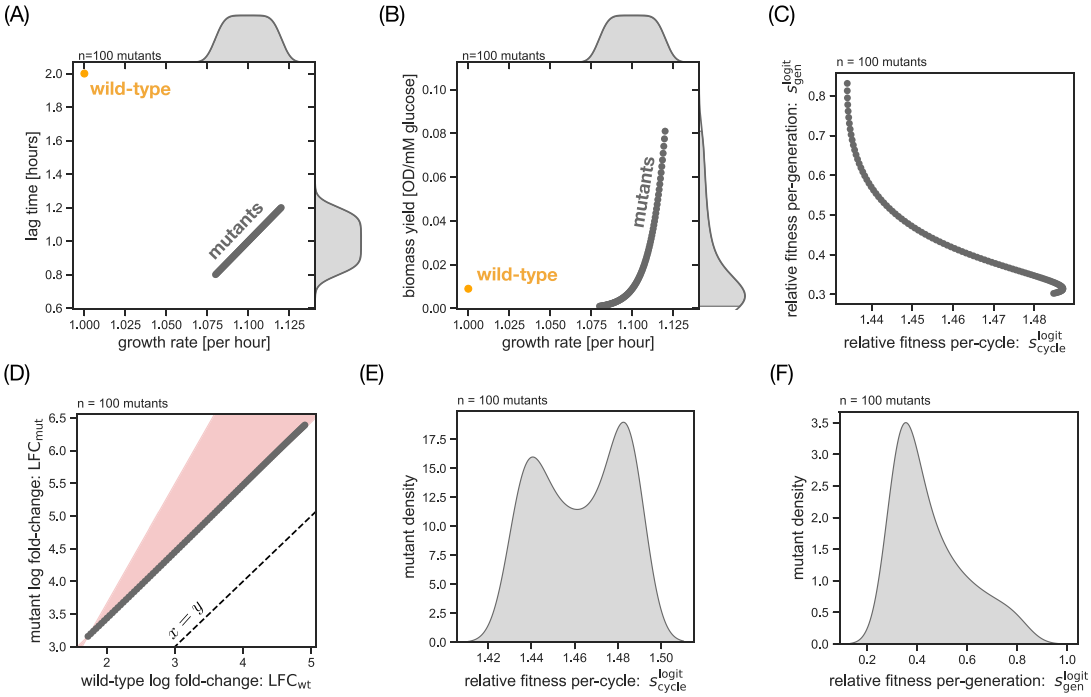
Appendix 1—figure 5. Replicate measurements for growth rate, lag time, and yield in our empirical trait data set. (**A**) Covariation of growth rate between replicate measurements of the knockouts (gray dots; Pearson correlation coefficient $r = 0.94$, $p = 0.00$). Each dot represents a mutant genotype from the single-gene knockout collection in *Saccharomyces cerevisiae* (***Warringer et al., 2003***). For the vast majority of genotypes in our data set (4163 out of 4492 knockouts) we are able to fit two traits from two independent growth curve measurements (***Appendix 1—figure 4A***; Methods). (**B**) Covariation of lag time between replicate measurements of the knockouts (gray dots; $r = 0.90$, $p = 0.00$) (**C**) Covariation of biomass yield between replicate measurements of the knockouts (gray dots; $r = 0.43$, $p = 4.81 \times 10^{-188}$).



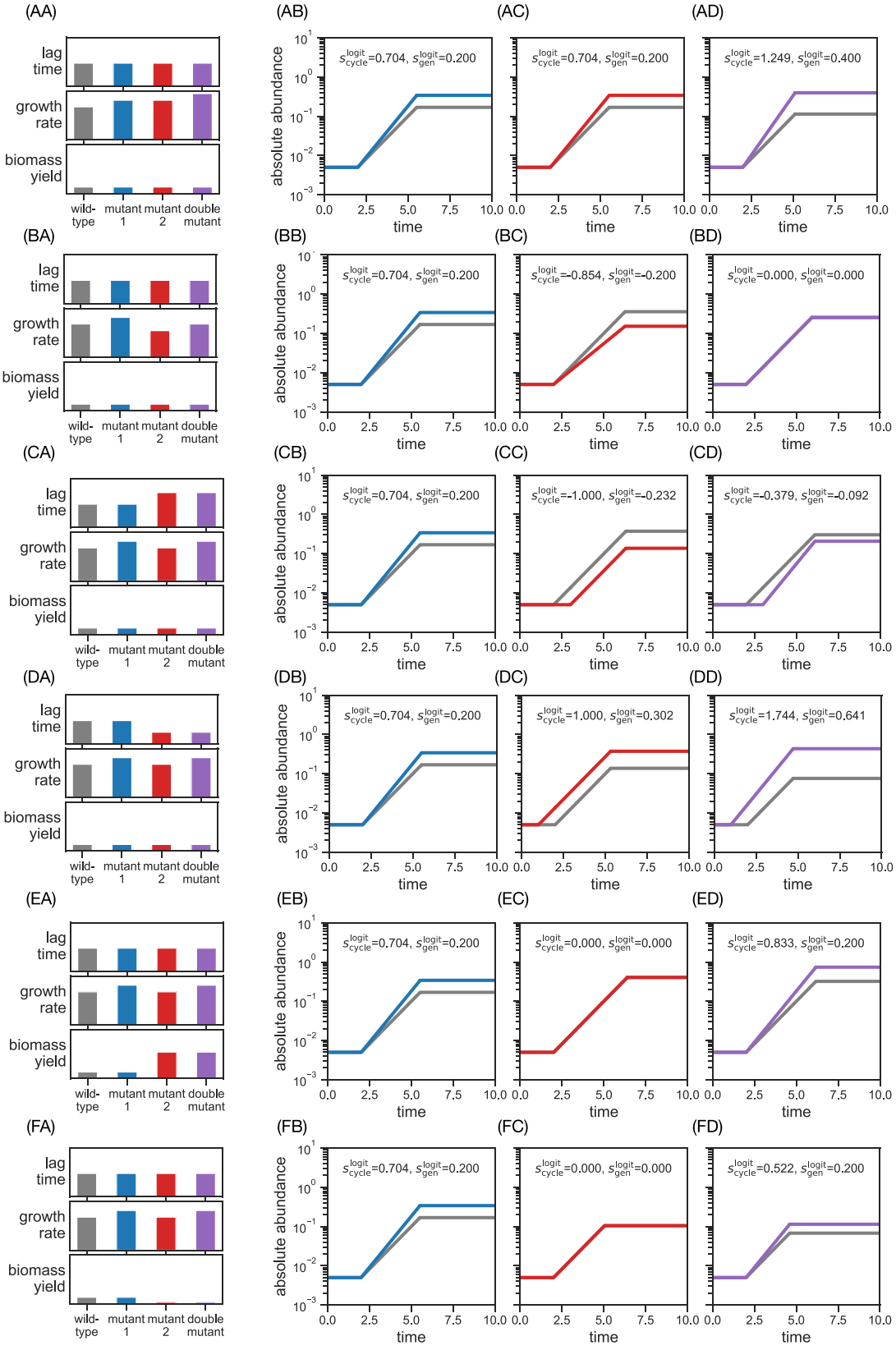
Appendix 1—figure 6. The distribution of fitness effects under relative fitness per-cycle and per-generation. (**A**) Distribution of relative fitness per-cycle $s^{\text{logit}}_{\text{cycle}}$ for the single-gene knockouts of yeast (gray) and wild-type replicates (orange) in our data set (***Appendix 1—figure 4A***, Methods) (***Warringer et al., 2003***), based on the fitness data from main text ***Figure 2B***. The vertical black line marks zero relative fitness (e.g., the median wild-type). (**B**) Same as panel A but with relative fitness per-generation $s^{\text{logit}}_{\text{gen}}$. (**C**) Covariation in fitness ranks between relative fitness per-cycle $s^{\text{logit}}_{\text{cycle}}$ and per-generation $s^{\text{logit}}_{\text{gen}}$. For each fitness statistic, we calculate the mutant ranking (higher rank means higher fitness and mutants with equal fitness are assigned the lowest rank in the group), based on the rank data from main text ***Figure 2B***.



Appendix 1—figure 7. Exploring alternative conditions for rank discrepancy between fitness statistics in yeast gene-deletion data. Plots columns A and B have the same format as ***Appendix 1—figure 4B, C***, and columns (**C**) and (**D**) match main text ***Figure 2B, C*** (in reverse order). Row (**A**): Low mutant frequency $x = 0.01$. Row (**B**): Standard mutant frequency $x = 0.5$, but where we artificially eliminate variation in lag time to test the effect on the fitness rank discrepancy. Row (**C**): Same as row B but no variation in growth rate. Row (**D**): Same as row B but no variation in biomass yield. Row (**E**): Same as row B, but yields of mutants lower than the median wild-type yield are set to the wild-type value.



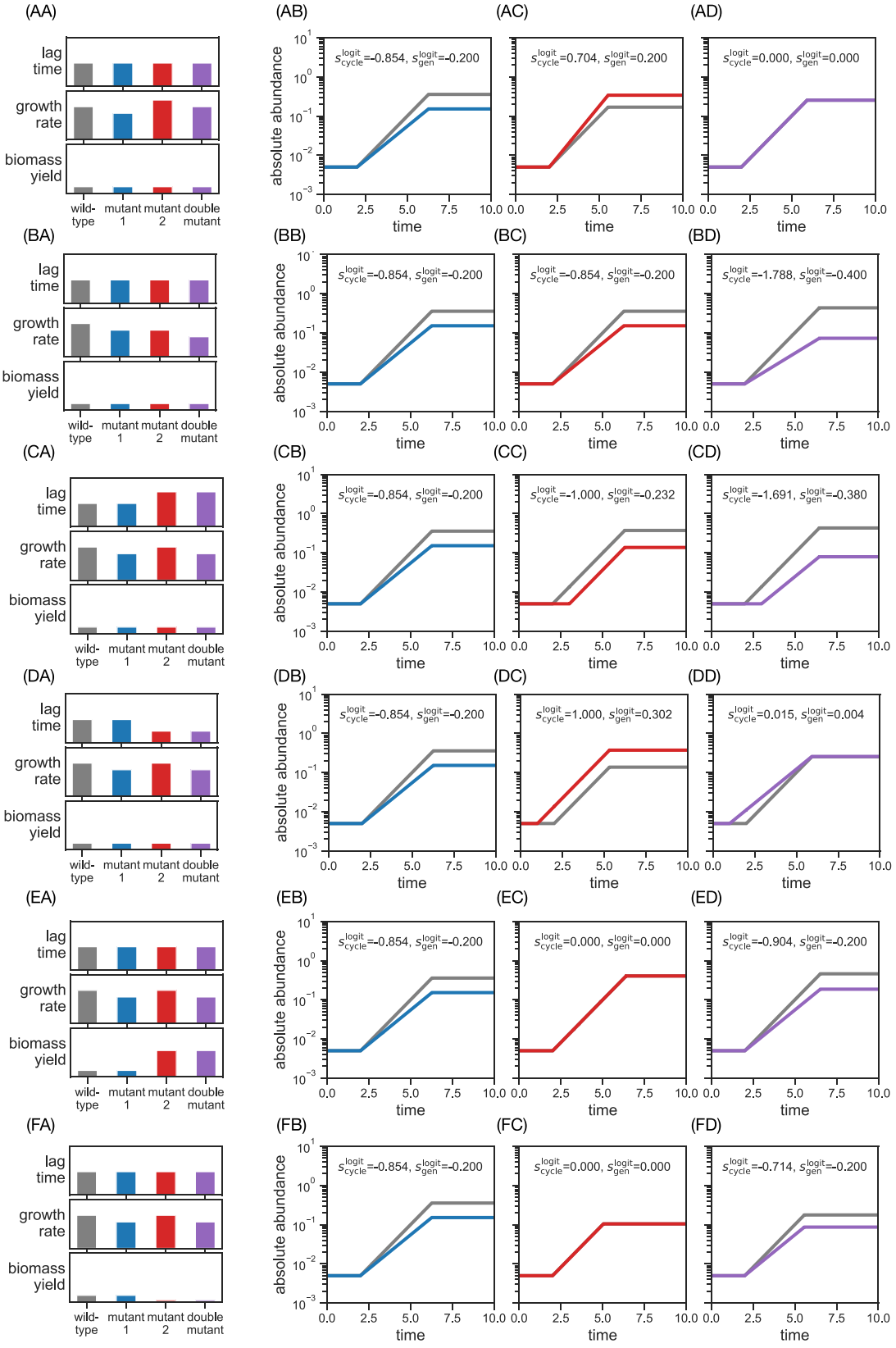
Appendix 1—figure 8. Hypothetical case where relative fitness per-cycle and per-generation are anticorrelated across mutants. (**A**) Covariation between growth rate and lag time for a synthetically generated set of mutants (gray dots) and a single wild-type (orange dot). The variation here may represent the standing variation in an evolved population with improved growth rate and lag time over the wild-type ancestor. The graphic overlap between points means they appear as a single line. (**B**) Covariation between growth rate and biomass yield for the mutants (gray dots) and wild-type (orange dot) in this synthetic data set. (**C**) Covariation between relative fitness per-cycle $s^{\text{logit}}_{\text{cycle}}$ and per-generation $s^{\text{logit}}_{\text{cycle}}$. We simulate pairwise competitions for all mutants against the wild-type with the exact same settings as for the empirical data set (main text ***Figure 2A***; Methods). (**D**) Covariation between mutant and wild-type fold-change in the competitions. Based on the competition data in panel C (gray dots), we estimate the LFC values for all mutant-to-wild-type competitions (gray dots). We highlight the bow tie-shaped area of rank discrepancy for the mutant with the lowest overall fold-change (red shading; compare ***Figure 1D***). The dashed black line shows the isocline for zero relative fitness per-cycle (main text ***Equation 9***). Distributions of relative fitness per-cycle $s^{\text{logit}}_{\text{cycle}}$ (**E**) and per-generation $s^{\text{logit}}_{\text{gen}}$ (**F**) for the mutants in panels A and B. Based on the fitness data from panel C.



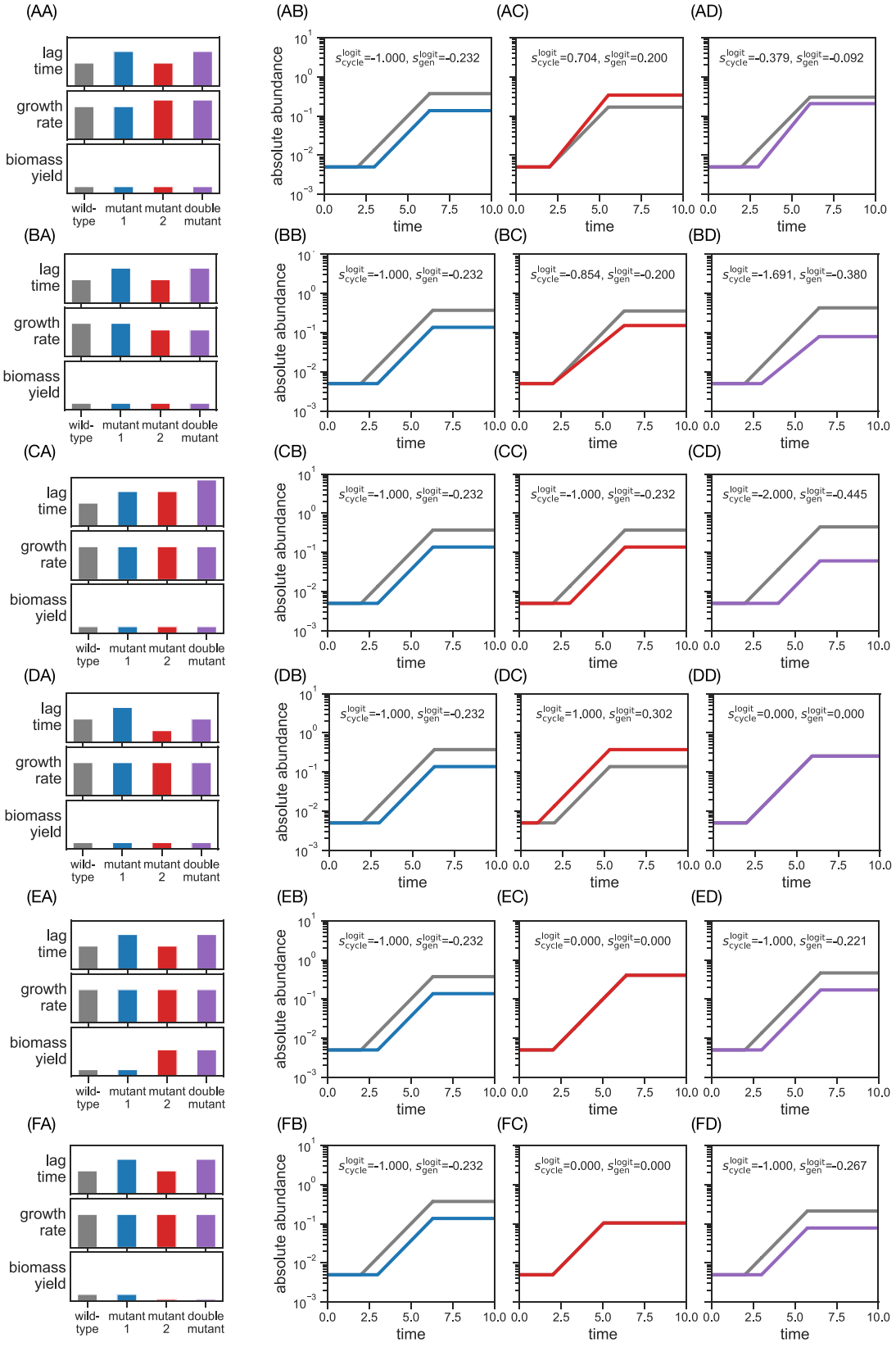
Appendix 1—figure 9. Competition growth cycles for double mutants—first column of main text ***Figure 3C, D***. Each row corresponds to a pair of mutations that perturb growth traits in the minimal model of population dynamics (main text ***Figure 2A***, Methods). This figure shows all combinations where the first mutant increases

Appendix 1—figure 9 continued on next page

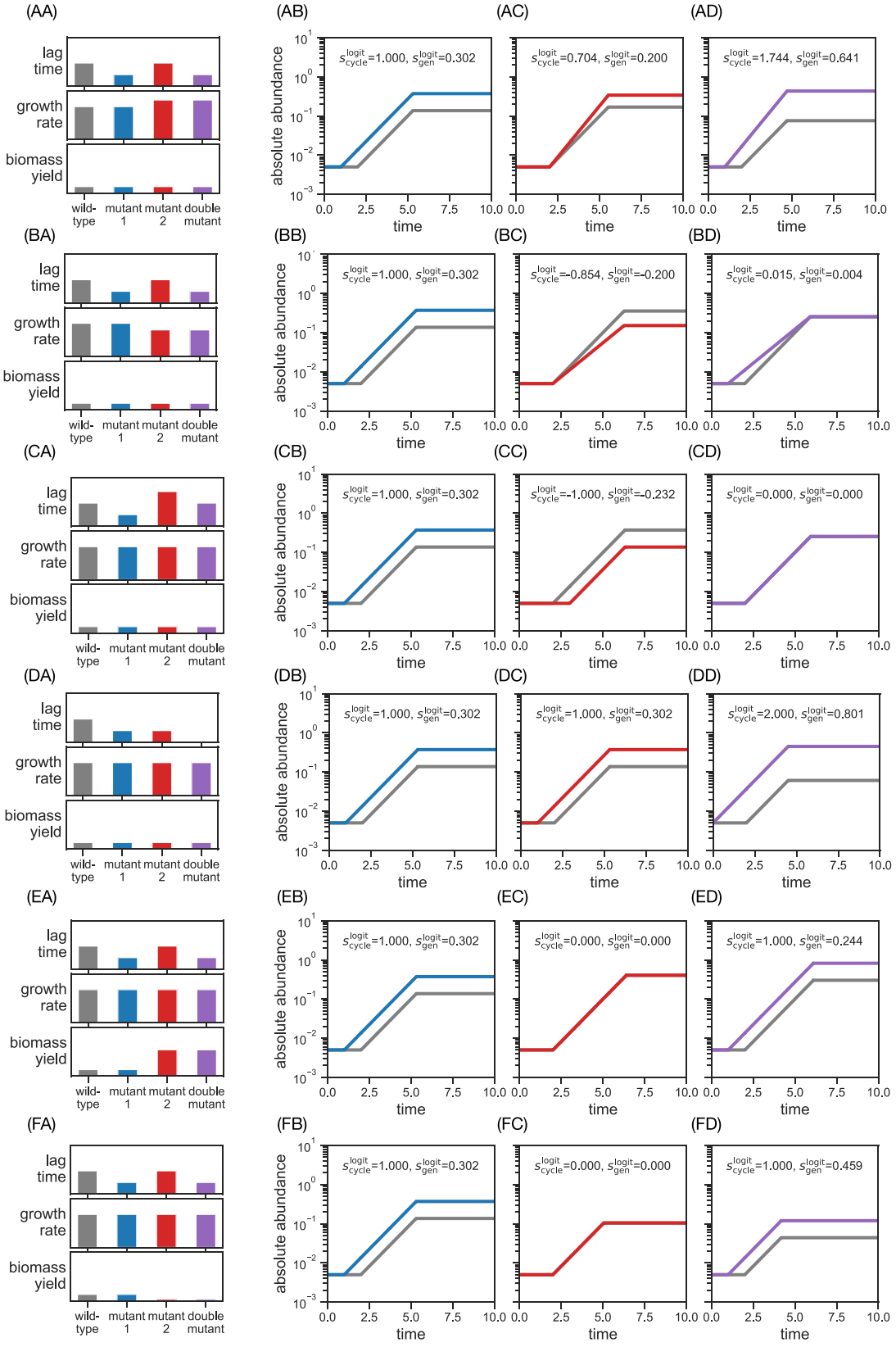
Appendix 1—figure 9 continued
growth rate (first column of main text ***Figure 3C, D***). Column (**A**): Perturbations of growth traits for single and double mutants. Column (**B**): Growth curves of wild-type (gray) and mutant 1 (blue). Column (**C**): Growth curves of wild-type (gray) and mutant 2 (red). Column (**D**): Growth curves of wild-type (gray) and double mutant (purple).



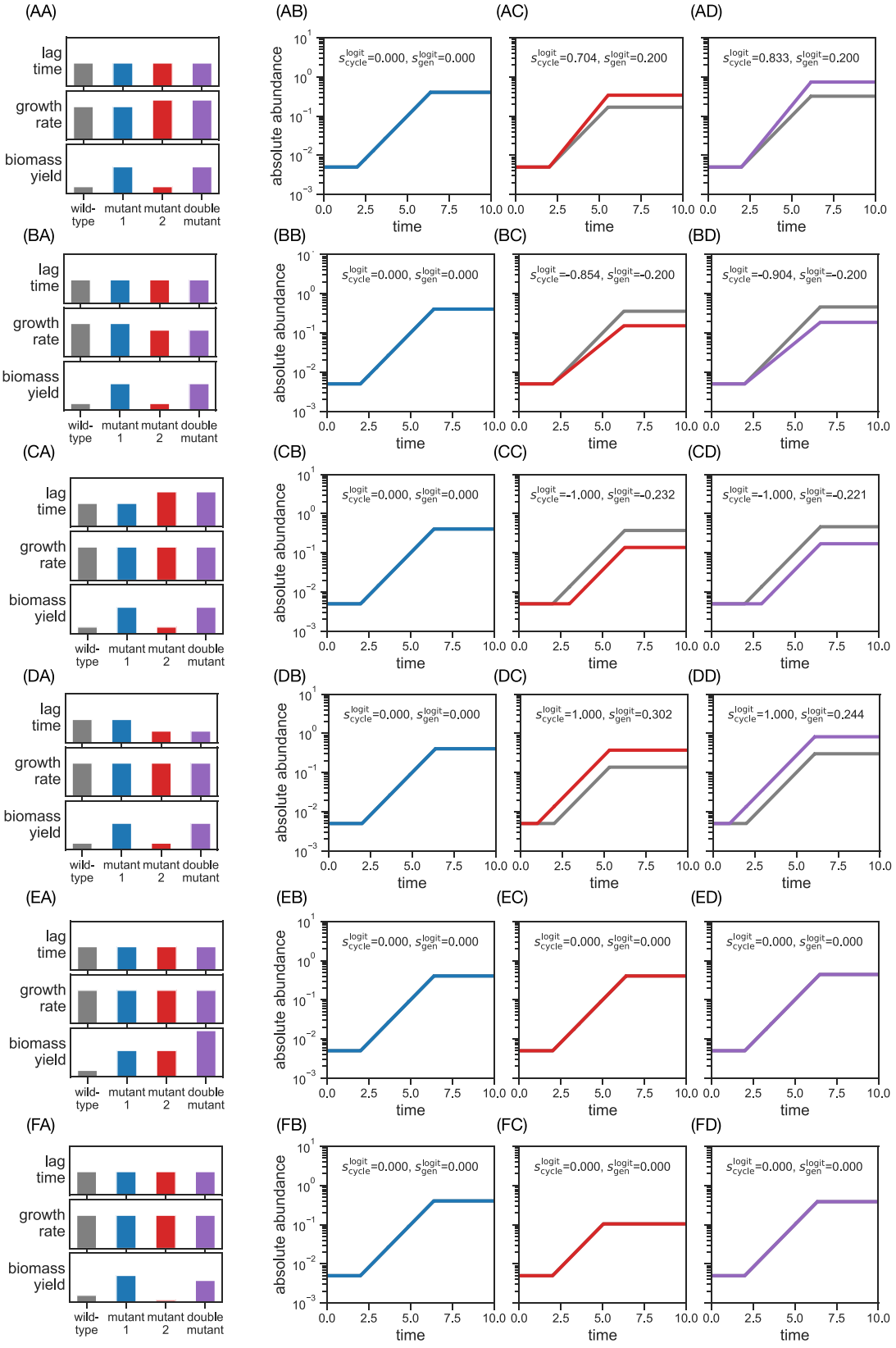
Appendix 1—figure 10. Competition growth cycles for double mutants—second column of main text ***Figure 3C, D***. Same as ***Appendix 1—figure 9*** but for mutant pairs where the first mutant decreases growth rate.



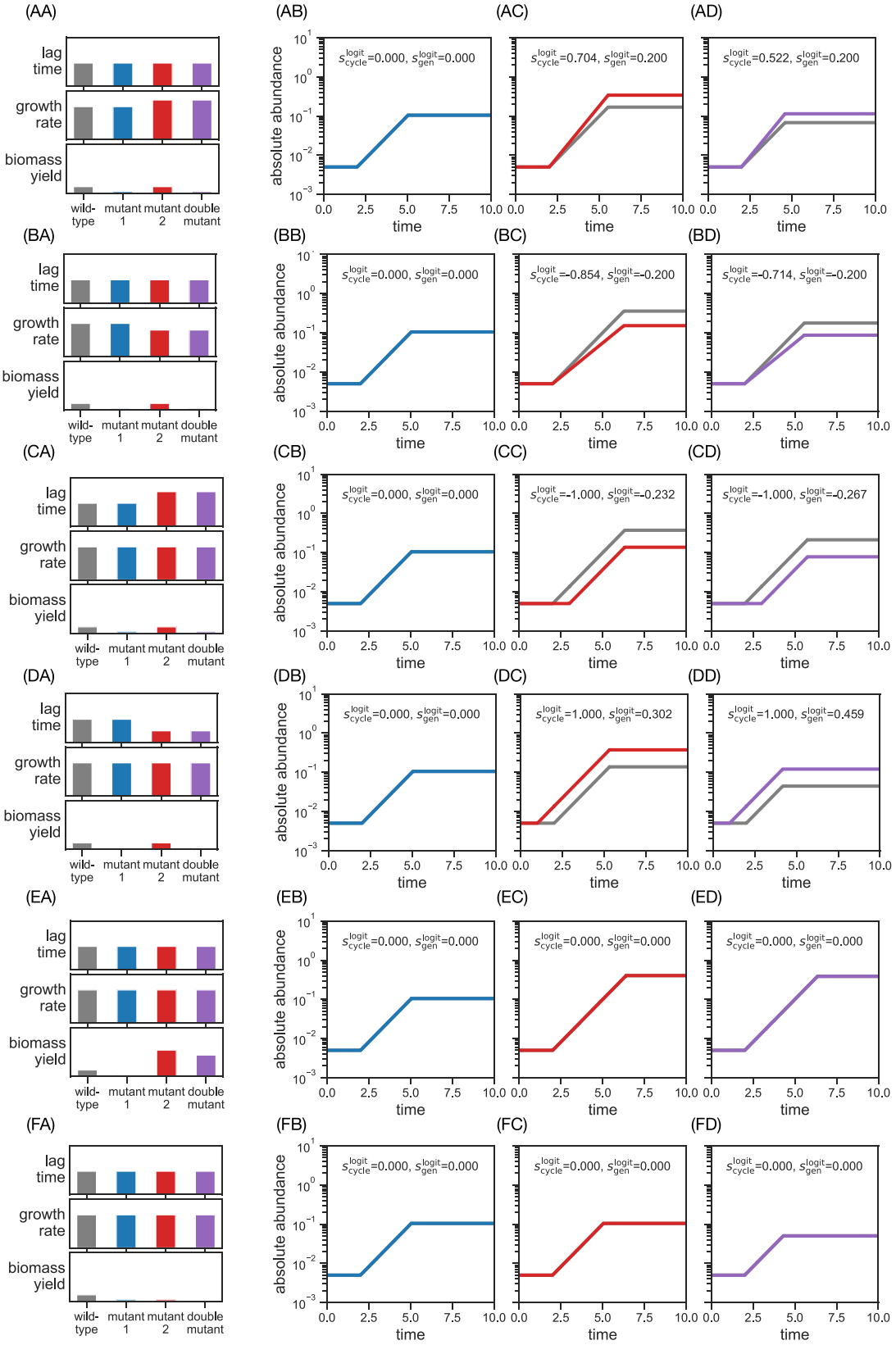
Appendix 1—figure 11. Competition growth cycles for double mutants—third column of main text ***Figure 3C, D***. Same as ***Appendix 1—figure 9*** but for mutant pairs where the first mutant increases lag time.



Appendix 1—figure 12. Competition growth cycles for double mutants—fourth column of main text ***Figure 3C, D***. Same as ***Appendix 1—figure 9*** but for mutant pairs where the first mutant decreases lag time.



Appendix 1—figure 13. Competition growth cycles for double mutants—fifth column of main text ***Figure 3C, D***. Same as ***Appendix 1—figure 9*** but for mutant pairs where the first mutant increases biomass yield.

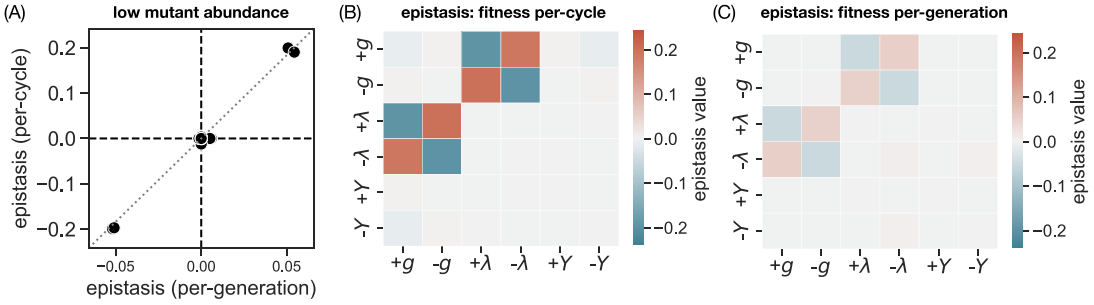


Appendix 1—figure 14. Competition growth cycles for double mutants—sixth column of main text ***Figure 3C, D***. Same as ***Appendix 1—figure 9*** but for mutant pairs where the first mutant decreases biomass yield. For the double mutant where the second mutant also decreases yield, we cannot use the additive mutation effects

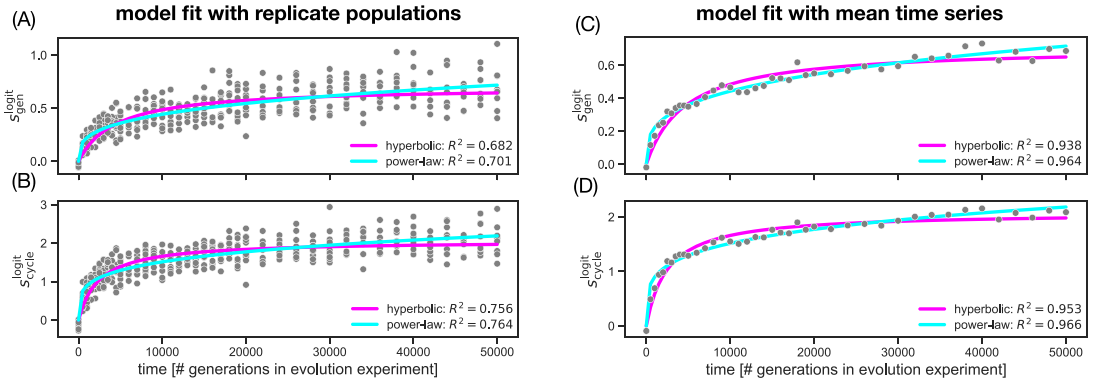
Appendix 1—figure 14 continued on next page

Appendix 1—figure 14 continued

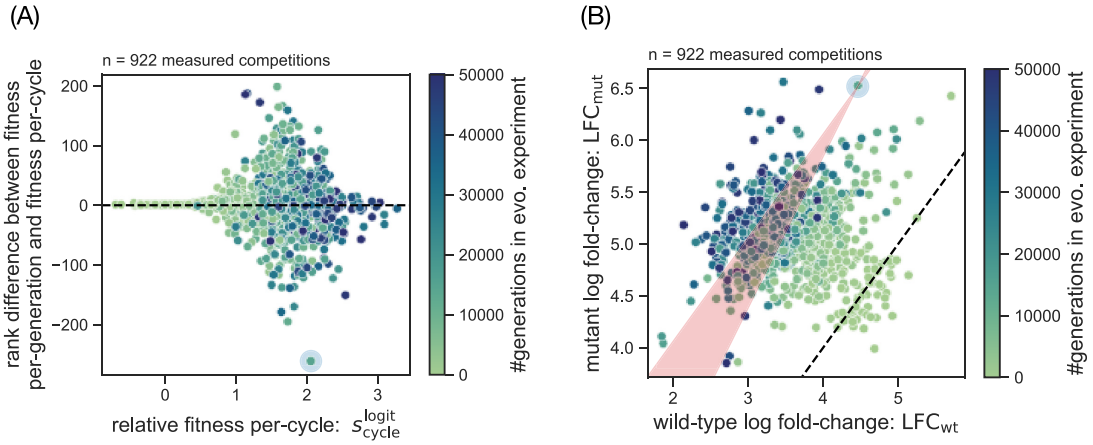
(Methods) because that would result in a negative yield for the double mutant. Here, we have defined the double mutant to have a yield value of $Y_{\mathrm{mut}} = 0.1$. This choice does not affect the fitness or epistasis, since biomass yield is a neutral trait with fitness zero in our model of population dynamics.



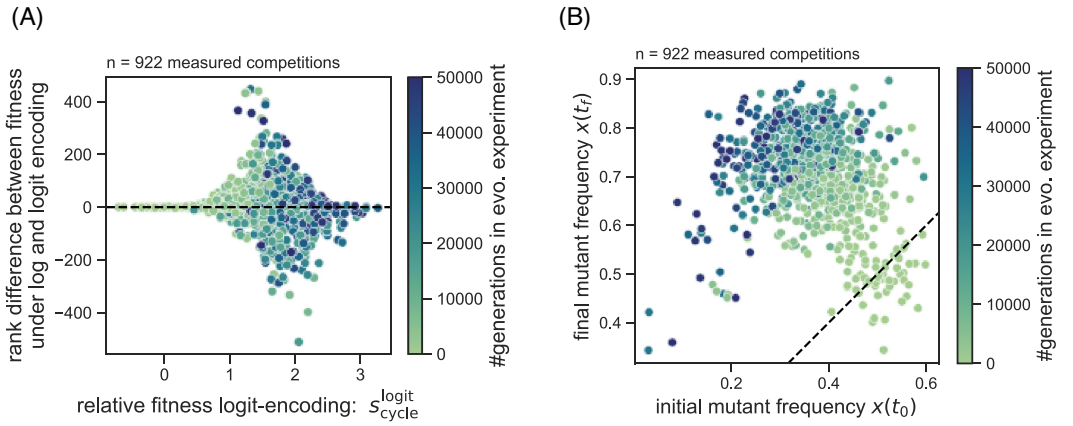
Appendix 1—figure 15. Epistasis patterns at low mutant relative abundance. Same as main text ***Figure 3B–D*** but where the mutant starts each competition at low relative abundance ($x_0 = 0.01$; Appendix 1—section S8), compared to the 1:1 initial conditions in main text ***Figure 3*** ($x_0 = 0.5$).



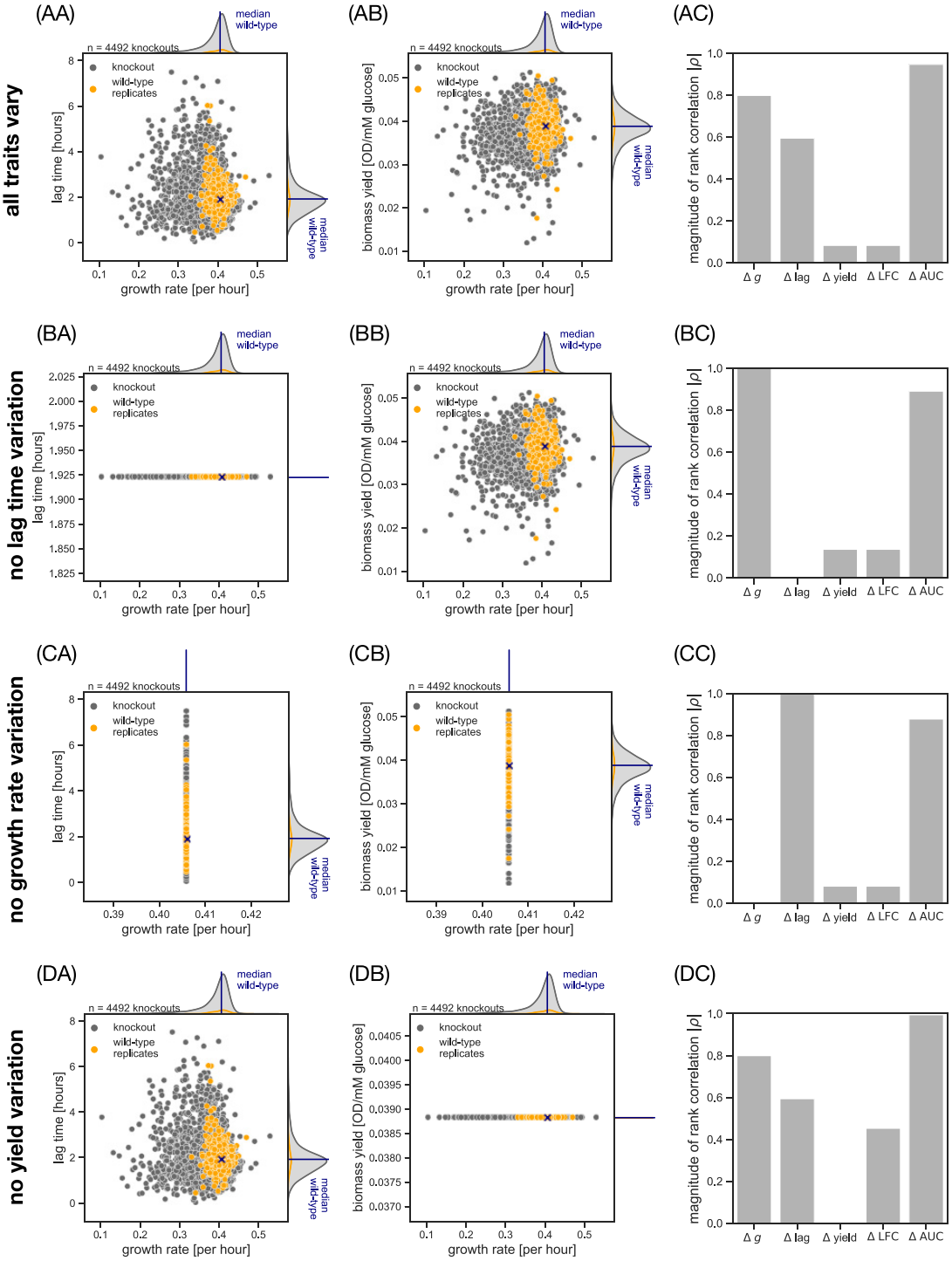
Appendix 1—figure 16. Long-term fitness trends in the LTEE under relative fitness per-cycle and per-generation. (**A**) Fit of a hyperbolic model (pink line; ***Equation S56*** in Appendix 1—section S9) and a power-law model (cyan line; ***Equation S57*** in Appendix 1—section S9) to a pooled time series of relative fitness per-generation $s_{\mathrm{gen}}^{\mathrm{logit}}$. We pool the fitness per-generation $s_{\mathrm{gen}}^{\mathrm{logit}}$ from all 12 lines of the LTEE into a single data set (gray dots) and repeat the fits of ***Wiser et al., 2013*** (Appendix 1—section S9). We compute the fraction of variance explained R^2 as a measure for the quality of fit. (**B**) Same as panel A but using relative fitness per-cycle $s_{\mathrm{cycle}}^{\mathrm{logit}}$. (**C**) Same as panel A but averaging fitness across all 12 lines at each time point. Note that the fraction of variance explained is much higher compared to panel A, because the averaged time series has fewer points (Appendix 1—section S9). (**D**) Same as panel C but using relative fitness per-cycle $s_{\mathrm{cycle}}^{\mathrm{logit}}$. For a comparison between our results and the original fit by ***Wiser et al., 2013***, see Appendix 1—section S9.



Appendix 1—figure 17. Comparison of relative fitness per-generation and per-cycle across the complete LTEE competition data set. (**A**) Rank discrepancy between relative fitness per-cycle $s^{\text{logit}}_{\text{cycle}}$ and per-generation $s^{\text{logit}}_{\text{gen}}$ for evolved populations of the LTEE. For each fitness statistic, we calculate a ranking (higher rank means higher fitness and mutants with equal fitness are assigned the lowest rank in the group; compare to main text ***Figure 2B***) across all 12 evolved lines and all time points. The rank difference is defined as the rank in $s^{\text{logit}}_{\text{gen}}$ minus the rank in $s^{\text{logit}}_{\text{cycle}}$. We highlight the evolved population with the greatest rank difference (blue halo). (**B**) Covariation between the wild-type and mutant fold-change for the competition data from the LTEE (***Wiser et al., 2013***). The term 'mutant' (*y*-axis) refers to an evolved population at a given time point from one of the 12 lines of the LTEE. We highlight the evolved population with the greatest rank difference (blue halo; same as in panel A) and draw its corresponding bow tie-shaped area of rank discrepancy between $s^{\text{logit}}_{\text{cycle}}$ and $s^{\text{logit}}_{\text{gen}}$ (red shading; compare to main text ***Figure 1D***). The coloring in both panels refers to the time point at which the evolved population was sampled from the LTEE.



Appendix 1—figure 18. Comparison of log encoding and logit encoding for relative fitness per-cycle in the LTEE competition data set. (**A**) Same as ***Appendix 1—figure 17A*** but for rank discrepancy between logit-encoded relative fitness per-cycle $s^{\text{logit}}_{\text{cycle}}$ and log-encoded relative fitness per-cycle $s^{\text{log}}_{\text{cycle}}$ for evolved populations of the LTEE. (**B**) Covariation between the wild-type relative abundance and mutant relative abundance at the start of the competition growth cycle for the competition data from the LTEE (***Wiser et al., 2013***). The term 'mutant' in the axis labels refers to an evolved population at a given time point from one of the 12 lines of the LTEE. The coloring in both panels refers to the time point at which the evolved population was sampled from the LTEE.

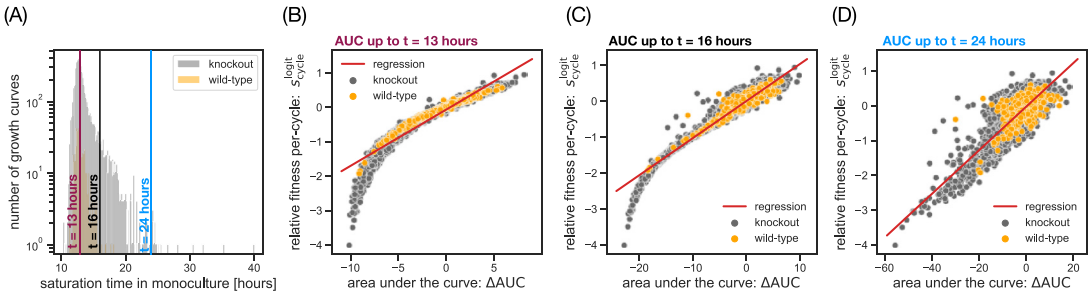


Appendix 1—figure 19. Predicting relative fitness with monoculture proxies (fitness potentials) under different scenarios of trait variation. Plots in columns (**A**) and (**B**) show growth trait variation across mutants, with the same format as ***Appendix 1—figure 4B,C***. Plots in column (**C**) show quality of prediction for different monoculture proxies under the trait distribution in columns A and B. As the ground truth, we estimate the relative fitness per-cycle $s_{\text{cycle}}^{\text{logit}}$ using a simulated 1:1 competition growth cycle (main text ***Figure 2A***; Methods). For each mutant i, we compute the growth rate difference $\Delta g = g_i - g_{\text{wt}}$, the lag time difference $\Delta\text{lag} = \lambda_i - \lambda_{\text{wt}}$, the difference in biomass yield $\Delta\text{yield} = Y_i - Y_{\text{wt}}$, the difference in log fold-change $\Delta\text{LFC} = \text{LFC}_i - \text{LFC}_{\text{wt}}$, and the difference in area under the growth curve $\Delta\text{AUC} = \text{AUC}_i - \text{AUC}_{\text{wt}}$ from simulated monoculture growth curves (Appendix 1—section S10). We quantify the agreement between the monoculture proxy and the relative fitness per-cycle $s_{\text{cycle}}^{\text{logit}}$

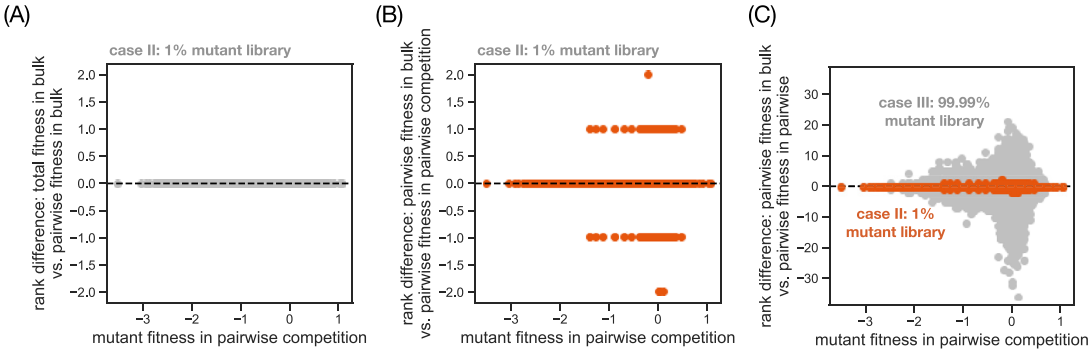
Appendix 1—figure 19 continued on next page

Appendix 1—figure 19 continued

using the Spearman correlation coefficient ρ. Row (**A**): Empirical growth trait variation from data on yeast single-gene knockout mutants (identical to ***Appendix 1—figure 4B,C***). Row (**B**): Same as row A but where we artificially eliminate variation in lag time to test the effect on the monoculture proxies. Row (**C**): Same as row A but with no variation in growth rate. Row (**D**): Same as row A but with no variation in biomass yield.



Appendix 1—figure 20. The choice of the cutoff time for evaluating the area under the curve (AUC). (**A**) Distribution of saturation times in monoculture for the knockouts (gray bars) and wild-type replicates (orange bars) in our empirical data set (***Appendix 1—figure 4***). The saturation time t_{sat} is defined as the time when the limiting resource is depleted ($R(t_{\text{sat}}) = 0$) and can be estimated numerically from the trait data (Methods). Three vertical lines indicate example choices for the cutoff time t_{eval} of the AUC: the most frequent saturation time ($t_{\text{eval}} = 13$ hr; red line), a saturation time halfway in the decay of the distribution ($t_{\text{eval}} = 16$ hr; black line), and an external time scale ($t_{\text{eval}} = 24$ hr; blue line). Covariation between relative fitness per-cycle $s^{\text{logit}}_{\text{cycle}}$ and AUC with the cutoff times marked in panel A: 13 hr (**B**), 16 hr (**C**), and 24 hr (**D**). We compute the AUC from simulated monoculture knockouts (gray dots) and wild-type replicates (orange dots). As the ground truth, we take the relative fitness per-cycle $s^{\text{logit}}_{\text{cycle}}$ from a pairwise competition (main text ***Figure 2A***). The red lines show the best fit from a linear regression of $s^{\text{logit}}_{\text{cycle}}$ to the AUC.



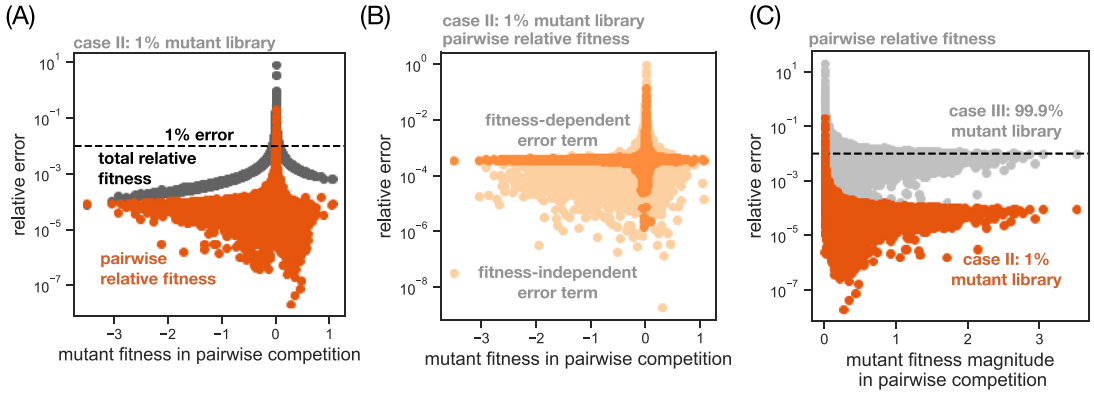
Appendix 1—figure 21. The error in mutant fitness rankings between bulk and pairwise competition experiments. (**A**) Rank difference between total relative fitness and pairwise relative fitness in a bulk competition growth cycle with low mutant library abundance (main text ***Figure 5A***, case II). Based on the fitness data in main text ***Figure 5C***, we calculate a mutant ranking for total relative fitness in bulk (main text ***Equation 24***) and a ranking for pairwise relative fitness in bulk (main text ***Equation 25***) (higher rank means higher fitness and mutants with equal fitness are assigned the lowest rank in the group). The rank difference is defined as the rank in total relative fitness $\sigma^{\text{logit}}_{i,\text{cycle}}$ minus the rank in pairwise relative fitness $s^{\text{logit}}_{i,\text{wt,cycle}}$. The ranks exactly match in this case because the mutants are sufficiently rare in case II that the population fitness is almost identical to the wild-type fitness. (**B**) Based on the pairwise relative fitness at low mutant library abundance in main text ***Figure 5C*** (orange dots; case II), we calculate a mutant ranking for pairwise relative fitness in bulk (main text ***Equation 25***) and a mutant ranking for the relative fitness per-cycle in pairwise competition (main text ***Equation 9***). The rank difference (orange dots) is defined as the rank in bulk competition minus the rank in pairwise competition. The rank differences are small because the mutants are sufficiently rare in case II that higher-order effects in the bulk competition are minor. (**C**) Based on the fitness data in the inset of main text ***Figure 5C***, we estimate a mutant ranking for pairwise relative fitness (main text ***Equation 25***) in the case of a bulk competition growth cycle with high mutant library abundance (gray dots; compare to main text ***Figure 5A***, case III). For each case, the rank difference is defined as the rank in the bulk

Appendix 1—figure 21 continued on next page

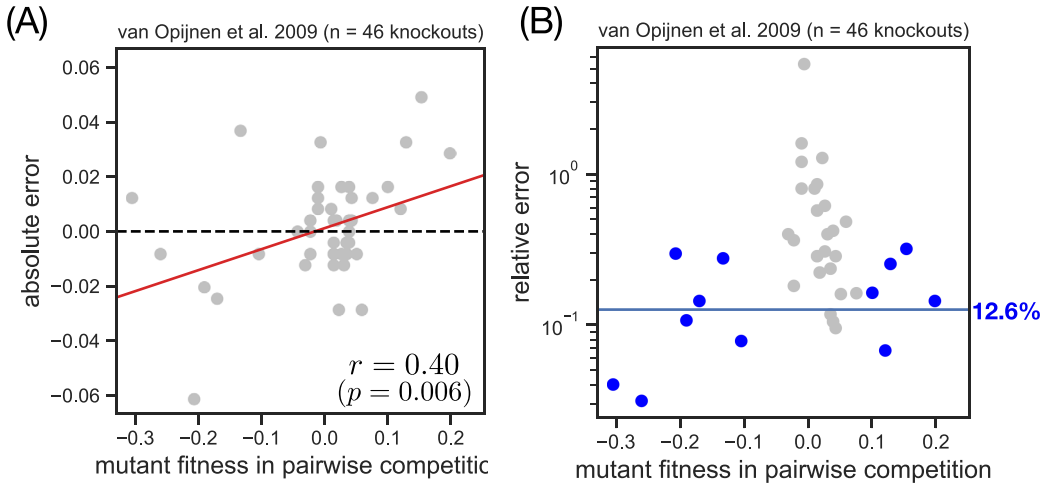
Appendix 1—figure 21 continued
competition minus the rank in pairwise competition. The rank difference for case II (orange dots) is identical to the data in panel B. All fitness statistics in this figure are based on the logit-encoding; however, since the underlying relative abundances are small ($x \ll 1$), it is approximately equivalent to the log encoding ($\log x \approx \operatorname{logit} x$).



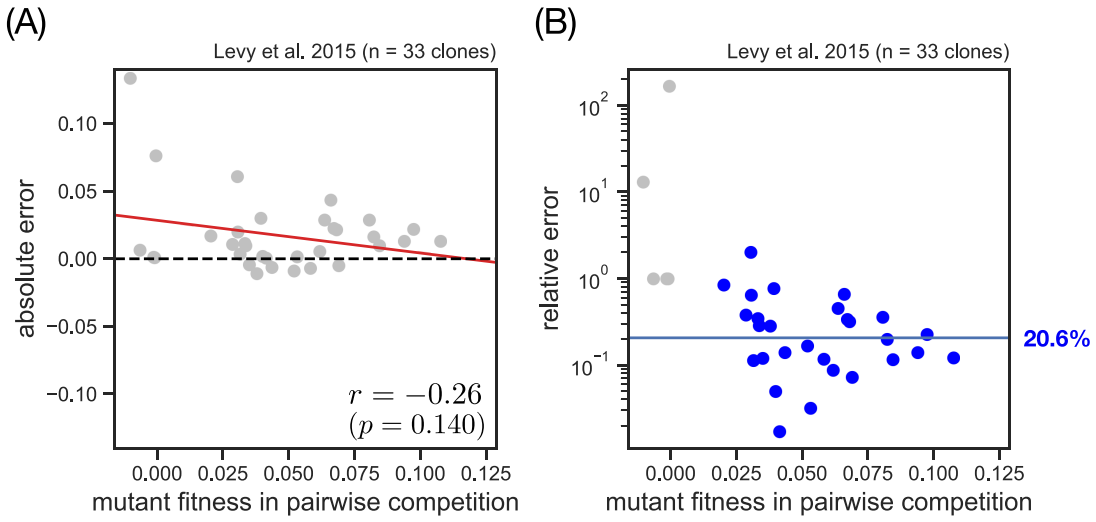
Appendix 1—figure 22. A decomposition for the error from higher-order interactions in bulk competition experiments. For a bulk competition growth cycle with low mutant library abundance (main text ***Figure 5A***, case II), we calculate the pairwise relative fitness (main text ***Equation 25***) for the knockouts in our empirical data set (***Appendix 1—figure 4A***) using a previously established approximation (***Manhart and Shakhnovich, 2018***) (Appendix 1—section S14). The error from higher-order interactions is defined as the pairwise fitness in bulk minus the fitness in pairwise competition. Based on the approximation for our model of population dynamics (Appendix 1—section S14), we derive a decomposition that separates the absolute error into two terms that we call the *fitness-dependent error term* (dark orange dots) and the *fitness-independent error term* (light orange dots). For full details on the decomposition, see Appendix 1—section S15.



Appendix 1—figure 23. The relative error between bulk and pairwise competition experiments. (**A**) Same as main text ***Figure 5C*** but showing relative rather than absolute error. The relative error of each bulk statistic is defined as the absolute error (main text ***Figure 5C***), divided by the fitness in pairwise competition (***Equation S102*** in Appendix 1—section S16). A dashed gray line indicates the threshold of 1% relative error. (**B**) Same as ***Appendix 1—figure 22*** but showing relative rather than absolute error. (**C**) Same as the inset of main text ***Figure 5C*** but showing relative rather than absolute error. On the *x*-axis, we plot the absolute value of relative fitness per-cycle in the pairwise competition.



Appendix 1—figure 24. The bulk fitness error based on measurements by ***van Opijnen et al., 2009***. (**A**) Absolute error $\Delta s_{\text{gen}}^{\text{logit}} = s_{\text{gen}}^{\text{logit,bulk}} - s_{\text{gen}}^{\text{logit,pair}}$ between the pairwise fitness measured in bulk competition $s_{\text{gen}}^{\text{logit,bulk}}$ and the pairwise fitness measured in pairwise competition $s_{\text{gen}}^{\text{logit,pair}}$ for the set of single-gene knockouts of *S. pneumoniae* shown in Figure 3C in the original publication. We calculate the Pearson correlation coefficient *r* and the p-value for the null hypothesis of zero correlation, and indicate the linear regression between the two variables with a red line. (**B**) Same as panel A but showing relative rather than absolute error. We define a set of knockouts with non-neutral fitness (blue dots; $|s_{\text{gen}}{}^{\text{logit,pair}}| > 0.1$) to calculate the geometric mean relative error (blue line). See main text ***Figure 6A*** for fitness data and experiment conditions.



Appendix 1—figure 25. The bulk fitness error based on measurements by ***Levy et al., 2015***. Same as ***Appendix 1—figure 24*** but for the set of evolved genotypes of *S. cerevisiae* shown in Figure 2D in the original publication. In (**A**), we calculate the Pearson correlation coefficient r and the p-value for the null hypothesis of zero correlation, and indicate the linear regression between the two variables with a red line. In (**B**), we define a set of knockouts with non-neutral fitness (blue dots; $|s_{\text{cycle}}{}^{\text{log,pair}}| > 0.02$) to calculate the geometric mean relative error (blue line). See main text ***Figure 6B*** for fitness data and experiment conditions.